

Aus der
Kinderklinik und Kinderpoliklinik im Dr. von Haunerschen Kinderspital
Klinikum der Ludwig-Maximilians-Universität München



**Plasma Metabolite Correlates of Immune Response in Health Care
Workers Post Two Doses of mRNA COVID-19 Vaccines and
Methodological Advances in Tissue Metabolomics for Clinical
Applications**

Dissertation
zum Erwerb des Doctor of Philosophy (Ph.D.)
an der Medizinischen Fakultät
der Ludwig-Maximilians-Universität München

vorgelegt von
Yuntao Hao

aus
Henan / China

Jahr
2025

Mit Genehmigung der Medizinischen Fakultät der
Ludwig-Maximilians-Universität München

Erstes Gutachten: Prof. Dr. Berthold Koletzko

Zweites Gutachten: Prof. Dr. Klaus Parhofer

Drittes Gutachten: Priv. Doz. Dr. Albrecht von Brunn

Viertes Gutachten: Priv. Doz. Dr. Rui Wang-Sattler

Dekan: Prof. Dr. med. Thomas Gudermann

Tag der mündlichen Prüfung: 04.08.2025

Table of content

Table of content	1
I. List of figures	4
II. List of tables	6
III. List of abbreviations	7
IV. Contribution to Research Studies	9
IV.1. RisCoin Study (Chapter 1)	9
IV.2. Tissue Homogenization Study (Chapter 2)	10
V. Summary of the Dissertation	11
Chapter 1 – RisCoin Study	13
1.1. Introduction	13
1.1.1. Background	13
1.1.1.1. Overview of SARS-CoV-2 and COVID-19 Pandemic	13
1.1.1.2. The Role of Vaccination in COVID-19 Prevention and Mitigation	14
1.1.1.3. Metabolomics and Immune Response	14
1.1.2. Aim of the study	15
1.2. Material and Methods	16
1.2.1. Study Design	16
1.2.2. Biosamples	16
1.2.3. Data Collection	17
1.2.4. Detection of Anti-SARS-CoV-2 Antibodies	17
1.2.5. Live-virus Neutralization Assay	17
1.2.6. Sample Preparation and LC-MS Measurements	18
1.2.7. Software Information and Statistical Data Analysis	19
1.3. Results	21
1.3.1. Characteristics of the Study Population	22

1.3.2. Characteristics of the Anti-Spike Antibody Concentrations	24
1.3.3. Association between Metabolites and Anti-Spike Antibody Levels	27
1.3.4. Association between Metabolites and Live-virus Neutralization	29
1.3.5. Relationship between Anti-Spike Antibody Titers and Live-virus Neutralization Activity	30
1.3.6. Pathway Analysis	30
1.3.7. Effect Modification	32
1.3.8. Sensitivity Analyses	34
1.4. Discussion	35
1.5. Conclusions	40
1.6. References	40
Chapter 2 – Tissue Homogenization Study	55
2.1. Introduction	55
2.1.1. Background	55
2.1.1.1. Importance of Tissue Homogenization in Biomedical Research	55
2.1.1.2. Challenges in Standardizing Homogenization Protocols	55
2.1.2. Tissue Homogenization in Clinical Metabolomics	56
2.1.2.1. High-Throughput Sample Preparation and Extraction Techniques	56
2.1.2.2. Impact of Solvent Selection on Metabolite Recovery	57
2.1.3. Aim of the Study	57
2.2. Material and Methods	58
2.2.1. Chemicals and Consumables	58
2.2.2. Sample Preparation	60
2.2.2.1. Processing of Pork Tissue	60
2.2.2.2. Processing of Mouse Pancreas Tissue	61
2.2.3 Tissue Homogenization	61
2.2.3.1 Temperature Management During Homogenization	61
2.2.3.2. Effect of Solvent Polarity on Tissue Homogenization	64

2.2.3.3. Background Contamination Check	64
2.2.4. Extraction for Polar and Non-polar Metabolites	65
2.2.4.1. Extraction for Polar Metabolites	65
2.2.4.2. Extraction of Lipids Using 25% and 75% MTBE in MeOH	66
2.2.5. Volume Adjustment for Homogenate Pipetting with Prewetting	68
2.2.6. Extraction for Mouse Pancreas Tissue	69
2.2.7. Instruments and Analytical Methods	69
2.2.8. Data Analysis	70
2.3. Results and discussion	71
2.3.1. Temperature Managed Homogenization	71
2.3.2. Prewetting Correction Factor for Volume Correction	71
2.3.3. Volume Choice of Homogenate and Extract	74
2.3.4. Comparison of Metabolite Extraction Efficiencies	81
2.3.5 Mouse Pancreas Tissue	85
2.4. Conclusions	86
2.5. References	88
Acknowledgements	95
Affidavit	97
Confirmation of congruency	98

I. List of figures

Figure 1.1. Flow chart for the selection of included subjects.	22
Figure 1.2a. Overview of the distribution of the log-transformed anti-spike antibody value among different groups.	25
Figure 1.2b. Overview of the distribution of the log-transformed anti-spike antibody value among different groups.	26
Figure 1.3a. Volcano plots presenting the associations between metabolites and anti-spike antibodies.	27
Figure 1.3b. Venn diagram showing intersection between significant metabolites from the main model (orange) and the extended model (purple).	28
Figure 1.3c. 95% CIs for the comparison of percent changes in anti-spike antibodies per 1% increase of metabolite concentration between the results from main and extended models.	28
Figure 1.4a. Volcano plots presenting the associations between metabolites and neutralization activity.	29
Figure 1.4b. 95% CIs for the comparison of odds ratio in of immune neutralization activity on metabolites between the results from main and extended models.	30
Figure 1.5. Metabolic pathways identified for the 18 significant metabolites from the main model.	31
Figure 1.6a. 95% CIs for the comparison of percent changes in anti-spike antibodies per 1% increase of metabolite concentrations.	33
Figure 1.6b. 95% CIs for the comparison of percent changes in anti-spike antibodies per 1% increase of metabolite metabolite concentrations.	34
Figure 1.7. Venn diagram showing information and intersections among significant metabolites for different sample sizes.	35
Figure 2.1. Temperature optimization test of tissue homogenization.	63
Figure 2.2. Workflow for tissue homogenization, followed by two-step extraction.	67

Figure 2.3a. Recoveries of selected lipid and polar metabolite for pork tissue samples (Bar charts).....	77
Figure 2.3b. Recoveries of selected lipid and polar metabolite for pork tissue samples (Line charts).....	80
Figure 2.4a. Upset Plot Analysis of Metabolite Extraction Recoveries Across Homogenization Solutions (Threshold A).....	83
Figure 2.4b. Upset Plot Analysis of Metabolite Extraction Recoveries Across Homogenization Solutions (Threshold B).....	84
Figure 2.5. Recoveries of selected lipid and polar metabolite for 9 mouse pancreas tissue pieces from three mice (Bar charts).....	86

II. List of tables

Table 1.1. Overview of the study population.	23
Table 1.2. Metabolic pathways identified from pathway analysis that were related to anti-spike antibodies induced by mRNA COVID-19 vaccine.	32
Table 2.1. Experiment conditions for temperature management test.	62
Table 2.2. Blank types for background contamination investigation.	65
Table 2.3a. Frequency of pipette tip blockage caused by the homogenate precipitate (n out of 10) and PWC-factor-II.	73
Table 2.3b. Pipette tip prewetting for different homogenate solutions.	73
Table 2.3c. Prewetting volume correction factor (PWC-factor) determination (n = 5 tips with each weighed 5 times) for different homogenization solvents	74
Table 2.4. Background contamination shown for a selection of metabolites.	81

III. List of abbreviations

ACN	Acetonitrile
BMI	Body Mass Index
Carn	Acylcarnitine
COVID-19	Coronavirus Disease 2019
CP	Control Plasma
Eq	Equation
EtOH	Ethanol
HCW	Healthcare Worker
HPLC-ESI-QTRAP-MS/MS	High-Performance Liquid Chromatography-Electrospray Ionization-Quadrupole Linear Ion Trap Mass Spectrometry
IBD	Inflammatory Bowel Disease
IPA	Isopropanol
ISTD	Internal Standard
LPCa	Acyl-Lysophosphatidylcholine
LPCe	Alkyl-Lysophosphatidylcholine
MeOH	Methanol
MTBE	Methyltert-butyl Ether
PBS	Phosphate Buffer Saline
PCaa	Diacyl-Phosphatidylcholine
PCae	Acyl-Alkyl-Phosphatidylcholine
PSY	Psychiatric Care Patient
PV	Pipetting Volume
PWC-factor	Pre-Wetting Correction Factor
QC	Quality Control
QqQ	The Triple Quadrupole
RHS	Residual Homogenate Slurry
RT-PCR	Real-Time Polymerase Chain Reaction

SARS-CoV-2	Severe Acute Respiratory Syndrome Coronavirus 2
SM	Sphingomyelin

IV. Contribution to Research Studies

IV.1. RisCoin Study (Chapter 1)

Yuntao Hao: Methodology, Formal Analysis, Software, Investigation, Visualization, Writing – original draft, Writing – review & editing.

Jeannie Horak: Conceptualization, Methodology, Project Administration, Supervision, Validation, Writing – review & editing.

Sultan Nilay Can: Formal Analysis, Software, Supervision, Visualization, Writing – review & editing.

Thu Giang Le Thi: Investigation, Project Administration, Data Curation, Writing – review & editing.

Luke Tu: Software, Investigation, Writing – review & editing.

Paul R. Wratil: Investigation, Methodology, Writing – review & editing.

Zorica Stijepic: Investigation, Methodology, Writing – review & editing.

Stephanie-Katrin Magdalena Winterstetter: Investigation, Methodology, Writing – review & editing.

Marcel Stern: Investigation, Methodology, Writing – review & editing.

Gaia Lupoli: Investigation, Methodology, Writing – review & editing.

Irina Badell: Investigation, Methodology, Writing – review & editing.

Ana Zhelyazkova: Investigation, Project Administration,

Andreas Osterman: Investigation, Data Curation, Writing – review & editing.

Sven P. Wichert: Data Curation, Writing – review & editing.

Alexander Choukér: Conceptualization, Project Administration, Writing – review & editing.

Veit Hornung: Conceptualization, Writing – review & editing.

Oliver T. Keppler: Conceptualization, Writing – review & editing.

Helga P. Török: Conceptualization, Writing – review & editing.

Kristina Adorjan: Conceptualization, Project Administration, Writing – review & editing.

Sibylle Koletzko: Conceptualization, Project Administration, Data Curation, Writing – review & editing.

Berthold Koletzko: Conceptualization of Metabolomics Analyses in the RisCoin Study and Respective Grant Application, Resources, Supervision, Project Administration, Writing – review & editing.

IV.2. Tissue Homogenization Study (Chapter 2)

Yuntao Hao: Formal analysis, Software, Investigation, Validation, Visualization, Data curation, Writing – original draft, Writing – review & editing.

Jeannie Horak: Conceptualization, Formal analysis, Software, Investigation, Methodology, Project Administration, Supervision, Validation, Visualization, Data curation, Writing – original draft, Writing – review & editing.

Zorica Stijepic: Investigation, Methodology, Validation, Writing – review & editing.

Sultan Nilay Can: Formal analysis, Software, Writing – review & editing.

Luke Tu: Software, Validation, Writing – review & editing.

Julia Alexandra Wolff: Resources, Writing – review & editing

Berthold Koletzko: Resources, Funding Acquisition, Writing – review & editing.

V. Summary of the Dissertation

This dissertation presents two studies, which respectively explored metabolite and lipid biomarkers in relation to immune response after mRNA COVID-19 vaccination, and introduced a comprehensive tissue sample preparation workflow to facilitate metabolomics and lipidomics analysis across a broad spectrum of biological samples.

The first part of the dissertation, shown in chapter 1, aimed to investigate the association between specific metabolite compounds and two key humoral response outcomes, namely levels of spike-specific anti-SARS-CoV-2 antibodies and their neutralization activity. Plasma and serum samples from healthcare workers (HCWs), as part of the RisCoin study, at a quaternary care hospital in Munich, Germany, were collected between October and December 2021. From over 4,000 participants, 412 were selected for detailed metabolomics and lipidomics analysis using high-performance liquid chromatography electrospray ionization triple quadrupole-linear ion trap mass spectrometry (HPLC-ESI-QTRAP-MS/MS), with 363 samples included in the final statistical analysis after data cleaning. Statistical analysis revealed significant positive correlations between elevated concentrations of three acylcarnitines and 15 lipid compounds, including sphingomyelins and ether lipids, with higher levels of spike-specific antibodies (FDR adjusted $p < 0.05$). However, no metabolites were significantly associated with neutralization activity, although neutralization activity showed a positive correlation with anti-spike antibody levels ($p < 0.001$). Pathway analysis further highlighted the involvement of sphingolipid, ether lipid, and glycerophospholipid metabolism in modulating the immune response to vaccination. These findings suggest that the metabolic state, particularly the activity of certain lipid pathways, played an important role in influencing the efficacy of mRNA COVID-19 vaccination. 18 reported discriminant metabolites, from sphingomyelin, ether phosphatidylcholine (ether PC), ether/acyl lysophosphatidylcholines (LPC), and acylcarnitine groups, emerged as potential biomarkers of vaccine-induced immune responses.

The second part of this thesis, described in chapter 2, has been successfully published in *Analytica Chimica Acta* on 25.01.2025 (DOI: [10.1016/j.aca.2025.343728](https://doi.org/10.1016/j.aca.2025.343728)). This section highlights the challenges associated with metabolomics and lipidomics analyses of tissue samples, which are less explored compared to other biological matrices due to complexities regarding collection, preparation, and standardization. To address these issues, we established a comprehensive robust tissue sample preparation and a workflow capable of quantitatively analysing a broad spectrum of metabolites, ranging from high polarity to high lipophilicity compounds. Using pork tissue as the model, six solvent mixtures with varying lipophilicity were evaluated for tissue homogenization, followed by metabolite extraction using methanol (MeOH) for polar compounds and methyl-tert-butyl ether (MTBE) in MeOH for lipophilic ones. To mitigate the issue of solvent-induced pipette tip blockage, a prewetting correction factor was introduced for highly lipophilic homogenization solutions and low-volume homogenate pipetting. Extraction efficiencies across 24 preparation conditions were assessed using Upset plots, with the optimal performance achieved using phosphate-buffered saline (PBS):MeOH (1:1, v/v) combined with a two-step extraction process involving MeOH for polar metabolites and 75% MTBE in MeOH for lipids. This optimized workflow was effectively applied to mouse pancreas tissues, uncovering anatomical region-specific metabolic activities and demonstrating its potential to advance metabolomics research.

Together, the findings from these two studies contribute to the understanding of metabolite and lipid biomarkers in both vaccination-induced immune responses and tissue-specific metabolic profiling, offering promise for advancing clinical and experimental metabolomics research.

Chapter 1 – RisCoin Study

Plasma Metabolite Correlates of Immune Response in Health Care Workers Post Two Doses of mRNA COVID-19 Vaccines: Analysis of A Riscoin Study Subsample

1.1. Introduction

1.1.1. Background

1.1.1.1. Overview of SARS-CoV-2 and COVID-19 Pandemic

The global outbreak of COVID-19, triggered by the highly transmissible severe acute respiratory syndrome coronavirus 2 (SARS-CoV-2), has emerged as one of the most profound public health crises of the 21st century [1-3]. SARS-CoV-2 virus primarily targets the lower respiratory tract, the COVID-19 disease can further inflict damage on multiple organs, including heart, gastrointestinal tract, lymph nodes, liver, and brain [4, 5]. Although most patients exhibit favourable prognoses, approximately one-fifth experience severe symptoms with a significant number requiring intensive care [6]. As of August 2025, the World Health Organization (WHO) reported over 778 million confirmed cases and 7.1 million deaths due to COVID-19, underscoring the disease's massive impact [7].

The rapid mutation of SARS-CoV-2 has led to the appearance of numerous variants, some of which have shown increased transmissibility, resistance to neutralizing antibodies, and, in some cases, enhanced virulence [8]. Notable variants include Alpha, Beta, Gamma, Delta, and Omicron, with the latter giving rise to several sublineages, including BA.2.86, JN.1, and EG.5 [8, 9]. Each of these variants presents unique challenges to public health efforts. The BA.2.86 variant carries numerous mutations in its spike protein, prompting concerns regarding its ability to bypass immune defenses established through prior infections or vaccinations [10]. Similarly, EG.5 and JN.1 have shown increased transmissibility, which could lead to new waves of infections even in populations with high vaccination coverage [10-12]. The continuous evolution of SARS-

CoV-2 variants underscores the importance of maintaining vigilance and advancing medical strategies to combat this infectious disease.

1.1.1.2. The Role of Vaccination in COVID-19 Prevention and Mitigation

Vaccination remains the cornerstone of efforts to control the COVID-19 disease by effectively preventing severe disease and death, even breakthrough infections, where vaccinated individuals still contract the virus, can happen, particularly with newer variants [13, 14]. The development of vaccines, particularly mRNA-based vaccines such as those produced by BioNTech & Pfizer and Moderna, has been a remarkable scientific achievement, offering high levels of efficacy in preventing SARS-CoV-2 infections or mitigating severity following breakthrough infections [13, 14]. These vaccines operate by delivering genetic instructions that encode the viral spike protein, prompting an immune response that involves the generation of antibodies directed against the spike antigen of SARS-CoV-2 [15]. Especially, the production of neutralizing antibodies, which commonly target the receptor-binding domain (RBD) of the viral spike protein, is recognized as a key indicator of immunity against severe COVID-19 [16].

It is worth noting that the concentrations and kinetics of anti-spike antibodies vary considerably among individuals following vaccination or infection [17, 18]. Understanding the underlying mechanisms of this variability is essential for optimizing vaccination strategies, particularly for vulnerable populations, who may not possess robust immune responses. Factors such as gender, age, health conditions and previous exposure to the virus have been shown to affect the strength and longevity of the immune response against SARS-CoV-2, while deeper underlying mechanisms are still not fully unveiled [19-23].

1.1.1.3. Metabolomics and Immune Response

Metabolomics, the comprehensive analysis of metabolites within biological systems, has provided substantial impetus to unveil the mechanism behind various health

conditions and progression of diseases [24-29]. Emerging evidence links metabolic regulation to adaptive immunity, involving several cellular metabolic pathways such as fatty acid metabolism, cholesterol synthesis, glycolysis, and oxidative phosphorylation [30-32]. Several studies have investigated changes in the metabolic state of COVID-19 patients relative to disease severity [33-35]. Blood sample-based metabolomics has also provided valuable insights into the mechanisms underlying influenza and DTaP (diphtheria, tetanus, and pertussis) vaccine-induced immune responses [36, 37]. However, limited research has examined the association between metabolites and the humoral immune response to COVID-19 vaccination. Metabolites such as amino acids, tricarboxylic acid cycle (TCA) organic acids, sphingomyelin (SM), free fatty acids, cholesterol, triglycerides, ceramides and lysophosphatidylcholine (LPC) have been linked to the immune response to COVID-19 vaccines [38-41].

1.1.2. Aim of the study

The present study, involving healthcare workers from the RisCoin (Risk Factors for COVID-19 Vaccination Failure) study, sought to uncover metabolite biomarkers linked to changes in humoral immunity against SARS-CoV-2 after mRNA COVID-19 vaccination. The study employed detailed metabolomics and lipidomics approaches [42], , utilizing advanced targeted high-performance liquid chromatography-electrospray ionization triple quadrupole linear ion trap mass spectrometry (HPLC-ESI-QTRAP-MS/MS) to precisely quantify organic acids, acylcarnitines and ether-linked lipids (such as ether phosphatidylcholine (PCae) and ether LPC (LPCe)). The latter have been reported in several studies to be promising predictive biomarkers for the outcome of COVID-19 patients and other diseases such as rheumatoid arthritis [43-45]. Linear regression and binomial logistic regression models, adjusted for covariates, were utilized to explore metabolites significantly correlated with humoral immune responses, i.e. anti-spike antibody concentrations and live-virus neutralization. Pathway analysis based on the most discriminant metabolite biomarkers was further

conducted to enhance understanding of the molecular mechanisms behind mRNA vaccine-induced protection against SARS-CoV-2.

1.2. Material and Methods

1.2.1. Study Design

The recruitment strategy and fundamental characteristics of the RisCoin Study have been previously outlined [42]. In brief, from October 7 to December 16, 2021, coinciding with Germany's fourth COVID-19 wave, all employees and trainees aged 18 and older at LMU University Hospital, the country's 2nd-largest quaternary care hospital, were invited to provide blood samples and fill out an online survey. Most healthcare workers participated during the last three weeks of October and first two weeks of December, aligned with a hospital-organized COVID-19 vaccination campaign. All participants were vaccinated at least twice, primarily with BNT162b2 (Comirnaty® by BioNTech & Pfizer) and mRNA-1273 (Spikevax® by Moderna), against COVID-19 before enrolment. Among > 4000 HCWs, 412 HCW samples (340 HCW considered healthy [HCW-H] and 72 with reported diseases [HCW-D]), while not representative for the total group (n > 4000), were selected and analysed for the here presented study. Regarding the selection criteria for these 412 HCWs, 294 HCW-H samples of them were selected by matching the distribution of gender, age, vaccine type, and absence of health issues (e.g., chronic lung diseases, diabetes) to the other two smaller RisCoin subcohorts: psychiatric patients (PSY, n = 116) and inflammatory bowel disease patients (IBD, n = 173) [42]. These 294 HCW samples will be further utilized as negative controls for investigating the PSY and IBD cohort. 46 extra HCW-H and 72 HCW-D samples were selected by matching gender, age, and health issue distributions from the CORKUM (LMU-Klinikum Biobank) study (n = 91). These 118 HCW samples will later be utilized as negative controls for the CORKUM study (46 HCW-H + 72 HCW-D).

1.2.2. Biosamples

Plasma samples were collected in LH-Plasma Monovette (Sarstedt) and transferred to the lab in ice boxes using crushed ice for cooling. Within 4 hours after sample collection, the following sample preparation steps were performed: centrifugation at 939 rcf for 10 minutes at 4°C, pipetting plasma into thermo matrix tubes in 96-tube-racks, scanning the bar code and QR-code information on each individual blood sample tube and their respective thermo matrix sample storage tube before storage at -80°C. Plasma samples were later selected for metabolomics and lipidomics profiling. The corresponding serum specimens of each plasma sample were tested for SARS-CoV-2-specific anti-spike antibodies, anti-nucleocapsid IgG, and live-virus neutralization activity.

1.2.3. Data Collection

The online questionnaire surveyed information on demographics, COVID-19 vaccination history, health conditions, medication intake, dietary patterns, supplement use, education level, and lifestyle.

1.2.4. Detection of Anti-SARS-CoV-2 Antibodies

Serum specimens were processed as described to assess the abundance of anti-SARS-CoV-2 antibodies targeting the nucleocapsid protein and the concentrations of anti-spike antibodies [46, 47]. The Elecsys Anti-SARS-CoV-2 assay (Roche, Basel, Switzerland, cat.: 09203095190) was conducted following the manufacturer's protocol to identify anti-nucleocapsid antibodies [46], while the Elecsys Anti-SARS-CoV-2 S assay to measure the concentrations of anti-spike antibodies.

1.2.5. Live-virus Neutralization Assay

Antibody mediated live-virus neutralization was measured as described [48] [49]. In brief, of the Omicron B.1.1.529 BA.1 SARS-CoV-2 variant (GISAID EPI ISL: 7808190) after clinical isolation was expanded in Vero-E6 cells (American Typ Culture Collection) and subsequently characterized using real-time RT-PCR as described [50]. Following expansion, the tissue culture infection dose resulting in 90% loss of target cell viability

(TCID₉₀) was incubated with different dilutions of the participants' sera for 2 h at room temperature. Afterwards, the virus serum mixture was introduced to MDA-MB-231 cells overexpressing hACE2. Cell viability was assessed at 48 h post infection by adding 10 μ L of CellTiter-Glo 2.0 reagent (Promega) and measuring the bioluminescence signal (no filter, 0.5 seconds integration time). IC₅₀ values for live-virus neutralization were determined through normalized sigmoidal dose-response curve fitting of the data. IC₅₀ values \leq 1:10 serum dilutions were corrected to IC₅₀ = 1:10 serum dilution.

1.2.6. Sample Preparation and LC-MS Measurements

For metabolomic analysis, we used 96-wellplates, analyzing 74 samples, 6 sample pool quality controls (QCs), 4 control plasmas (CPs), one internal standard (ISTD), one H₂O blank for system contamination check, and 6 to 10 calibration solutions depending on the individual single platform analysis. 450 μ L of the methanol containing all ISTDs (MeOH-ISTD solution) was dispensed simultaneously with an epMotion 96XL device from Eppendorf (Hamburg, Germany) into the wells of a 1.2 mL 96-well plate (Brand, obtained from Sigma-Aldrich, Schnelldorf, Germany), followed by pipetting 50 μ L LH-plasma directly into the MeOH-ISTD solution. By drawing and ejecting 20 times, a homogeneous protein precipitate was obtained. The plates were sealed by adhesive foil, shaken at 700 rpm and 25°C for 20 minutes on a ThermoMixer C from Eppendorf (Wesseling, Germany), and then refrigerated at -20°C for 20 minutes to finalize protein precipitation. The extract slurry was transferred to a PTFE-membrane filter wellplate, which was attached with adhesive tape to a new 1.2 mL 96-wellplate. The dual wellplates were centrifuged at 2113 rcf and 22°C for 15 minutes. The lower wellplate was sealed with an adhesive foil and stored at -30°C prior to LC-MS/MS sample preparation and analysis.

For organic acid and lipid analysis, an Agilent 1260 HPLC system equipped with a degaser (G1379B), a binary pump (G1312B), and a 1260 multi-sampler (G7167A) (Agilent Technologies, Waldbronn, Germany) combined with MayLab column oven

(MayLab, Vienna, Austria) were utilized. This HPLC system was coupled to a hybrid QTRAP 4000 featuring an ESI source (AB SCIEX Pte. Ltd., Concord, Canada). The Kinetex F5 column (2.6 μ m, 2.1 mm x 150 mm) used for separating keto acids and organic acids (15 analytes) [51] as well as a Kinetex EVO C18 column (2.6 μ m, 2.1 x 150 mm) utilized for separating acyl-carnitines (60 analytes) were obtained from Phenomenex (Aschaffenburg, Germany) [52, 53]. Phosphocholine lipids (LPCa, LPCe, PCaa, PCae, and SM) were addressed through flow-injection-analysis (FIA) mode, , which operates without the need for a chromatographic column [54].

1.2.7. Software Information and Statistical Data Analysis

Sigmoidal dose response curve approximations for the IC₅₀ calculations of live-virus neutralization were performed using Prism 9 (Graphpad Inc.). Data acquisition was performed with Analyst 1.6.1, while quantitative data analysis was carried out using MultiQuantTM 3.0.3 (SCIEX, Ontario, Canada). Participants were considered to have had COVID-19, if they tested positive for anti-SARS-CoV-2 antibodies against viral nucleocapsid protein or had a specific positive PCR test. Statistical analysis and visualization were executed using R programming version 4.4.0 from R foundation, (Vienna, Austria). An in-house developed R script was used for automated peak integration, isotopic correction, and quantification of phosphatidylcholine lipids.

Prior to statistical analysis, metabolomics data cleaning was performed according to the following main steps: 1) Exclusion of all metabolites with 100% missingness and all samples with 100% missingness. 2) Exclusion of experimental sample outliers based on missingness analysis, PCA outliers test. Checking if the outliers in PCA could be explained by high missingness (> 30%). 3) Exclusion of QC sample outliers (needed for Batch Correction): threshold = Mean \pm 3*SD (on log₂-transformed data). If one QC sample show outlier values for all or most of the metabolites (> 90%), then that QC sample was excluded. Otherwise, only changing certain QC outliers values to NA. 4) Batch correction for both experimental samples and QC samples (Correction factor =

batch QC sample mean/ global QC sample mean). 5) Calculation of CV of QC samples, and dispersion ratio (D-ratio: SD (QC samples)/SD (experimental samples)). 6) Exclusion of metabolites: Metabolites were excluded only if QC-CV > 30% and if the D-ratio > 50%. Both criteria had to be met for exclusion. 7) Construction of final non-imputed file: Final non-imputed file were created by combining all platforms in the same file. All non-experimental samples (QC) were excluded from the final files. 8) Before imputation, excluding samples that were not measured in all 3 platforms, excluding samples with missingness > 30% and metabolites with missingness > 30%. 9) Imputation with “missForest” function from the missForest R package.

Afterwards, multivariate analysis was performed using linear regression for anti-spike antibodies and binomial logistic regression for neutralization activity. To improve the conformity of residual distributions to normality, all metabolite and anti-spike antibody outcomes were natural-log transformed prior to analysis. The main regression model adjusted for gender, age, 2nd vaccination interval (interval of second vaccination prior to sample collection), BMI and vaccine type. An extended regression model was created, additionally adjusted for smoking behaviour, alcohol consumption, physical activity, education level, vegetable consumption, fish consumption, ready-to-eat meal consumption, vitamin/mineral/fish oil supplements intake, cardiovascular disease status, chronic lung disease status, diabetes mellitus status, lipid metabolism disorder status, thyroid dysfunction status, chronic kidney disease status, chronic hepatic or gastrointestinal disease status, chronic neurological disorder status, cancer status, transplantation status, rheumatological disease status, chronic immune disease status, medication intake variables, taking into account previously identified variables related to antibody response [19, 46, 47]. Two models were utilized for both linear regression and logistic regression analysis. Effect estimates were expressed as percent changes in anti-spike antibody titres (together with 95% confidence intervals [95% CI]) per 1% increase of metabolites, or the odds ratio of immune neutralization activity (along with 95% CI) on metabolites between the results from main and extended models. Point-

biserial correlation analysis and partial correlation analysis, after controlling the covariates from the main model were performed to check the association between anti-spike antibodies and neutralization activity [55, 56].

Effect modification was assessed by incorporating an interaction term for the potential effect modifier. The examined modifiers included gender (female vs male), age (≤ 45 years vs > 45 years, to keep sample size statistically similar in two groups), 2nd vaccination interval (≤ 6 months vs > 6 months), vaccine type for twice vaccination (BioNTech vs Moderna, all 363 participants in this study received same vaccine type (BioNTech (n = 348) or Moderna (n = 15)) for 1st and 2nd vaccination), HCW group (HCW-healthy (HCW-H, without disease status, n = 305) vs HCW-disease (HCW-D, with disease status, n = 58)), smoking behaviour (No vs Yes), alcohol consumption (No vs Yes), regular physical activity (No vs Yes), regular vegetable consumption (No vs Yes), regular fish consumption (No vs Yes), regular ready-to-eat food consumption (No vs Yes), regular vitamin/mineral/fish oil supplements intake (No vs Yes) and education level (Without university degree vs University degree). Effect modification analyses were exclusively performed for metabolites showing significant associations with anti-spike antibody levels based on the main model, and corresponding samples with unknown information were excluded when analyzing each effect modifier [57-59]. Sensitivity analyses were performed including the following restrictions, i) participants belonging to HCW-H, ii) participants vaccinated with the BioNTech vaccine, and iii) participants who did not have unknown information for all variables included in the extended model [58, 59]. To account for multiple comparisons, the Benjamini-Hochberg procedure was applied to control the false discovery rate (FDR) with a cut-off threshold of 0.05 to filter metabolites showing significant associations with anti-spike antibodies from the main model. For these significant metabolites, pathway analysis was performed using MetaboAnalyst 6.0 combined with KEGG mapper [60, 61].

1.3. Results

1.3.1. Characteristics of the Study Population

During the data cleaning procedure, of 412 HCWs who were selected from over 4000 HCW participants in RisCoin study, in total 49 were further excluded due to missing information, previous SARS-CoV-2 infection, having received the second COVID-19 vaccination within the preceding 28 days or having received a third vaccination, use of vaccines other than BioNTech or Moderna, or use of immunosuppressive drugs, leaving 363 participants, not a representative subsample of the total group ($n > 4000$), for following data analysis (**Figure 1.1**). The relative distributions of gender, age, HCW group, education, 2nd vaccination interval, applied vaccine type for both vaccinations, weight class, neutralization activity, smoking behaviour, alcohol consumption, regular physical activity, diet habits, cardiovascular disease, medication intake and other disease status among study participants are shown in **Table 1.1**

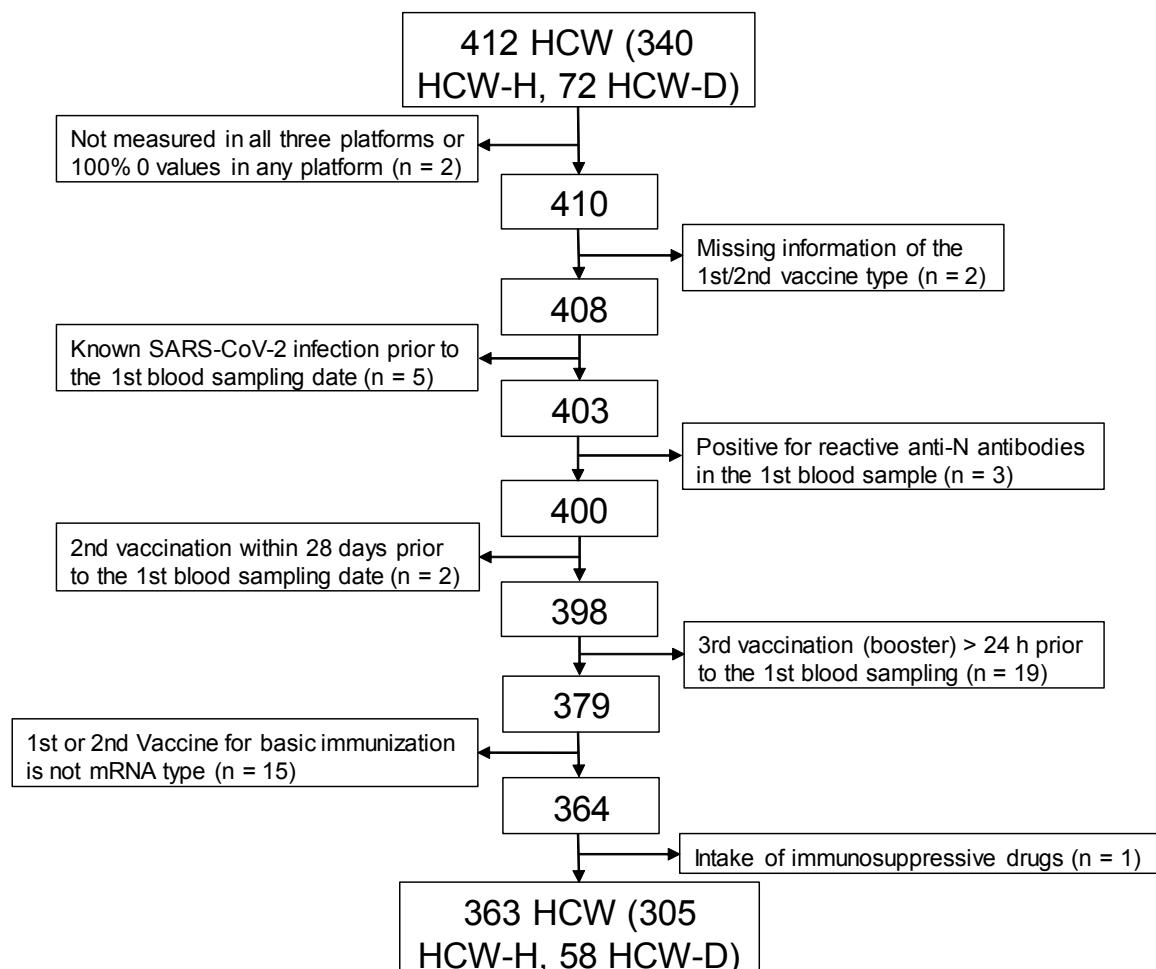


Figure 1.1. Flow chart for the selection of included subjects.

HCW = Healthcare Worker, HCW-H = HCW considered healthy, HCW-D, HCW with reported disease.

Table 1.1. Overview of the study population.

Characteristics	RisCoin Selection (n = 363)
Gender (Female)	165 (45.5%)
Age (years)	
18-30	80 (22.0%)
31-40	60 (16.5%)
41-50	59 (16.3%)
51-60	86 (23.7%)
≥ 60	78 (21.5%)
HCW subgroup (HCW-H)	305 (84%)
2 nd vaccination interval (≤ 6 months)	236 (65%)
Vaccine type (BioNTech)	348 (95.9%)
Weight class	
Underweight	5 (1.4%)
Normal weight	210 (57.9%)
Pre-obesity	118 (32.5%)
Obesity	30 (8.3%)
Neutralization activity (Negative)	154 (42.4%)
Smoking behaviour	
Non-smoker	339 (93.4%)
Unknown	1 (0.3%)
Smoker	23 (6.3%)
Alcohol consumption	
No	173 (47.6%)
Unknown	10 (2.8%)
Yes	180 (49.6%)
Regular physical activity (No)	50 (13.8%)
Regular vegetables consumption (No)	166 (45.7%)
Regular fish consumption (No)	301 (82.9%)
Regular ready-to-eat meal (No)	336 (92.6%)
Regular vitamin/mineral/fish oil supplements	
No	257 (70.8%)
Unknown	7 (1.9%)
Yes	99 (27.3%)
University degree	
No	192 (52.9%)
Unknown	12 (3.3%)
Yes	159 (43.8%)
Cardiovascular disease (No)	334 (92.0%)
Chronic lung disease (No)	356 (98.1%)
Diabetes mellitus (No)	351 (96.7%)
Lipid metabolism disorder (No)	355 (97.8%)
Thyroid dysfunction	
No	344 (94.7%)
Unknown	1 (0.3%)
Yes	18 (5.0%)
Chronic kidney disease	
No	360 (99.2%)
Unknown	1 (0.3%)
Yes	2 (0.6%)
Chronic hepatic gastrointestinal disease	
No	358 (98.6%)
Unknown	1 (0.3%)

Characteristics	RisCoin Selection (n = 363)
Yes	4 (1.1%)
Chronic neurological disorder	
No	359 (98.9%)
Unknown	1 (0.3%)
Yes	3 (0.8%)
Cancer	
No	350 (96.4%)
Unknown	2 (0.6%)
Yes_ Cured	10 (2.8%)
Yes_ Remission	1 (0.3%)
Transplantation	
No	361 (99.4%)
Unknown	1 (0.3%)
Yes	1 (0.3%)
Rheumatological disease	
No	359 (98.9%)
Unknown	1 (0.3%)
Yes	3 (0.8%)
Chronic immune disease	
No	360 (99.2%)
Unknown	1 (0.3%)
Yes	2 (0.6%)
Hematological disease	
No	357 (99.2%)
Unknown	5 (1.4%)
Yes	1 (0.3%)
Medication intake	
No	301 (82.9%)
Unknown	4 (1.1%)
Yes	58 (16.0%)

Data was shown as total number plus percentage (in parenthesis) among all participants (N = 363) for each sub-class of each group. Weight class was set according to the BMI (body mass index) definitions for adults by the WHO [62].

1.3.2. Characteristics of the Anti-Spike Antibody Concentrations

The distribution of anti-spike titres among different groups showed that the factors, female gender, younger age, shorter distance between the second vaccination prior to sample collection, receiving the Moderna vaccine, being healthy, not having a cardiovascular disease, lipid metabolism disorder, or cancer history, regularly eating ready-to-eat meals and no regular medicine intake, illustrated significantly positive correlations with the measured anti-spike antibody levels (**Figure 1.2a** and **Figure 1.2b**).

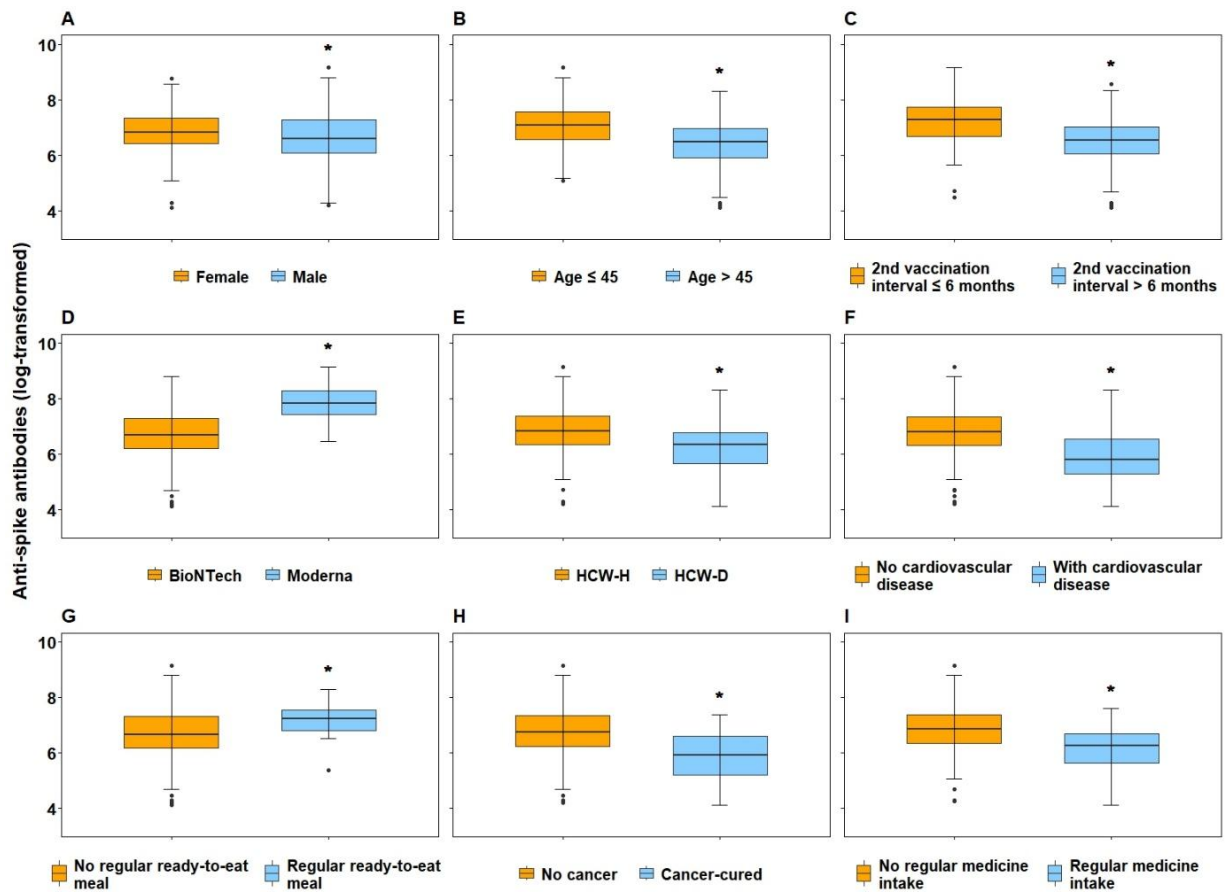


Figure 1.2a. Overview of the distribution of the log-transformed anti-spike antibody value among different groups.

(A) gender, (B) age group, (C) 2nd vaccination interval, (D) vaccine type for twice vaccination, (E) HCW group, (F) cardiovascular disease status, (G) ready-to-eat meal consumption, (H) cancer status, (I) medication intake. The line within the box means median. Box boundaries depict the interquartile range. Whiskers indicate outlier threshold (Lower one: 25 percentile – 1.5 * interquartile. Upper one: 75 percentile + 1.5 * interquartile). Independent t-test was employed to calculate the statistical significance of differences between each group pair. * $p < 0.05$.

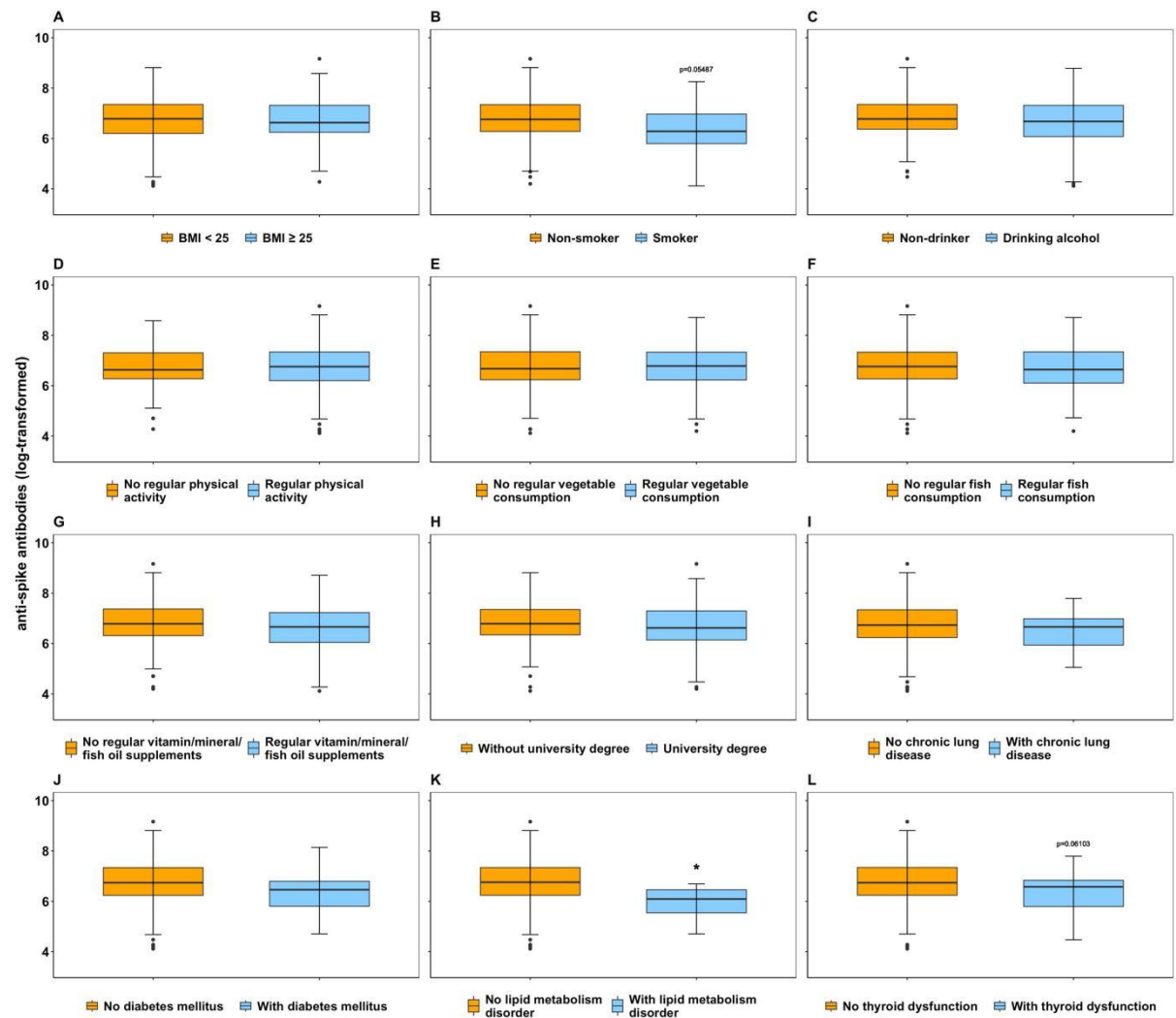


Figure 1.2b. Overview of the distribution of the log-transformed anti-spike antibody value among different groups.

(A) BMI, (B) smoking behavior, (C) alcohol consumption, (D) regular physical activity, (E) regular vegetable consumption, (F) regular fish consumption, (G) regular vitamins/minerals/fish oil supplements consumption, (H) education level, (I) chronic lung disease status, (J) diabetes mellitus status, (K) lipid metabolism disorder, (L) thyroid dysfunction. The line within the box means median. Box boundaries depict the interquartile range. Whiskers indicate outlier threshold (Lower one: 25 percentile – 1.5 * interquartile. Upper one: 75 percentile + 1.5 * interquartile). Independent t-test was employed to calculate the statistical significance of differences between each group pair. * $p < 0.05$.

After controlling the covariates from the main model, a significant trend was no longer found for regular ready-to-eat meal consumption ($p = 0.06$) and lipid metabolism disorder ($p = 0.1$), while $\text{BMI} \geq 25 \text{ kg/m}^2$ showed positive correlations with anti-spike antibody concentrations ($p < 0.01$). However, no apparent correlation was found between immune response and regular fish or vegetable intake, or vitamin/mineral/fish

oil supplementation as well as physical activity, education level and other reported diseases (**Figure 1.2b**).

1.3.3. Association between Metabolites and Anti-Spike Antibody Levels

In the main model, 18 metabolites from the acylcarnitine, phosphatidylcholine and sphingomyelin groups showed significant positive associations with anti-spike antibody concentrations (**Figure 1.3a**). In the extended model, 14 metabolites from the same metabolite groups showed significant positive associations with anti-spike antibody concentrations (**Figure 1.3a**). These significant metabolites among two models shared

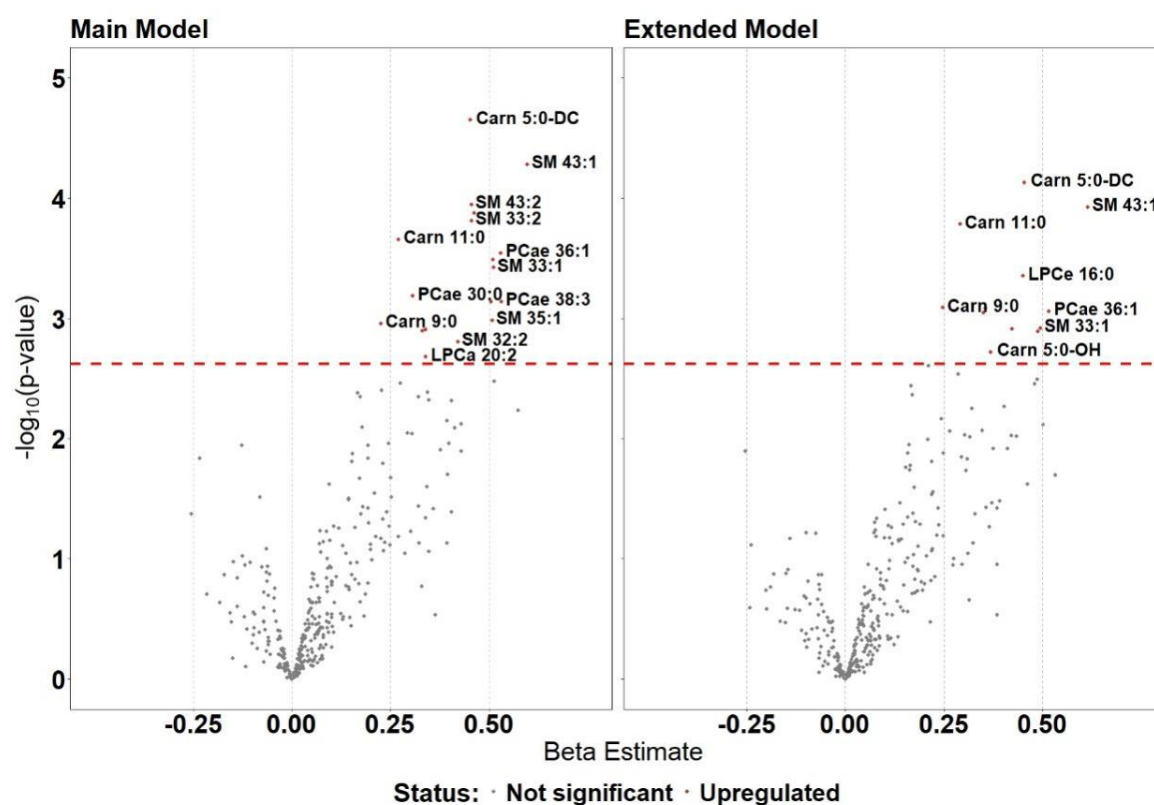


Figure 1.3a. Volcano plots presenting the associations between metabolites and anti-spike antibodies.

The Y axis indicates negative logarithm ($-\log_{10}$) of the p-value. The X axis represents the association between metabolites and anti-spike antibodies. The red dashed line shows adjusted statistical significance cut-off according to the Benjamini-Hochberg (FDR) method. Carn: acylcarnitine, PCae: acyl-alkyl phosphatidylcholine, LPCa: alkyl lysophosphatidylcholine, LPCe: acyl lysophosphatidylcholine, SM: alkyl sphingomyelin.

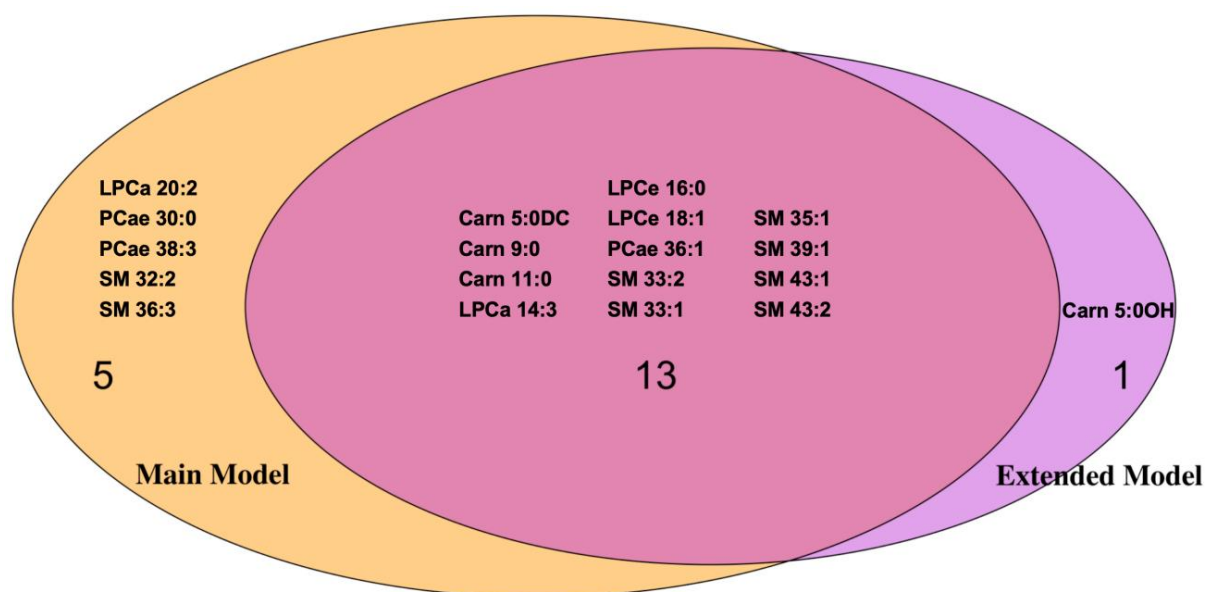


Figure 1.3b. Venn diagram showing intersection between significant metabolites from the main model (orange) and the extended model (purple).

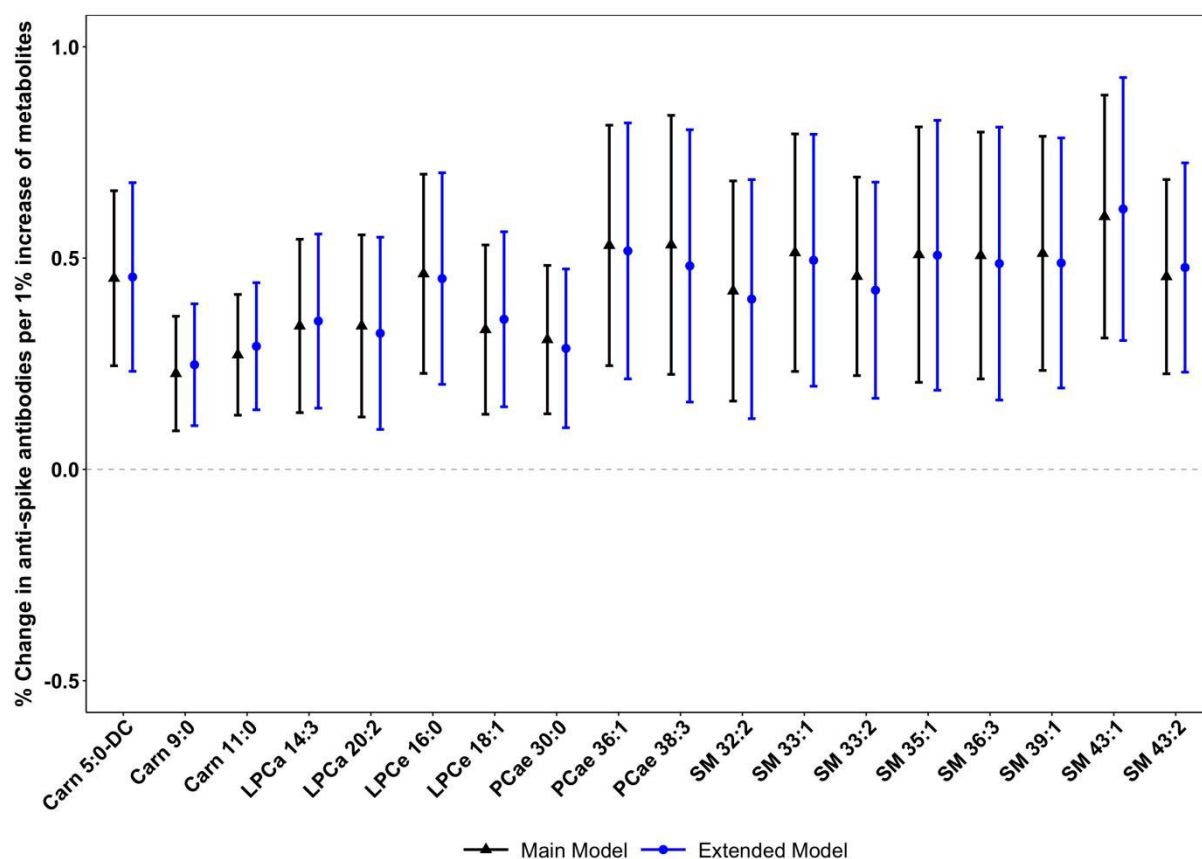


Figure 1.3c. 95% CIs for the comparison of percent changes in anti-spike antibodies per 1% increase of metabolite concentration between the results from main and extended models.

The triangle and dot mean Beta estimate for each compound from main and extended models respectively.

a big overlap (13 metabolites), indicating that the results are robust (**Figure 1.3b**). In addition, the vertical line chart of 18 metabolites in the main model also showed a similar positive trend in the extended model (**Figure 1.3c**).

1.3.4. Association between Metabolites and Live-virus Neutralization

The volcano plots clearly show that no metabolites were significantly correlated with the participants live-virus neutralization activity against SARS-CoV-2 variant Omicron BA.1 neither in the main nor in the extended model (**Figure 1.4a**). In addition, the vertical line chart of most of the 18 metabolites from the main model for anti-spike antibodies did not show a clear trend for neutralization activity using both models (**Figure 1.4b**).

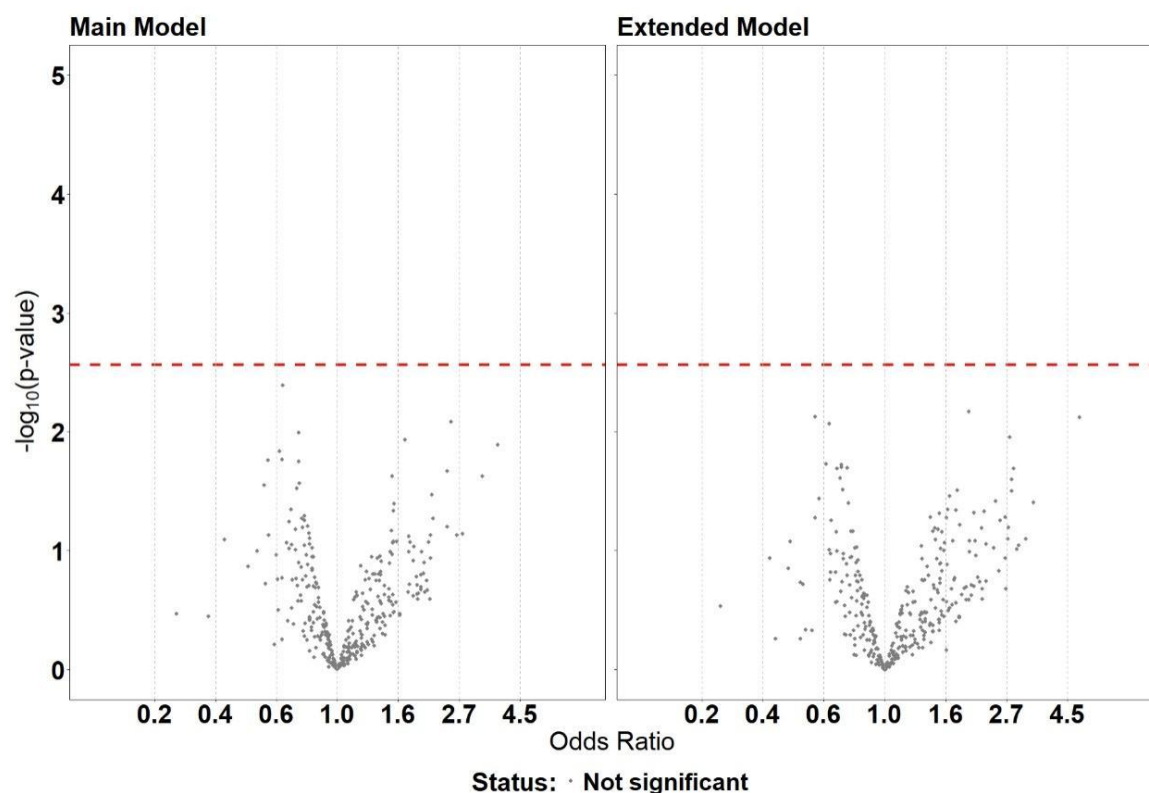


Figure 1.4a. Volcano plots presenting the associations between metabolites and neutralization activity.

The Y axis indicates negative logarithm ($-\log_{10}$) of the p-value. The X axis represents the association between metabolites and neutralization activity. The red dashed lines shows adjusted statistical significance cut-off according to the Benjamini-Hochberg (FDR) method.

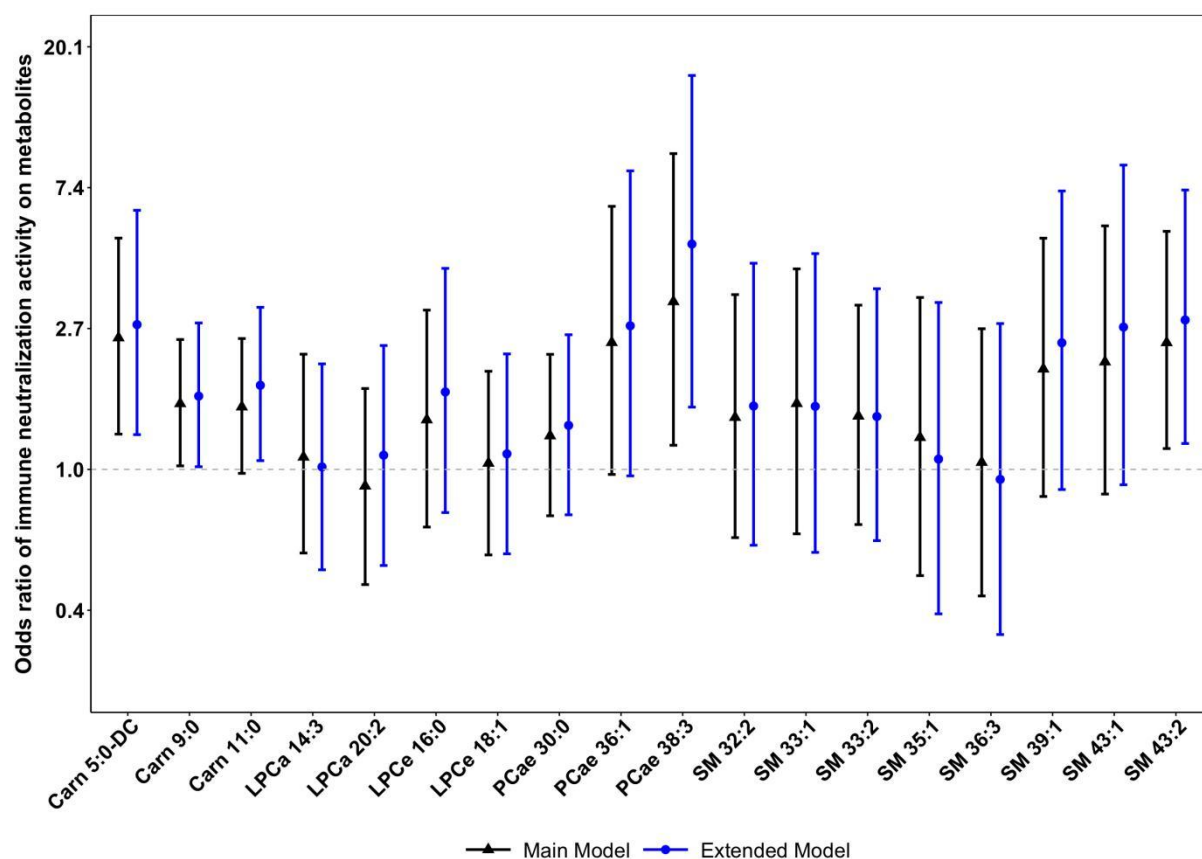


Figure 1.4b. 95% CIs for the comparison of odds ratio in of immune neutralization activity on metabolites between the results from main and extended models.

The triangle and dot mean Beta estimate for each compound from main and extended models respectively.

1.3.5. Relationship between Anti-Spike Antibody Titers and Live-virus

Neutralization Activity

The point-biserial correlation analysis demonstrated that anti-spike antibody titers were significantly correlated with neutralization activity ($\text{cor} = 0.615$, $p < 0.001$). The partial correlation analysis also showed a significant association between both immune response variables ($\text{cor} = 0.531$, $p < 0.001$).

1.3.6. Pathway Analysis

For pathway analysis, 18 metabolites from the main model, which were significantly associated with altered anti-spike antibody levels were uploaded to MetaboAnalyst 6.0, and three metabolic pathways were identified. Specifically, LPCa 20:2 and LPCa 14:3

were designated to the glycerophospholipid metabolism pathway ($p = 0.07$, impact value = 0.02), SM 32:2, SM 33:1, SM 33:2, SM 35:1, SM 36:3, SM 39:1, SM 43:1 and SM 43:2 were associated with the sphingolipid metabolism pathway ($p = 0.06$, impact value = 0), and PCae 30:0, PCae 36:1, PCae 38:3, LPCe 16:0, and LPCe 18:1 were related to the ether lipid metabolism pathway (p -value = 0.04, impact value = 0.08). However, they were found to be insignificant after using the FDR method for p -value correction (**Figure 1.5** and **Table 1.2**). According to the KEGG database, Carn 5:0-DC, Carn 9:0, and Carn 11:0 were not correlated.

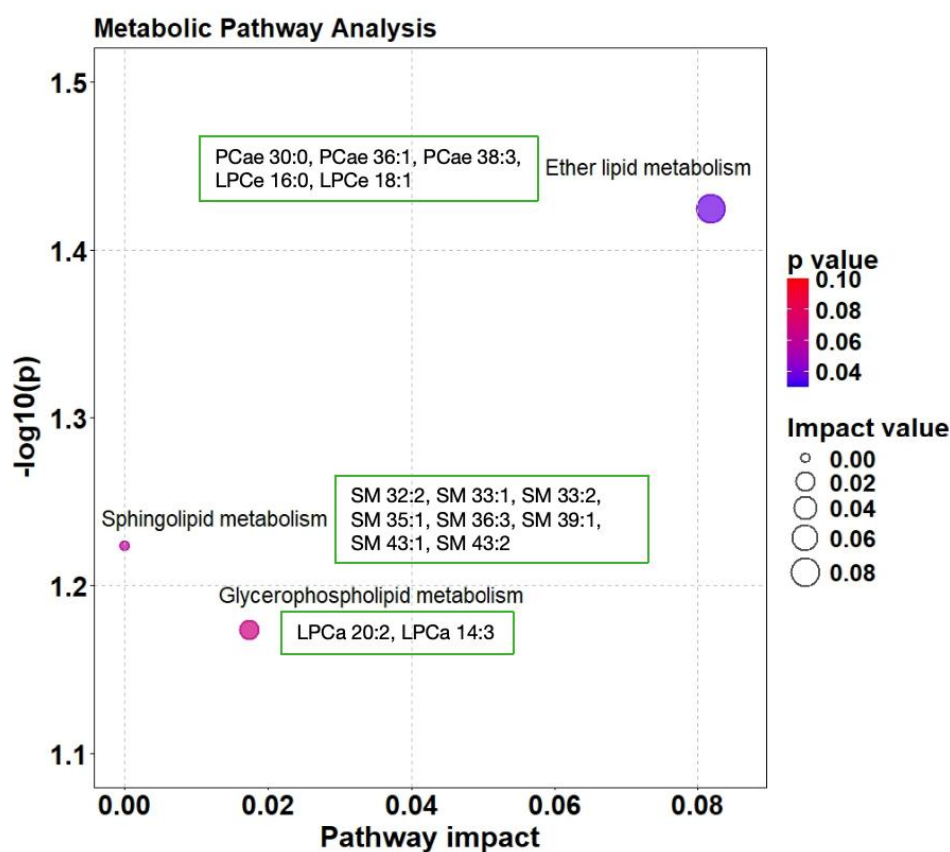


Figure 1.5. Metabolic pathways identified for the 18 significant metabolites from the main model.

The Y-axis shows the negative logarithm ($-\log_{10}$) of the p -value from the enrichment test, while the X-axis represents the structural impact of anti-spike antibodies related metabolites in the enriched pathways, determined by the cumulative importance of all significant metabolites within the pathway. The bubble size indicates the impact value, while the bubble colour reflects the enrichment significance. Pathways with a p -value ≤ 0.1 or an impact value > 0.5 (with p -value ≤ 0.3) were deemed most relevant, where the p -values were derived from enrichment analysis and the impact values were from topology analysis [58, 63].

Table 1.2. Metabolic pathways identified from pathway analysis that were related to anti-spike antibodies induced by mRNA COVID-19 vaccine.

	Total	Hits	<i>p</i> -value	FDR	Impact factor
Ether lipid metabolism	20	1	0.03763	1	0.08176
Sphingolipid metabolism	32	1	0.05976	1	0
Glycerophospholipid metabolism	36	1	0.06705	1	0.01736

Total refers to the number of metabolites within the pathway; while Hits indicates the matched count from uploaded data; The *p*-value is originally derived from enrichment analysis; and the FDR represents *p*-value adjusted using False Discovery Rate; The impact factor is the pathway impact value determined through pathway topology analysis.

1.3.7. Effect Modification

Effect modification analyses were conducted for the 18 metabolites, which were significantly associated with altered anti-spike antibody levels from the main model, while the continuous variable age, 2nd vaccination interval, and BMI were respectively replaced by their corresponding effect modifier, when analyzing effect modification for their corresponding categorical modifiers. Results presented in **Figure 1.6a** showed that the association between Carn 5:0-DC and anti-spike antibodies was significantly modified by smoking (FDR corrected $p < 0.05$). Participants who reported smoking behaviour showed stronger effects. Besides, elevated age (>45 years old), 2nd vaccination interval greater than 6 months, and regular vegetable consumption demonstrated higher modification between LPCa 20:2 and immune response (uncorrected $p < 0.05$). Similarly, higher modification on LPCe 16:0, LPCe 18:1, and PCae 36:1 was detected, when the interval between blood sampling and the 2nd vaccination was > 6 months. Regular physical activity also showed higher modification on PCae 36:1, while no alcohol consumption showed stronger modification on LPCe 18:1 (uncorrected $p < 0.05$). In addition, higher age showed stronger modification on PCae 38:3 and SM 39:1, and female gender also displayed higher modification on PCae 38:3 (uncorrected $p < 0.05$). Results also indicated the stronger modification with a university degree on SM 43:1 (uncorrected $p < 0.05$). No significant effect modification on the correlation between 18 metabolites and anti-spike antibody

concentrations from other categories was found, namely, BMI, vaccine type, HCW group, regular fish consumption, regular ready-to-eat food consumption, and regular vitamin/mineral/fish oil supplements (**Figure 1.6b**)

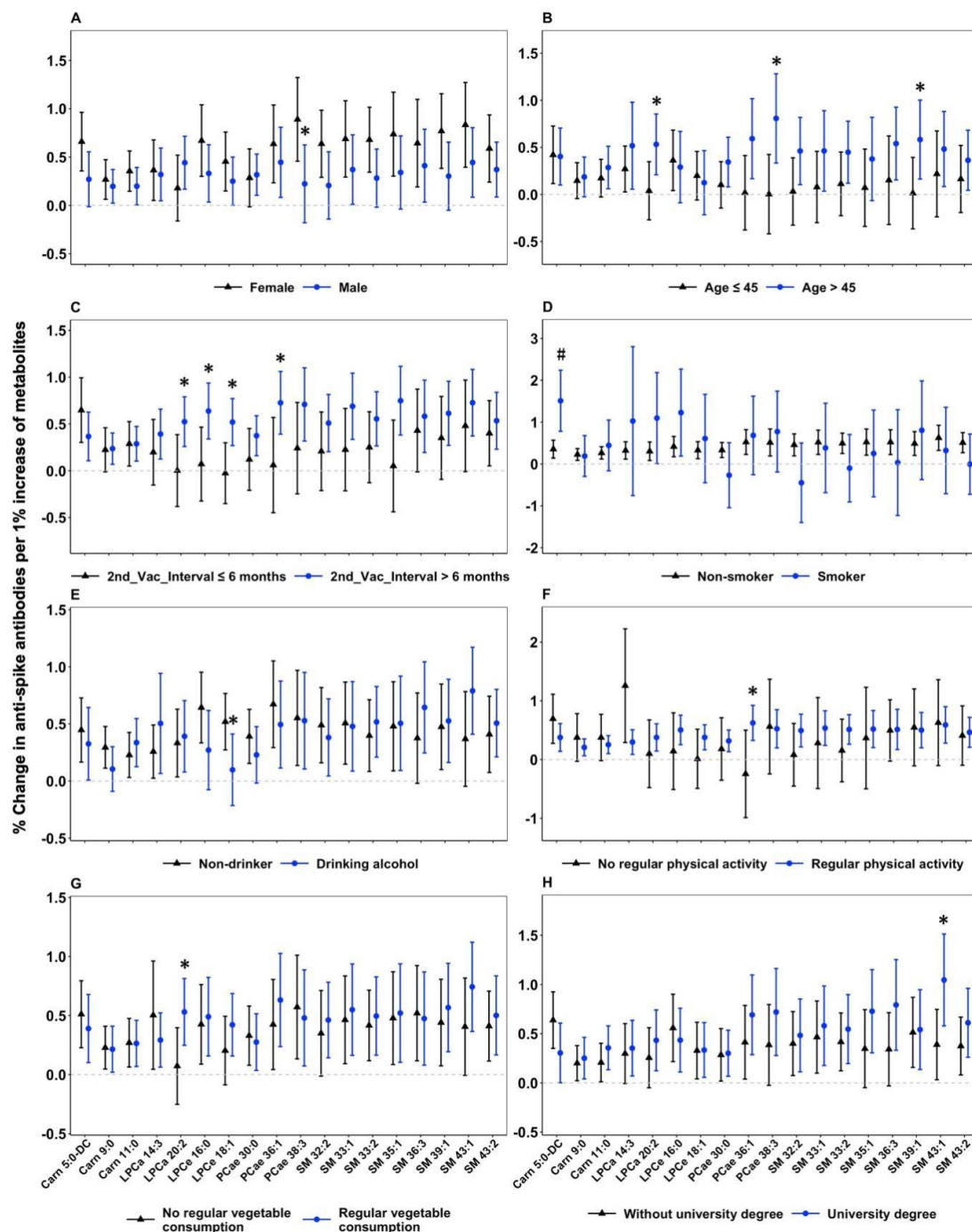


Figure 1.6a. 95% CIs for the comparison of percent changes in anti-spike antibodies per 1% increase of metabolite concentrations.

Metabolite concentrations were stratified by gender, age, 2nd vaccination interval, smoking behavior, physical activity, vegetable consumption, and education level. The triangle and dot mean Beta estimate for each compound from the main model. * $p < 0.05$, # FDR corrected $p < 0.05$.

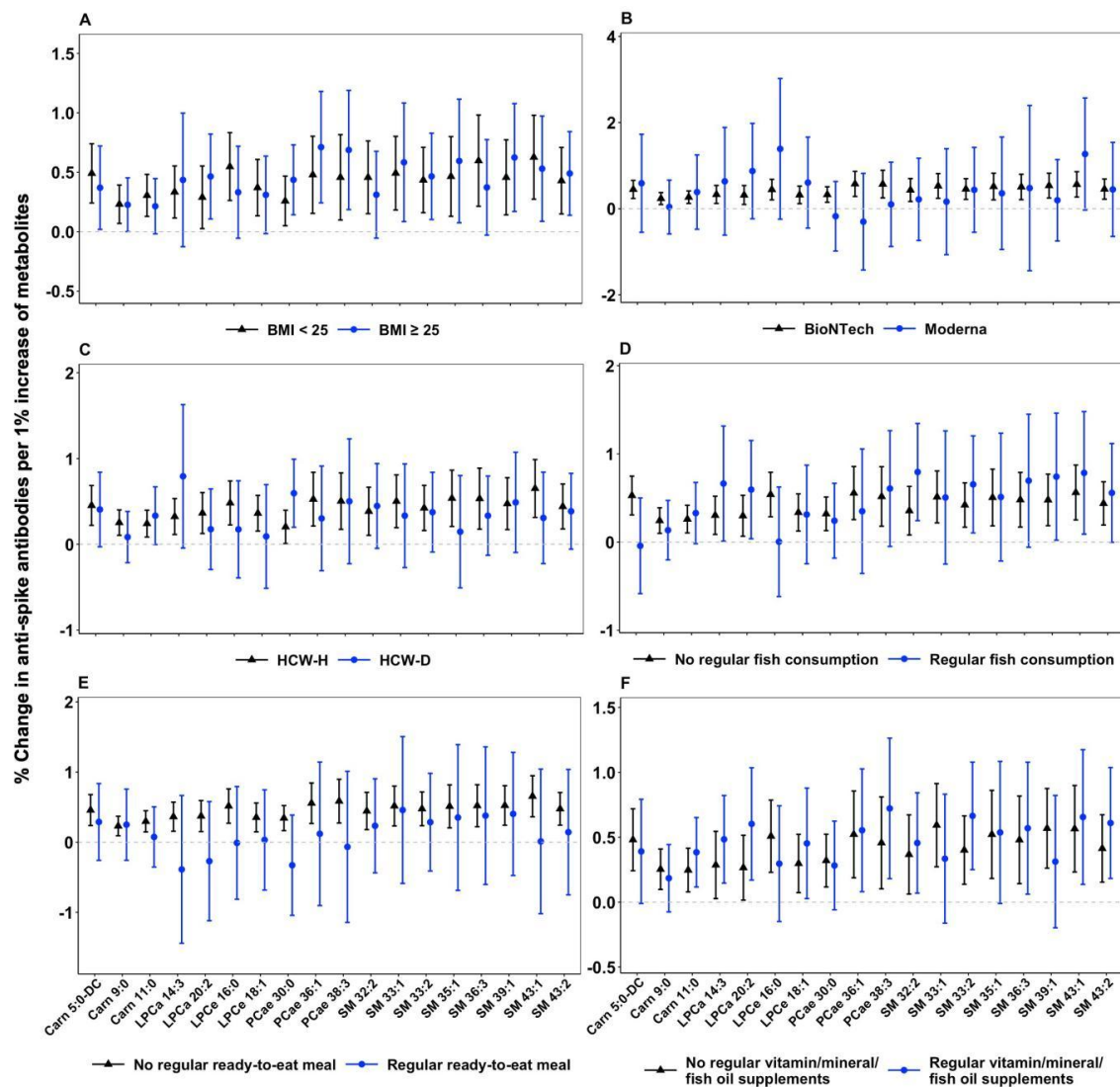


Figure 1.6b. 95% CIs for the comparison of percent changes in anti-spike antibodies per 1% increase of metabolite concentrations.

Metabolite concentrations were stratified by BMI, vaccine type, HCW, regular fish consumption, regular ready-to-eat food consumption and regular vitamins/minerals/fish oil supplements. The triangle and dot mean Beta estimate for each compound from main model.

1.3.8. Sensitivity Analyses

The associations between anti-spike antibody levels and the 18 significant metabolites, found from the main model for anti-spike antibodies analysis, generally remained consistent across various sensitivity analyses. When limiting the participants to HCW-H participants or the individuals who only received the BioNTech vaccine or additionally, excluding the participants with unknown information among the variables included by

the extended model, results shared notable Venn diagram overlaps (≥ 15) with original results from all participants (**Figure 1.7**).

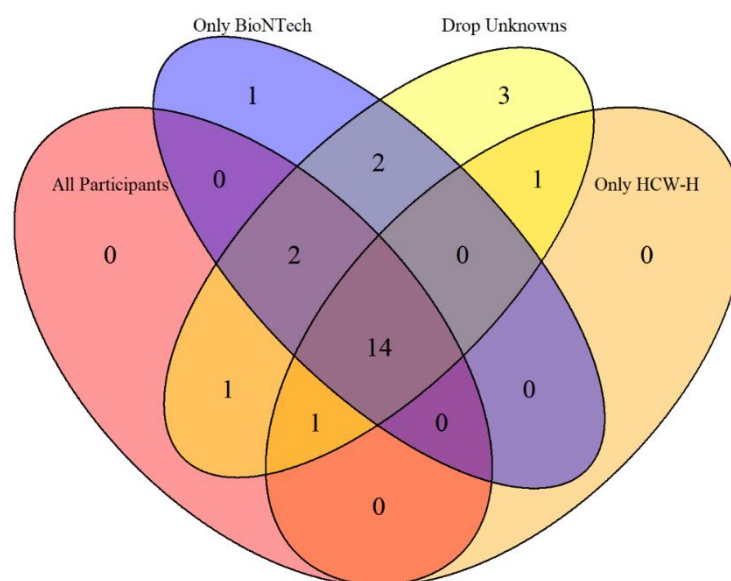


Figure 1.7. Venn diagram showing information and intersections among significant metabolites for different sample sizes.

4 different sample sizes: all participants, participants who were only vaccinated with the BioNTech vaccine, participants without unknown information among the variables included by the extended model, as well as only HCW-H individuals.

1.4. Discussion

This study investigated the relationship between humoral immune responses in healthcare workers post two doses of COVID-19 mRNA vaccine and participants' metabolic states, identifying 18 key metabolites, including 3 acylcarnitines (Carn 5:0-DC, Carn 9:0 and Carn 11:0), 2 LPCa (LPCa 20:2 and LPCa 14:3), 2 LPCe (LPCe 16:0 and LPCe 18:1), 3 PCae (PCae 30:0, PCae 36:1 and PCae 38:3) and 8 SMs (SM 32:2, SM 33:1, SM 33:2, SM 35:1, SM 36:3, SM 39:1, SM 43:1 and SM 43:2), positively associated with variations of spike-specific anti-SARS-CoV-2 antibodies, along with pertinent metabolic pathways relevant to COVID-19 vaccination and vaccine-induced immunity. The identified potential biomarkers hold promise for predicting humoral immunity to COVID-19 and may grant insight into underlying mechanisms influencing

antibody concentrations. Our study also indicated that older age, female gender, second vaccine dose interval, smoking, non-alcohol consumption, and university education were associated with stronger metabolic responses than their counterparts. In addition, after restricting our study to healthy participants, those who received only the BioNTech vaccine, and participants with completely valid information for the factors in our extended model, the substantial overlap of significant metabolites with the original results indicated the robustness of our findings.

Vaccines represent the primary defence against future infections or severe symptoms upon exposure. Live-virus neutralization activities measured in serum specimens are a strong predictor for protection against severe COVID-19 in vaccinated and/or convalescent individuals [13, 64, 65]. Moreover, these neutralization activities often positively correlate with the individual's anti-spike antibody concentration, as reported in several studies [64, 66, 67]. In our results, analysis of anti-spike antibody concentrations across different groups revealed significant positive associations with several epidemiological and lifestyle-dependent factors. After accounting for covariates in our main model, these associations generally persisted, while BMI ≥ 25 kg/m² exhibited a positive correlation with anti-spike antibody levels ($p < 0.01$). These findings align with prior investigations [19, 68, 69], while one clinical study noted lower levels of anti-spike antibodies and neutralization activity among individuals with severe obesity (BMI > 40 kg/m²), vaccinated with BioNTech or AstraZeneca COVID-19 vaccines, compared to those with normal BMI [70]. Notably, we did not identify any metabolites that were significantly correlated with live-virus neutralization activity, possibly due to the limited selected sample size (412 out of over 4000) being analysed. We found, however, a strong positive association of neutralization activity with anti-spike antibody levels before and after adjusting for covariates in the main model was consistent with other reports [15, 71, 72].

Three acylcarnitines (Carn 5:0-DC, Carn 9:0, and Carn 11:0) were identified in this study, whereas the relationship between acylcarnitines and immune response induced by vaccines has received very limited attention in previous research. It is worth noting that recent findings in sepsis non-survivors imply a role of elevated long- and medium-chain acylcarnitines in immune cell proinflammatory activation through cytokines such as interleukin-6 and interleukin-4, which can facilitate immune response by enhancing antibody production [73-75]. This activation process might account for the metabolism of enhancing humoral immune response associated with the three acylcarnitine compounds showed in our results.

Canonically, lysophosphatidylcholine (LPC) is produced from phosphatidylcholine (PC) by the hydrolyzation of Phospholipase A2 (PLA2), which in turn mediates cell signalling pathways in macrophages and T cells, and thus plays a role in the inflammatory response [76, 77]. PCs and LPCs also function as reservoirs and transporters of glycerophospholipid components, regulating homeostatic and inflammatory processes. Increased LPC and PLA2, along with decreased PCs can indicate disturbances in glycerophospholipid metabolism and elevated PC turnover for the production of both pro- and anti-inflammatory mediators [78, 79]. PCs are important for generating germinal center-derived B cells and antibody-secreting cells, with the latter having a higher demand for PCs [80]. Long et al. discovered elevated plasma PCaa 36:0, PCaa 34:4, PCae 40:4 and PCae 42:5 as reliable biomarkers distinguishing tuberculosis (TB) patients from healthy controls and those with latent infection. Their analysis revealed significant alterations in ether lipid and linolenic acid metabolism pathways, alongside changes in immune response signaling pathways, highlighting the role of lipid-related gene enrichment in TB pathology [81]. Another study revealed elevated plasma PC level, while decreased plasma lysoplasmenylcholine (LPC-P) level in septic patients, plasma plasmenylcholine (PC-P) and LPC-P were decreased in septic rats, and plasma PC-P was also decreased in SARS-CoV-2 infected mice [44]. Elevated PC level had also been reported to correlate with higher antibody level following influenza

vaccine [36]. This study proposed that increase of certain plasma PCae, LPCa and LPCe compounds has the potential to improve immune response following COVID-19 vaccination. The underlying mechanism may involve modulation of post-transcriptional mechanisms by PCs for driving the differentiation of naïve T cells to T follicular helper cells, which can further enhance the humoral immunity post vaccine [82].

The downstream metabolites of sphingomyelins (SMs), including ceramides and sphingosine-1-phosphate (S1P), play critical roles in immune cell development, proliferation, and signalling [83-85]. Reduced sphingomyelin levels in circulating lipoproteins of COVID-19 patients compared to healthy controls were reported [84]. Our study found significant positive association between 8 novel SMs and anti-spike antibody concentration, which might be indirectly mediated by the downstream sphingolipids of SMs through regulating neutrophil phagocytosis, differentiation of Th1 and Th2 T cells, and T cell apoptosis [86].

Pathway analysis showed that the significant metabolites were related to glycerophospholipid, sphingolipid, and ether lipid metabolism pathways, consistent with one similar research that investigated metabolic correlates of the antibody response in recipients of the inactivated COVID-19 vaccine and identified sphingolipid metabolism via pathway analysis [87]. Additionally, early administration of the Bacille Calmette–Guérin (BCG) vaccine in newborns is associated with metabolic changes, notably in sphingolipid production, including N-acylsphingosine, sphingomyelin, glucosylceramide and S1P, as well as PCs and LPCs, indicating a significant enrichment in sphingolipid and glycerophospholipid metabolism pathways [88, 89]. Interestingly, one study demonstrated perturbations in the same three metabolic pathways as our findings in plasma samples from COVID-19 patients and noted that modifying the metabolite profile by inhibiting the phosphatidate-phosphatase-1 (PAP-1) enzyme could suppress SARS-CoV-2 replication [90].

There are some limitations of our study. Study participants were not required to fast (≥ 8 hours) before donating blood samples, and we did not collect food intake information at the time of sampling, preventing us from assessing potential changes in results based on dietary intake on the sample collection day [91, 92]. The included sample size ($n = 363$) was informative, but did not allow detailed sub-group analysis, for example only 15 participants received the Moderna vaccine, 12 had diabetes and seven participants had chronic lung disease. Our sample selection criteria are inappropriate, resulting in the selected group ($n = 412$) and the final group after data cleaning ($n = 363$) being unrepresentative of the total population ($n > 4000$). Although the multivariate regression analysis we performed could help mitigate the issue of a non-representative subsample, bias stemming from unmeasured or excluded variables persists and could benefit from more reasonable future sampling and further analysis [93]. We used a flow-injection-analysis (FIA) method for the quantitative analysis of lipid metabolites, which offers high throughput and speed, but lacks detailed structural information such as fatty acid position, fatty acid chain length distribution, double bond position and branched chain identification. Compared to untargeted metabolomics analysis, our targeted metabolomics method could avoid misleading false annotation for metabolites, while limiting the discovery of additional biomarkers which are not included in the targeted method and does not completely capture the entire metabolome.

To date, only one study has examined the metabolite profile related to immune response triggered by mRNA-type vaccine, as opposed to inactivated vaccine against SARS-CoV-2 [41]. Our study comparatively investigated bigger sample size and covered broader range of metabolites, especially within the group of lipids. The expanded scope is more likely to offer new insights into potential biomarkers for enhancing vaccine efficacy. Given that analogues of bioactive sphingolipids are being utilized to treat immune disorders and daily oral L-carnitine supplementation has been shown to mitigate the organ lesion among COVID-19 patients, the 18 discriminative

metabolites identified in this study are worth considering as promising candidates to develop specific therapeutic supplements for enhancing immune response after receiving mRNA vaccines [83, 93].

1.5. Conclusions

Our study provides novel insights into the metabolic characteristics linked to the humoral immune response elicited by the BioNTech and Moderna mRNA COVID-19 vaccines, particularly focusing on sphingomyelins, ether PCs, (ether) lysoPCs, and acylcarnitines. The observed metabolic alterations suggest that an enhanced immune response is likely mediated by changes in the profiles of elevated concentrations of these key metabolites, while the precise mechanisms underlying these associations remain unclear and warrant further investigation. These findings offer potential modifiable target metabolite candidates, which hold the promise to adjust immune response post mRNA vaccination in clinical practice. The results from this sub-cohort, especially the association between metabolites and live-virus neutralization activity, will be further confirmed and explored in the whole cohort later.

1.6. References

- [1] A.e. Gorbalenya, S.C. baker, R.S. baric, R.J.d. Groot, C. Drosten, A.A. Gulyaeva, B.I. Haagmans, C. lauber, A.M. leontovich, B.W. Neuman, D. Penzar, S. Perlman, L.I.M. Poon, D.V. Samborskiy, I.A. Sidorov, I. Sola, J. Ziebuhr, The species Severe acute respiratory syndrome-related coronavirus: classifying 2019-nCoV and naming it SARS-CoV-2, *Nature microbiology* 5(4) (2020) 536-544. <https://doi.org/10.1038/s41564-020-0695-z>.
- [2] S. Bokaie, S. Daneshi, A. Bahonar, A. Haghdooost, E. Barfar, D. Patrick Moran, Estimating the disability adjusted life years associated with COVID-19 in Iran for the first 2 years of the pandemic, *Front Public Health* 11 (2023) 1303549. <https://doi.org/10.3389/fpubh.2023.1303549>.

- [3] M. Ghafari, M. Hall, T. Golubchik, D. Ayoubkhani, T. House, G. MacIntyre-Cockett, H.R. Fryer, L. Thomson, A. Nurtay, S.A. Kemp, L. Ferretti, D. Buck, A. Green, A. Trebes, P. Piazza, L.J. Lonie, R. Studley, E. Rourke, D.L. Smith, M. Bashton, A. Nelson, M. Crown, C. McCann, G.R. Young, R. Santos, Z. Richards, M.A. Tariq, R. Cahuantzi, J. Barrett, C. Fraser, D. Bonsall, A.S. Walker, K. Lythgoe, Prevalence of persistent SARS-CoV-2 in a large community surveillance study, *Nature* 626(8001) (2024) 1094-1101. <https://doi.org/10.1038/s41586-024-07029-4>.
- [4] D. Wang, B. Hu, C. Hu, F. Zhu, X. Liu, J. Zhang, B. Wang, H. Xiang, Z. Cheng, Y. Xiong, Y. Zhao, Y. Li, X. Wang, Z. Peng, Clinical Characteristics of 138 Hospitalized Patients With 2019 Novel Coronavirus-Infected Pneumonia in Wuhan, China, *Jama* 323(11) (2020) 1061-1069. <https://doi.org/10.1001/jama.2020.1585>.
- [5] C. Huang, Y. Wang, X. Li, L. Ren, J. Zhao, Y. Hu, L. Zhang, G. Fan, J. Xu, X. Gu, Z. Cheng, T. Yu, J. Xia, Y. Wei, W. Wu, X. Xie, W. Yin, H. Li, M. Liu, Y. Xiao, H. Gao, L. Guo, J. Xie, G. Wang, R. Jiang, Z. Gao, Q. Jin, J. Wang, B. Cao, Clinical features of patients infected with 2019 novel coronavirus in Wuhan, China, *Lancet* 395(10223) (2020) 497-506. [https://doi.org/10.1016/S0140-6736\(20\)30183-5](https://doi.org/10.1016/S0140-6736(20)30183-5).
- [6] S. Richardson, J.S. Hirsch, M. Narasimhan, J.M. Crawford, T. McGinn, K.W. Davidson, C.-R.C. the Northwell, D.P. Barnaby, L.B. Becker, J.D. Chelico, S.L. Cohen, J. Cookingham, K. Coppa, M.A. Diefenbach, A.J. Dominello, J. Duer-Hefe, L. Falzon, J. Gitlin, N. Hajizadeh, T.G. Harvin, D.A. Hirschwerk, E.J. Kim, Z.M. Kozel, L.M. Marrast, J.N. Mogavero, G.A. Osorio, M. Qiu, T.P. Zanos, Presenting Characteristics, Comorbidities, and Outcomes Among 5700 Patients Hospitalized With COVID-19 in the New York City Area, *Jama* 323(20) (2020) 2052-2059. <https://doi.org/10.1001/jama.2020.6775>.
- [7] WHO, Coronavirus (COVID-19), 2025. <https://covid19.who.int/>. (Accessed 05th August 2025).
- [8] A.M. Carabelli, T.P. Peacock, L.G. Thorne, W.T. Harvey, J. Hughes, S.J. Peacock, W.S. Barclay, T.I. de Silva, G.J. Towers, D.L. Robertson, SARS-CoV-2 variant biology: immune escape, transmission and fitness, *Nat Rev Microbiol* 21(3) (2023) 162-177. <https://doi.org/10.1038/s41579-022-00841-7>.
- [9] K. Gangavarapu, A.A. Latif, J.L. Mullen, M. Alkuzweny, E. Hufbauer, G. Tsueng, E. Haag, M. Zeller, C.M. Aceves, K. Zaiets, M. Cano, X. Zhou, Z. Qian, R. Sattler, N.L.

- Matteson, J.I. Levy, R.T.C. Lee, L. Freitas, S. Maurer-Stroh, M.A. Suchard, C. Wu, A.I. Su, K.G. Andersen, L.D. Hughes, Outbreak.info genomic reports: scalable and dynamic surveillance of SARS-CoV-2 variants and mutations, *Nat Methods* 20(4) (2023) 512-522. <https://doi.org/10.1038/s41592-023-01769-3>.
- [10] T. Tamura, K. Mizuma, H. Nasser, S. Deguchi, M. Padilla-Blanco, Y. Oda, K. Uriu, J.E.M. Tolentino, S. Tsujino, R. Suzuki, I. Kojima, N. Nao, R. Shimizu, L. Wang, M. Tsuda, M. Jonathan, Y. Kosugi, Z. Guo, A.A. Hinay, Jr., O. Putri, Y. Kim, Y.L. Tanaka, H. Asakura, M. Nagashima, K. Sadamasu, K. Yoshimura, C. Genotype to Phenotype Japan, A. Saito, J. Ito, T. Irie, S. Tanaka, J. Zahradnik, T. Ikeda, K. Takayama, K. Matsuno, T. Fukuhara, K. Sato, Virological characteristics of the SARS-CoV-2 BA.2.86 variant, *Cell Host Microbe* 32(2) (2024) 170-180 e12. <https://doi.org/10.1016/j.chom.2024.01.001>.
- [11] R. Rubin, As COVID-19 Cases Surge, Here's What to Know About JN.1, the Latest SARS-CoV-2 "Variant of Interest", *Jama* 331(5) (2024) 382-383. <https://doi.org/10.1001/jama.2023.27841>.
- [12] A. Esmaeilzadeh, F. Ebrahimi, A. Jahani Maleki, A. Siahmansouri, EG.5 (Eris) and BA.2.86 (Pirola) two new subvariants of SARS-CoV-2: a new face of old COVID-19, *Infection* 52(2) (2024) 337-343. <https://doi.org/10.1007/s15010-023-02146-0>.
- [13] D.S. Khoury, D. Cromer, A. Reynaldi, T.E. Schlub, A.K. Wheatley, J.A. Juno, K. Subbarao, S.J. Kent, J.A. Triccas, M.P. Davenport, Neutralizing antibody levels are highly predictive of immune protection from symptomatic SARS-CoV-2 infection, *Nat Med* 27 (2021) 1205-1211. <https://doi.org/10.1038/s41591-021-01377-8>.
- [14] A. Wajnberg, F. Amanat, A. Firpo, D.R. Altman, M.J. Bailey, M. Mansour, M. McMahon, P. Meade, D.R. Mendu, K. Muellers, D. Stadlbauer, K. Stone, S. Strohmeier, V. Simon, J. Aberg, D.L. Reich, F. Krammer, C. Cordon-Cardo, Robust neutralizing antibodies to SARS-CoV-2 infection persist for months, *Science* 370(6521) (2020) 1227-1230. <https://doi.org/10.1126/science.abd7728>.
- [15] N. Lin, H. Fu, D. Pu, Y. Quan, Y. Li, X. Yin, Y. Wei, H. Wang, X. Ma, X. Wei, Criteria for judging the immune markers of COVID-19 disease vaccines, *MedComm* 3(1) (2022) 1-12. <https://doi.org/10.1002/mco2.109>.
- [16] W.F. Garcia-Beltran, E.C. Lam, M.G. Astudillo, D. Yang, T.E. Miller, J. Feldman, B.M. Hauser, T.M. Caradonna, K.L. Clayton, A.D. Nitido, M.R. Murali, G. Alter, R.C.

Charles, A. Dighe, J.A. Branda, J.K. Lennerz, D. Lingwood, A.G. Schmidt, A.J. Iafrate, A.B. Balazs, COVID-19-neutralizing antibodies predict disease severity and survival, *Cell* 184(2) (2021) 476-488 e11. <https://doi.org/10.1016/j.cell.2020.12.015>.

[17] J. Wei, P.C. Matthews, N. Stoesser, T. Maddox, L. Lorenzi, R. Studley, J.I. Bell, J.N. Newton, J. Farrar, I. Diamond, E. Rourke, A. Howarth, B.D. Marsden, S. Hoosdally, E.Y. Jones, D.I. Stuart, D.W. Crook, T.E.A. Peto, K.B. Pouwels, A.S. Walker, D.W. Eyre, T. Thomas, D. Cook, D. Ayoubkhani, R. Black, A. Felton, M. Crees, J. Jones, L. Lloyd, E. Sutherland, E. Pritchard, K.-D. Vihta, G. Doherty, J. Kavanagh, K.K. Chau, S.B. Hatch, D. Ebner, L.M. Ferreira, T. Christott, W. Dejnirattisai, J. Mongkolsapaya, S. Cameron, P. Tamblin-Hopper, M. Wolna, R. Brown, R. Cornall, G. Screaton, K. Lythgoe, D. Bonsall, T. Golubchik, H. Fryer, S. Cox, K. Paddon, T. James, T. House, J. Robotham, P. Birrell, H. Jordan, T. Sheppard, G. Athey, D. Moody, L. Curry, P. Brereton, I. Jarvis, A. Godsmark, G. Morris, B. Mallick, P. Eeles, J. Hay, H. VanSteenhouse, J. Lee, S. White, T. Evans, L. Bloembergen, K. Allison, A. Pandya, S. Davis, D.I. Conway, M. MacLeod, C. Cunningham, C.-I.S.t. the, Anti-spike antibody response to natural SARS-CoV-2 infection in the general population, *Nature Communications* 12(1) (2021) 6250. <https://doi.org/10.1038/s41467-021-26479-2>.

[18] M. Nakai, D. Yokoyama, T. Sato, R. Sato, C. Kojima, T. Shimosawa, Variation in antibody titers determined by Abbott and Roche Elecsys SARS-CoV-2 assays in vaccinated healthcare workers, *Heliyon* 9(6) (2023) e16547. <https://doi.org/10.1016/j.heliyon.2023.e16547>.

[19] X. Ren, W. Wen, X. Fan, W. Hou, B. Su, P. Cai, J. Li, Y. Liu, F. Tang, F. Zhang, Y. Yang, J. He, W. Ma, J. He, P. Wang, Q. Cao, F. Chen, Y. Chen, X. Cheng, G. Deng, X. Deng, W. Ding, Y. Feng, R. Gan, C. Guo, W. Guo, S. He, C. Jiang, J. Liang, Y.M. Li, J. Lin, Y. Ling, H. Liu, J. Liu, N. Liu, S.Q. Liu, M. Luo, Q. Ma, Q. Song, W. Sun, G. Wang, F. Wang, Y. Wang, X. Wen, Q. Wu, G. Xu, X. Xie, X. Xiong, X. Xing, H. Xu, C. Yin, D. Yu, K. Yu, J. Yuan, B. Zhang, P. Zhang, T. Zhang, J. Zhao, P. Zhao, J. Zhou, W. Zhou, S. Zhong, X. Zhong, S. Zhang, L. Zhu, P. Zhu, B. Zou, J. Zou, Z. Zuo, F. Bai, X. Huang, P. Zhou, Q. Jiang, Z. Huang, J.X. Bei, L. Wei, X.W. Bian, X. Liu, T. Cheng, X. Li, P. Zhao, F.S. Wang, H. Wang, B. Su, Z. Zhang, K. Qu, X. Wang, J. Chen, R. Jin, Z. Zhang, COVID-19 immune features revealed by a large-scale single-cell transcriptome atlas, *Cell* 184(7) (2021) 1895-1913.e19. <https://doi.org/10.1016/j.cell.2021.01.053>.

- [20] M. Rizzi, S. Tonello, C. Brinno, E. Zecca, E. Matino, M. Cittone, E. Rizzi, G.F. Casciaro, D. D'Onghia, D. Colangelo, R. Minisini, M. Bellan, L.M. Castello, A. Chiocchetti, M. Pirisi, C. Rigamonti, D. Lilleri, F. Zavaglio, F. Bergami, D. Sola, P.P. Sainaghi, SARS-CoV-2 infection risk is higher in vaccinated patients with inflammatory autoimmune diseases or liver transplantation treated with mycophenolate due to an impaired antiviral immune response: results of the extended follow up of the RIVALSA prospective cohort, *Front Immunol* 14 (2023) 1185278. <https://doi.org/10.3389/fimmu.2023.1185278>.
- [21] B. Yuan, W. Li, H. Liu, X. Cai, S. Song, J. Zhao, X. Hu, Z. Li, Y. Chen, K. Zhang, Z. Liu, J. Peng, C. Wang, J. Wang, Y. An, Correlation between immune response and self-reported depression during convalescence from COVID-19, *Brain, behavior, and immunity* 88 (2020) 39-43. <https://doi.org/10.1016/j.bbi.2020.05.062>.
- [22] C.E. Murray, C. O'Brien, S. Alamin, S.H. Phelan, R. Argue, R. Kiersey, M. Gardiner, A. Naughton, E. Keogh, P. Holmes, S. Naughton, A. Scanlon, A. Sloan, P. McCrea, J. Sui, J. Dunne, N. Conlon, Cellular and humoral immunogenicity of the COVID-19 vaccine and COVID-19 disease severity in individuals with immunodeficiency, *Front Immunol* 14 (2023) 1131604. <https://doi.org/10.3389/fimmu.2023.1131604>.
- [23] I. Owsianka, A. Pac, E. Jachowicz, K. Gutkowska, W. Szczuciński, B. Maziarz, E. Sochacka-Tatara, P. Heczko, W. Sydor, B. Żółtowska, J. Wójkowska-Mach, SARS-CoV-2 antibody response after mRNA vaccination in healthcare workers with and without previous COVID-19, a follow-up study from a university hospital in Poland during 6 months 2021, *Front Immunol* 13 (2022) 1071204. <https://doi.org/10.3389/fimmu.2022.1071204>.
- [24] C.H. Johnson, J. Ivanisevic, G. Siuzdak, Metabolomics: beyond biomarkers and towards mechanisms, *Nat Rev Mol Cell Biol* 17(7) (2016) 451-459. <https://doi.org/10.1038/nrm.2016.25>.
- [25] T. Baumruker, F. Bornancin, A. Billich, The role of sphingosine and ceramide kinases in inflammatory responses, *Immunology letters* 96(2) (2005) 175-185. <https://doi.org/10.1016/j.imlet.2004.09.001>.
- [26] G. Di Paolo, P. De Camilli, Phosphoinositides in cell regulation and membrane dynamics, *Nature* 443(7112) (2006) 651-657. <https://doi.org/10.1038/nature05185>.

- [27] D.R. Schmidt, R. Patel, D.G. Kirsch, C.A. Lewis, M.G. Vander Heiden, J.W. Locasale, Metabolomics in cancer research and emerging applications in clinical oncology, *CA Cancer J Clin* 71(4) (2021) 333-358. <https://doi.org/10.3322/caac.21670>.
- [28] M. Masoodi, A. Gastaldelli, T. Hyötyläinen, E. Arretxe, C. Alonso, M. Gaggini, J. Brosnan, Q.M. Anstee, O. Millet, P. Ortiz, J.M. Mato, J.F. Dufour, M. Orešič, Metabolomics and lipidomics in NAFLD: biomarkers and non-invasive diagnostic tests, *Nat Rev Gastroenterol Hepatol* 18(12) (2021) 835-856. <https://doi.org/10.1038/s41575-021-00502-9>.
- [29] X. Han, Lipidomics for studying metabolism, *Nature reviews. Endocrinology* 12(11) (2016) 668-679. <https://doi.org/10.1038/nrendo.2016.98>.
- [30] V. Barili, C. Boni, M. Rossi, A. Vecchi, A. Zecca, A. Penna, G. Missale, C. Ferrari, P. Fisicaro, Metabolic regulation of the HBV-specific T cell function, *Antiviral Res* 185 (2021) 104989. <https://doi.org/10.1016/j.antiviral.2020.104989>.
- [31] A.M. Kabat, E.L. Pearce, E.J. Pearce, Metabolism in type 2 immune responses, *Immunity* 56(4) (2023) 723-741. <https://doi.org/10.1016/j.immuni.2023.03.007>.
- [32] R.J. Arts, B. Novakovic, R. Ter Horst, A. Carvalho, S. Bekkering, E. Lachmandas, F. Rodrigues, R. Silvestre, S.C. Cheng, S.Y. Wang, E. Habibi, L.G. Gonçalves, I. Mesquita, C. Cunha, A. van Laarhoven, F.L. van de Veerdonk, D.L. Williams, J.W. van der Meer, C. Logie, L.A. O'Neill, C.A. Dinarello, N.P. Riksen, R. van Crevel, C. Clish, R.A. Notebaart, L.A. Joosten, H.G. Stunnenberg, R.J. Xavier, M.G. Netea, Glutaminolysis and Fumarate Accumulation Integrate Immunometabolic and Epigenetic Programs in Trained Immunity, *Cell Metab* 24(6) (2016) 807-819. <https://doi.org/10.1016/j.cmet.2016.10.008>.
- [33] C. Bruzzzone, M. Bizkarguenaga, R. Gil-Redondo, T. Diercks, E. Arana, A. Garcia de Vicuna, M. Seco, A. Bosch, A. Palazon, I. San Juan, A. Lain, J. Gil-Martinez, G. Bernardo-Seisdedos, D. Fernandez-Ramos, F. Lopitz-Otsoa, N. Embade, S. Lu, J.M. Mato, O. Millet, SARS-CoV-2 Infection Dysregulates the Metabolomic and Lipidomic Profiles of Serum, *iScience* 23(10) (2020) 101645. <https://doi.org/10.1016/j.isci.2020.101645>.
- [34] D. Wu, T. Shu, X. Yang, J.-X. Song, M. Zhang, C. Yao, W. Liu, M. Huang, Y. Yu, Q. Yang, T. Zhu, J. Xu, J. Mu, Y. Wang, H. Wang, T. Tang, Y. Ren, Y. Wu, S.-H. Lin, Y. Qiu, D.-Y. Zhang, Y. Shang, X. Zhou, Plasma metabolomic and lipidomic alterations

associated with COVID-19, *National Science Review* 7(7) (2020) 1157-1168.
<https://doi.org/10.1093/nsr/nwaa086>.

[35] M. Caterino, M. Gelzo, S. Sol, R. Fedele, A. Annunziata, C. Calabrese, G. Fiorentino, M. D'Abbraccio, C. Dell'Isola, F.M. Fusco, R. Parrella, G. Fabbrocini, I. Gentile, I. Andolfo, M. Capasso, M. Costanzo, A. Daniele, E. Marchese, R. Polito, R. Russo, C. Missero, M. Ruoppolo, G. Castaldo, Dysregulation of lipid metabolism and pathological inflammation in patients with COVID-19, *Sci Rep* 11(1) (2021) 2941.
<https://doi.org/10.1038/s41598-021-82426-7>.

[36] C.H. Chou, S. Mohanty, H.A. Kang, L. Kong, J. Avila-Pacheco, S.R. Joshi, I. Ueda, L. Devine, K. Raddassi, K. Pierce, S. Jeanfavre, K. Bullock, H. Meng, C. Clish, F.R. Santori, A.C. Shaw, R.J. Xavier, Metabolomic and transcriptomic signatures of influenza vaccine response in healthy young and older adults, *Aging Cell* 21(9) (2022) e13682. <https://doi.org/10.1111/accel.13682>.

[37] S.C. Hammel, S. Nordone, S. Zhang, A.M. Lorenzo, B. Eichner, M.A. Moody, L. Harrington, J. Gandee, L. Schmidt, S. Smith, H.M. Stapleton, K. Hoffman, Infants' diminished response to DTaP vaccine is associated with exposure to organophosphate esters, *Sci Total Environ* 837 (2022) 155782.
<https://doi.org/10.1016/j.scitotenv.2022.155782>.

[38] J. de Souza Nogueira, C.B. Santos-Reboucas, R.M. Piergiorgio, A.P. Valente, M.C. Gama-Almeida, T. El-Bacha, M.L. Lopes Moreira, B.S. Baptista Marques, J.R. de Siqueira, E.M. de Carvalho, O. da Costa Ferreira, Jr., L.C. Porto, T. Kelly da Silva Fidalgo, G. Costa Dos Santos, Jr., Metabolic Adaptations Correlated with Antibody Response after Immunization with Inactivated SARS-CoV-2 in Brazilian Subjects, *J Proteome Res* 22(6) (2023) 1908-1922. <https://doi.org/10.1021/acs.jproteome.3c00014>.

[39] S. Yu, Y. He, W. Ji, R. Yang, Y. Zhao, Y. Li, Y. Liu, L. Ding, M. Ma, H. Wang, X. Yang, Metabolic and Proteomic Profiles Associated with Immune Responses Induced by Different Inactivated SARS-CoV-2 Vaccine Candidates, *Int J Mol Sci* 23(18) (2022).
<https://doi.org/10.3390/ijms231810644>.

[40] Y. Wang, X. Wang, L.D.W. Luu, S. Chen, F. Jin, S. Wang, X. Huang, L. Wang, X. Zhou, X. Chen, X. Cui, J. Li, J. Tai, X. Zhu, Proteomic and Metabolomic Signatures Associated With the Immune Response in Healthy Individuals Immunized With an

Inactivated SARS-CoV-2 Vaccine, *Front Immunol* 13 (2022) 848961. <https://doi.org/10.3389/fimmu.2022.848961>.

[41] I. Dagla, A. Iliou, D. Benaki, E. Gikas, E. Mikros, T. Bagratuni, E. Kastritis, M.A. Dimopoulos, E. Terpos, A. Tsarbopoulos, Plasma Metabolomic Alterations Induced by COVID-19 Vaccination Reveal Putative Biomarkers Reflecting the Immune Response, *Cells* 11(7) (2022) 1241. <https://doi.org/10.3390/cells11071241>.

[42] S. Koletzko, T.G. Le Thi, A. Zhelyazkova, A. Osterman, S.P. Wichert, S. Breitenreicher, L. Koletzko, T. Schwerd, S. Volk, T. Jebrini, J. Horak, M. Tuschen, A. Chouker, V. Hornung, O.T. Keppler, B. Koletzko, H.P. Torok, K. Adorjan, G. Members of Riscoin Study, A prospective longitudinal cohort study on risk factors for COVID-19 vaccination failure (RisCoin): methods, procedures and characterization of the cohort, *Clin Exp Med* 23 (2023) 4901-4917. <https://doi.org/10.1007/s10238-023-01170-6>.

[43] A.M. Abdallah, A. Doudin, T.O. Sulaiman, O. Jamil, R. Arif, F.A. Sada, H.M. Yassine, M.A. Elrayess, A.N. Elzouki, M.M. Emara, N.B. Thillaiappan, F.S. Cyprian, Metabolic predictors of COVID-19 mortality and severity: a survival analysis, *Front Immunol* 15 (2024) 1353903. <https://doi.org/10.3389/fimmu.2024.1353903>.

[44] D.P. Pike, R.M. McGuffee, E. Geerling, C.J. Albert, D.F. Hoft, M.G.S. Shashaty, N.J. Meyer, A.K. Pinto, D.A. Ford, Plasmalogen Loss in Sepsis and SARS-CoV-2 Infection, *Front Cell Dev Biol* 10 (2022) 912880. <https://doi.org/10.3389/fcell.2022.912880>.

[45] J.H. Koh, S.J. Yoon, M. Kim, S. Cho, J. Lim, Y. Park, H.S. Kim, S.W. Kwon, W.U. Kim, Lipidome profile predictive of disease evolution and activity in rheumatoid arthritis, *Exp Mol Med* 54(2) (2022) 143-155. <https://doi.org/10.1038/s12276-022-00725-z>.

[46] P.R. Wratil, N.A. Schmacke, A. Osterman, T. Weinberger, J. Rech, B. Karakoc, M. Zeilberger, J. Steffen, T.T. Mueller, P.M. Spaeth, M. Stern, M. Albanese, H. Thun, J. Reinbold, B. Sandmeyer, P. Kressirer, B. Grabein, P. Falkai, K. Adorjan, V. Hornung, L. Kaderali, M. Klein, O.T. Keppler, In-depth profiling of COVID-19 risk factors and preventive measures in healthcare workers, *Infection* 50(2) (2022) 381-394. <https://doi.org/10.1007/s15010-021-01672-z>.

[47] P.R. Wratil, T.G. Le Thi, A. Osterman, I. Badell, M. Huber, A. Zhelyazkova, S.P. Wichert, A. Litwin, S. Hormansdorfer, F. Strobl, V. Grote, T. Jebrini, H.P. Torok, V. Hornung, A. Chouker, B. Koletzko, K. Adorjan, S. Koletzko, O.T. Keppler, g. RisCoin

study, Dietary habits, traveling and the living situation potentially influence the susceptibility to SARS-CoV-2 infection: results from healthcare workers participating in the RisCoin Study, *Infection* (2024). <https://doi.org/10.1007/s15010-024-02201-4>.

[48] P.R. Wrtil, M. Stern, A. Priller, A. Willmann, G. Almanzar, E. Vogel, M. Feuerherd, C.C. Cheng, S. Yazici, C. Christa, S. Jeske, G. Lupoli, T. Vogt, M. Albanese, E. Mejías-Pérez, S. Bauernfried, N. Graf, H. Mijocevic, M. Vu, K. Tinnefeld, J. Wettengel, D. Hoffmann, M. Muenchhoff, C. Daechert, H. Mairhofer, S. Krebs, V. Fingerle, A. Graf, P. Steininger, H. Blum, V. Hornung, B. Liebl, K. Überla, M. Prelog, P. Knolle, O.T. Keppler, U. Protzer, Three exposures to the spike protein of SARS-CoV-2 by either infection or vaccination elicit superior neutralizing immunity to all variants of concern, *Nat Med* 28(3) (2022) 496-503. <https://doi.org/10.1038/s41591-022-01715-4>.

[49] A. Keppler-Hafkemeyer, C. Greil, P.R. Wrtil, K. Shoumariyeh, M. Stern, A. Hafkemeyer, D. Ashok, A. Hollaus, G. Lupoli, A. Priller, M.L. Bischof, G. Ihorst, M. Engelhardt, R. Marks, J. Finke, H. Bertrand, C. Dächert, M. Muenchhoff, I. Badell, F. Emmerich, H. Halder, P.M. Spaeth, P.A. Knolle, U. Protzer, M. von Bergwelt-Baildon, J. Duyster, T.N. Hartmann, A. Moosmann, O.T. Keppler, Potent high-avidity neutralizing antibodies and T cell responses after COVID-19 vaccination in individuals with B cell lymphoma and multiple myeloma, *Nat Cancer* 4(1) (2023) 81-95. <https://doi.org/10.1038/s43018-022-00502-x>.

[50] M. Muenchhoff, H. Mairhofer, H. Nitschko, N. Grzimek-Koschewa, D. Hoffmann, A. Berger, H. Rabenau, M. Widera, N. Ackermann, R. Konrad, S. Zange, A. Graf, S. Krebs, H. Blum, A. Sing, B. Liebl, R. Wölfel, S. Ciesek, C. Drosten, U. Protzer, S. Boehm, O.T. Keppler, Multicentre comparison of quantitative PCR-based assays to detect SARS-CoV-2, Germany, March 2020, *Euro Surveill* 25(24) (2020). <https://doi.org/10.2807/1560-7917.Es.2020.25.24.2001057>.

[51] K.L. Lindsay, C. Hellmuth, O. Uhl, C. Buss, P.D. Wadhwa, B. Koletzko, S. Entringer, Longitudinal Metabolomic Profiling of Amino Acids and Lipids across Healthy Pregnancy, *PLoS One* 10(12) (2015) e0145794. <https://doi.org/10.1371/journal.pone.0145794>.

[52] P. Giesbertz, J. Ecker, A. Haag, B. Spanier, H. Daniel, An LC-MS/MS method to quantify acylcarnitine species including isomeric and odd-numbered forms in plasma and tissues, *J Lipid Res* 56(10) (2015) 2029-39. <https://doi.org/10.1194/jlr.D061721>.

- [53] J. Marques, E. Shokry, O. Uhl, L. Baber, F. Hofmeister, S. Jarmusch, M. Bidlingmaier, U. Ferrari, B. Koletzko, M. Drey, Sarcopenia: investigation of metabolic changes and its associated mechanisms, *Skelet Muscle* 13(1) (2023) 2. <https://doi.org/10.1186/s13395-022-00312-w>.
- [54] S. Rauschert, O. Uhl, B. Koletzko, F. Kirchberg, T.A. Mori, R.-C. Huang, L.J. Beilin, C. Hellmuth, W.H. Oddy, Lipidomics reveals associations of phospholipids with obesity and insulin resistance in young adults, *Journal of Clinical Endocrinology & Metabolism* 101(3) (2016) 871-879. <https://doi.org/10.1210/jc.2015-3525>.
- [55] J. Lukac, K. Dhaygude, M. Saraswat, S. Joenväärä, S.O. Syrjälä, E.J. Holmström, R. Krebs, R. Renkonen, A.I. Nykänen, K.B. Lemström, Plasma proteome of brain-dead organ donors predicts heart transplant outcome, *J Heart Lung Transplant* 41(3) (2022) 311-324. <https://doi.org/10.1016/j.healun.2021.11.011>.
- [56] L. Guo, S. Deng, S. Sun, X. Wang, Y. Li, Respiratory syncytial virus seasonality, transmission zones, and implications for seasonal prevention strategy in China: a systematic analysis, *The Lancet. Global health* 12(6) (2024) e1005-e1016. [https://doi.org/10.1016/s2214-109x\(24\)00090-1](https://doi.org/10.1016/s2214-109x(24)00090-1).
- [57] J.S. Chandan, D.T. Zemedikun, R. Thayakaran, N. Byne, S. Dhalla, D. Acosta-Mena, K.M. Gokhale, T. Thomas, C. Sainsbury, A. Subramanian, J. Cooper, A. Anand, K.O. Okoth, J. Wang, N.J. Adderley, T. Taverner, A.K. Denniston, J. Lord, G.N. Thomas, C.D. Buckley, K. Raza, N. Bhala, K. Nirantharakumar, S. Haroon, Nonsteroidal Antiinflammatory Drugs and Susceptibility to COVID-19, *Arthritis & rheumatology (Hoboken, N.J.)* 73(5) (2021) 731-739. <https://doi.org/10.1002/art.41593>.
- [58] Y. Yao, A. Schneider, K. Wolf, S. Zhang, R. Wang-Sattler, A. Peters, S. Breitner, Longitudinal associations between metabolites and long-term exposure to ambient air pollution: Results from the KORA cohort study, *Environ Int* 170 (2022) 107632. <https://doi.org/10.1016/j.envint.2022.107632>.
- [59] W. Ni, N. Nikolaou, C.K. Ward-Caviness, S. Breitner, K. Wolf, S. Zhang, R. Wilson, M. Waldenberger, A. Peters, A. Schneider, Associations between medium- and long-term exposure to air temperature and epigenetic age acceleration, *Environ Int* 178 (2023) 108109. <https://doi.org/10.1016/j.envint.2023.108109>.
- [60] Z. Pang, Y. Lu, G. Zhou, F. Hui, L. Xu, C. Viau, A.F. Spigelman, P.E. MacDonald, D.S. Wishart, S. Li, J. Xia, MetaboAnalyst 6.0: towards a unified platform for

metabolomics data processing, analysis and interpretation, *Nucleic Acids Res* (2024).
<https://doi.org/10.1093/nar/gkae253>.

[61] M. Kanehisa, Y. Sato, M. Kawashima, M. Furumichi, M. Tanabe, KEGG as a reference resource for gene and protein annotation, *Nucleic Acids Res* 44(D1) (2016) D457-62. <https://doi.org/10.1093/nar/gkv1070>.

[62] WHO, A healthy lifestyle - WHO recommendations, 2010.
<https://www.who.int/europe/news-room/fact-sheets/item/a-healthy-lifestyle---who-recommendations>. (Accessed 23rd October 2024).

[63] Y. Yao, A. Schneider, K. Wolf, S. Zhang, R. Wang-Sattler, A. Peters, S. Breitner, Longitudinal associations between metabolites and immediate, short- and medium-term exposure to ambient air pollution: Results from the KORA cohort study, *Sci Total Environ* 900 (2023) 165780. <https://doi.org/10.1016/j.scitotenv.2023.165780>.

[64] S. Feng, D.J. Phillips, T. White, H. Sayal, P.K. Aley, S. Bibi, C. Dold, M. Fuskova, S.C. Gilbert, I. Hirsch, H.E. Humphries, B. Jepson, E.J. Kelly, E. Plested, K. Shoemaker, K.M. Thomas, J. Vekemans, T.L. Villafana, T. Lambe, A.J. Pollard, M. Voysey, Correlates of protection against symptomatic and asymptomatic SARS-CoV-2 infection, *Nat Med* 27(11) (2021) 2032-2040. <https://doi.org/10.1038/s41591-021-01540-1>.

[65] S. Cele, I. Gazy, L. Jackson, S.H. Hwa, H. Tegally, G. Lustig, J. Giandhari, S. Pillay, E. Wilkinson, Y. Naidoo, F. Karim, Y. Ganga, K. Khan, M. Bernstein, A.B. Balazs, B.I. Gosnell, W. Hanekom, M.S. Moosa, R.J. Lessells, T. de Oliveira, A. Sigal, Escape of SARS-CoV-2 501Y.V2 from neutralization by convalescent plasma, *Nature* 593(7857) (2021) 142-146. <https://doi.org/10.1038/s41586-021-03471-w>.

[66] E.A. Omran, R.E. El Naggar, L.A. Ezz Elarab, M.H. Hashish, M.A. El-Barrawy, I.A. Abdelwahab, M.M. Fekry, Anti-Spike and Neutralizing Antibodies after Two Doses of COVID-19 Sinopharm/BIBP Vaccine, *Vaccines* (Basel) 10(8) (2022).
<https://doi.org/10.3390/vaccines10081340>.

[67] Correlation of SARS-CoV-2 Viral NA Titers with Anti-S Antibodies and ACE-2 Inhibition among Vaccinated Individuals--2022-10-e0131522.pdf>, *Microbiol Spectr* 10(5) (2022) e0131522. <https://doi.org/10.1128/spectrum.01315-22>.

[68] N.V. Tolan, A.C. Sherman, G. Zhou, K.G. Nabel, M. Desjardins, S. Melanson, S. Kanjilal, S. Moheed, J. Kupelian, R.M. Kaufman, E.T. Ryan, R.C. LaRocque, J.A.

- Branda, A.S. Dighe, J. Abraham, L.R. Baden, R.C. Charles, S.E. Turbett, The Effect of Vaccine Type and SARS-CoV-2 Lineage on Commercial SARS-CoV-2 Serologic and Pseudotype Neutralization Assays in mRNA Vaccine Recipients, *Microbiol Spectr* 10(2) (2022) e00211-22. <https://doi.org/doi:10.1128/spectrum.00211-22>.
- [69] M. Talaei, S. Faustini, H. Holt, D.A. Jolliffe, G. Vivaldi, M. Greenig, N. Perdek, S. Maltby, C.M. Bigogno, J. Symons, G.A. Davies, R.A. Lyons, C.J. Griffiths, F. Kee, A. Sheikh, A.G. Richter, S.O. Shaheen, A.R. Martineau, Determinants of pre-vaccination antibody responses to SARS-CoV-2: a population-based longitudinal study (COVIDENCE UK), *BMC Medicine* 20(1) (2022) 87. <https://doi.org/10.1186/s12916-022-02286-4>.
- [70] A.A. van der Klaauw, E.C. Horner, P. Pereyra-Gerber, U. Agrawal, W.S. Foster, S. Spencer, B. Vergese, M. Smith, E. Henning, I.D. Ramsay, J.A. Smith, S.M. Guillaume, H.J. Sharpe, I.M. Hay, S. Thompson, S. Innocentin, L.H. Booth, C. Robertson, C. McCowan, S. Kerr, T.E. Mulroney, M.J. O'Reilly, T.P. Gurugama, L.P. Gurugama, M.A. Rust, A. Ferreira, S. Ebrahimi, L. Ceron-Gutierrez, J. Scotucci, B. Kronsteiner, S.J. Dunachie, P. Klenerman, A.J. Park, F. Rubino, A.A. Lamikanra, H. Stark, N. Kingston, L. Estcourt, H. Harvala, D.J. Roberts, R. Doffinger, M.A. Linterman, N.J. Matheson, A. Sheikh, I.S. Farooqi, J.E.D. Thaventhiran, Accelerated waning of the humoral response to COVID-19 vaccines in obesity, *Nat Med* 29(5) (2023) 1146-1154. <https://doi.org/10.1038/s41591-023-02343-2>.
- [71] M. Franzese, L. Coppola, R. Silva, S.A. Santini, L. Cinquanta, C. Ottomano, M. Salvatore, M. Incoronato, SARS-CoV-2 antibody responses before and after a third dose of the BNT162b2 vaccine in Italian healthcare workers aged ≤ 60 years: One year of surveillance, *Front Immunol* 13 (2022) 947187. <https://doi.org/10.3389/fimmu.2022.947187>.
- [72] G. Fedele, I. Schiavoni, F. Trentini, P. Leone, E. Olivetta, A. Fallucca, S. Fiore, A. Di Martino, S. Abrignani, V. Baldo, T. Baldovin, A. Bandera, P. Clerici, M. De Paschale, F. Diaco, A. Domnich, F. Fortunato, I. Giberti, A. Gori, R. Grifantini, T. Lazzarotto, V. Lodi, C.M. Mastroianni, R. Prato, V. Restivo, F. Vitale, S. Brusaferro, S. Merler, A.T. Palamara, P. Stefanelli, A 12-month follow-up of the immune response to SARS-CoV-2 primary vaccination: evidence from a real-world study, *Front Immunol* 14 (2023) 1272119. <https://doi.org/10.3389/fimmu.2023.1272119>.

- [73] R.J. Langley, E.L. Tsalik, J.C. van Velkinburgh, S.W. Glickman, B.J. Rice, C. Wang, B. Chen, L. Carin, A. Suarez, R.P. Mohny, D.H. Freeman, M. Wang, J. You, J. Wulff, J.W. Thompson, M.A. Moseley, S. Reisinger, B.T. Edmonds, B. Grinnell, D.R. Nelson, D.L. Dinwiddie, N.A. Miller, C.J. Saunders, S.S. Soden, A.J. Rogers, L. Gazourian, L.E. Fredenburgh, A.F. Massaro, R.M. Baron, A.M. Choi, G.R. Corey, G.S. Ginsburg, C.B. Cairns, R.M. Otero, V.G. Fowler, Jr., E.P. Rivers, C.W. Woods, S.F. Kingsmore, An integrated clinico-metabolomic model improves prediction of death in sepsis, *Science translational medicine* 5(195) (2013) 195ra95. <https://doi.org/10.1126/scitranslmed.3005893>.
- [74] M.A. Puskarich, C.R. Evans, A. Karnovsky, A.K. Das, A.E. Jones, K.A. Stringer, Septic Shock Nonsurvivors Have Persistently Elevated Acylcarnitines Following Carnitine Supplementation, *Shock* 49(4) (2018) 412-419. <https://doi.org/10.1097/shk.0000000000000997>.
- [75] A.A. Al-Qahtani, F.S. Alhamlan, A.A. Al-Qahtani, Pro-Inflammatory and Anti-Inflammatory Interleukins in Infectious Diseases: A Comprehensive Review, *Trop Med Infect Dis* 9(1) (2024) 13. <https://doi.org/10.3390/tropicalmed9010013>.
- [76] J.H. Kabarowski, G2A and LPC: regulatory functions in immunity, Prostaglandins & other lipid mediators 89(3-4) (2009) 73-81. <https://doi.org/10.1016/j.prostaglandins.2009.04.007>.
- [77] J. Oestvang, B. Johansen, PhospholipaseA2: a key regulator of inflammatory signalling and a connector to fibrosis development in atherosclerosis, *Biochim Biophys Acta* 1761(11) (2006) 1309-16. <https://doi.org/10.1016/j.bbalip.2006.06.003>.
- [78] W. Liao, G. Tan, Z. Zhu, Q. Chen, Z. Lou, X. Dong, W. Zhang, W. Pan, Y. Chai, Combined metabonomic and quantitative real-time PCR analyses reveal systems metabolic changes in Jurkat T-cells treated with HIV-1 Tat protein, *J Proteome Res* 11(11) (2012) 5109-23. <https://doi.org/10.1021/pr300173c>.
- [79] M. Kertys, M. Grendar, P. Kosutova, D. Mokra, J. Mokry, Plasma based targeted metabolomic analysis reveals alterations of phosphatidylcholines and oxidative stress markers in guinea pig model of allergic asthma, *Biochimica et biophysica acta. Molecular basis of disease* 1866(1) (2020) 165572. <https://doi.org/10.1016/j.bbadis.2019.165572>.

- [80] J.W. Brewer, V. Solodushko, I. Aragon, R.A. Barrington, Phosphatidylcholine as a metabolic cue for determining B cell fate and function, *Cell Immunol* 310 (2016) 78-88. <https://doi.org/10.1016/j.cellimm.2016.08.002>.
- [81] N.P. Long, N.K. Anh, N.T.H. Yen, N.K. Phat, S. Park, V.T.A. Thu, Y.S. Cho, J.G. Shin, J.Y. Oh, D.H. Kim, Comprehensive lipid and lipid-related gene investigations of host immune responses to characterize metabolism-centric biomarkers for pulmonary tuberculosis, *Sci Rep* 12(1) (2022) 13395. <https://doi.org/10.1038/s41598-022-17521-4>.
- [82] G. Fu, C.S. Guy, N.M. Chapman, G. Palacios, J. Wei, P. Zhou, L. Long, Y.D. Wang, C. Qian, Y. Dhungana, H. Huang, A. Kc, H. Shi, S. Rankin, S.A. Brown, A. Johnson, R. Wakefield, C.G. Robinson, X. Liu, A. Sheyn, J. Yu, S. Jackowski, H. Chi, Metabolic control of T(FH) cells and humoral immunity by phosphatidylethanolamine, *Nature* 595(7869) (2021) 724-729. <https://doi.org/10.1038/s41586-021-03692-z>.
- [83] Y.A. Hannun, L.M. Obeid, Sphingolipids and their metabolism in physiology and disease, *Nat Rev Mol Cell Biol* 19(3) (2018) 175-191. <https://doi.org/10.1038/nrm.2017.107>.
- [84] M. Abusukhun, M.S. Winkler, S. Pöhlmann, O. Moerer, K. Meissner, B. Tampe, H. Hofmann-Winkler, M. Bauer, M.H. Gräler, R.A. Claus, Activation of Sphingomyelinase-Ceramide-Pathway in COVID-19 Purposes Its Inhibition for Therapeutic Strategies, *Front Immunol* 12 (2021) 784989. <https://doi.org/10.3389/fimmu.2021.784989>.
- [85] S. Spiegel, S. Milstien, The outs and the ins of sphingosine-1-phosphate in immunity, *Nat Rev Immunol* 11(6) (2011) 403-15. <https://doi.org/10.1038/nri2974>.
- [86] T. Baumruker, E.E. Prieschl, Sphingolipids and the regulation of the immune response, *Semin Immunol* 14(1) (2002) 57-63. <https://doi.org/10.1006/smim.2001.0342>.
- [87] Y. Zhang, Q. Yue, H. Zhu, J. Song, D. Li, W. Liu, S. Jiang, N. Jiang, C. Qiu, J. Ai, Y. Zhang, W. Zhang, Serum Metabolic Correlates of the Antibody Response in Subjects Receiving the Inactivated COVID-19 Vaccine, *Vaccines (Basel)* 10(11) (2022). <https://doi.org/10.3390/vaccines10111890>.
- [88] V. Koeken, C. Qi, V.P. Mourits, L.C.J. de Bree, S. Moorlag, V. Sonawane, H. Lemmers, H. Dijkstra, L.A.B. Joosten, A. van Laarhoven, C.J. Xu, R. van Crevel, M.G. Netea, Y. Li, Plasma metabolome predicts trained immunity responses after antituberculosis BCG vaccination, *PLoS biology* 20(9) (2022) e3001765. <https://doi.org/10.1371/journal.pbio.3001765>.

- [89] J. Diray-Arce, A. Angelidou, K.J. Jensen, M.G. Conti, R.S. Kelly, M.A. Pettengill, M. Liu, S.D. van Haren, S.D. McCulloch, G. Michelloti, O. Idoko, T.R. Kollmann, B. Kampmann, H. Steen, A. Ozonoff, J. Lasky-Su, C.S. Benn, O. Levy, Bacille Calmette-Guérin vaccine reprograms human neonatal lipid metabolism in vivo and in vitro, *Cell Rep* 39(5) (2022) 110772. <https://doi.org/10.1016/j.celrep.2022.110772>.
- [90] B. Yan, S. Yuan, J. Cao, K. Fung, P.M. Lai, F. Yin, K.H. Sze, Z. Qin, Y. Xie, Z.W. Ye, T.T. Yuen, K.K. Chik, J.O. Tsang, Z. Zou, C.C. Chan, C. Luo, J.P. Cai, K.H. Chan, T.W. Chung, A.R. Tam, H. Chu, D.Y. Jin, I.F. Hung, K.Y. Yuen, R.Y. Kao, J.F. Chan, Phosphatidic acid phosphatase 1 impairs SARS-CoV-2 replication by affecting the glycerophospholipid metabolism pathway, *Int J Biol Sci* 18(12) (2022) 4744-4755. <https://doi.org/10.7150/ijbs.73057>.
- [91] B.J. Anderson, A.M. Curtis, A. Jen, J.A. Thomson, D.O. Clegg, P. Jiang, J.J. Coon, K.A. Overmyer, H. Toh, Plasma metabolomics supports non-fasted sampling for metabolic profiling across a spectrum of glucose tolerance in the Nile rat model for type 2 diabetes, *Lab Anim (NY)* 52(11) (2023) 269-277. <https://doi.org/10.1038/s41684-023-01268-0>.
- [92] B.G. Nordestgaard, A Test in Context: Lipid Profile, Fasting Versus Nonfasting, *J Am Coll Cardiol* 70(13) (2017) 1637-1646. <https://doi.org/10.1016/j.jacc.2017.08.006>.
- [93] E.C. Alexopoulos, Introduction to multivariate regression analysis, *Hippokratia* 14(Suppl 1) (2010) 23-8.
- [94] R. Badaro, J.D.V. Barbosa, C.A. de Araujo Neto, B.A.S. Machado, M.B.P. Soares, V. de Senna, M. Taddeo, L.T. de Araújo, S. Durkee, R. Donninger, K. Judge, Z. Saiyed, A randomized clinical trial to evaluate the efficacy of L-carnitine L-tartrate to modulate the effects of SARS-CoV-2 infection, *Front Nutr* 10 (2023) 1134162. <https://doi.org/10.3389/fnut.2023.1134162>.

Chapter 2 – Tissue Homogenization Study

2.1. Introduction

2.1.1. Background

2.1.1.1. Importance of Tissue Homogenization in Biomedical Research

Tissue homogenization is a fundamental step in biomedical research, enabling the extraction of biomolecules essential for downstream analyses. Biological tissues contain a diverse range of analytes, including DNA, RNA and proteins, as well as relatively smaller molecules such as lipids and polar metabolites [1-5], necessitating specialized homogenization protocols tailored to the specific molecular class of interest. Various homogenization techniques are available, each with distinct advantages and limitations. Traditional approaches include ultrasonic disruption [6], mechanical grinding using a pestle and mortar (with or without liquid nitrogen), and ultra-turrax homogenization [2, 3, 7-13]. Bead-based homogenization has recently obtained popularity for its efficiency in high-throughput workflows [8, 14, 15].

Although single-sample homogenization is often sufficient in basic biological and biochemical research, large-scale studies, such as those in clinical research and routine diagnostics, require parallel processing of big amount of samples. Automated homogenization platforms, such as Precellys, Beadbug and Bullet Blender homogenizers, have been developed to improve efficiency, minimize processing time, and enhance sample-to-sample reproducibility [8, 16, 17]. These systems also offer cooling options to prevent heat-induced degradation of metabolites, further ensuring the integrity of extracted compounds.

2.1.1.2. Challenges in Standardizing Homogenization Protocols

One of the major challenges in tissue homogenization is the substantial variability across different protocols, which can lead to inconsistencies in downstream analyses. Variations arise from differences in homogenization tools, solvent composition, and extraction conditions. For example, while a pestle-based homogenization method

primarily relies on shear forces to break open cells, it does not necessarily disrupt organelles or lipid membranes. In contrast, bead-based homogenization can completely disrupt dense structures, including bones [18].

Additionally, many homogenization protocols were initially optimized for extracting specific biomolecular classes, meaning that different extraction protocols are required for the analysis of multiple analyte types. This is particularly problematic when dealing with small biopsy samples, such as brain or tumour tissues, where maximizing the extracted biochemical information from a single tissue section is critical. Recent technological progress has facilitated real-time metabolite analysis through rapid evaporative ionization mass spectrometry (REIMS) with the Harmonic scalpel (iKnife), alongside tissue imaging mass spectrometry as well as spatial multi-omics methods [19-22]. However, these advanced methodologies require expensive instrumentation and highly specialized expertise, limiting their routine clinical application.

2.1.2. Tissue Homogenization in Clinical Metabolomics

2.1.2.1. High-Throughput Sample Preparation and Extraction Techniques

Efficient and cost-effective sample processing in clinical metabolomics field necessitates the automation of various preparation steps, such as analyte extraction and derivatization [23]. A shift from single 15 mL glass tubes to 96-well plates can improve throughput, while replacing two-phase extraction methods, like what E.G. Bligh, et al reported [24], with single-phase solvent extraction techniques [25]. Sequential solid-liquid extraction using solvents of increasing lipophilicity has been shown to significantly enhance metabolite and lipid recovery [7, 17, 26]. However, employing more than two extraction steps can cause time-intensive and cumbersome, particularly when homogenization is conducted manually with a pestle [7] rather than using a bead homogenizer compatible with multiple tubes [12]. An often-overlooked aspect is the variability in metabolic profiles across different sample fractions, including the tissue homogenate slurry, residual debris and supernatant. Recent research highlights that

homogenate slurry and debris pellets contain substantial lipid content when water-rich homogenization solvents are used, whereas non-aqueous solvents like methanol yield similar lipid levels in both homogenate and supernatant [10]. Despite this, the supernatant remains the most commonly used fraction for metabolite and lipid extraction [26-28], with the homogenate gaining attention only in recent studies [10, 29].

2.1.2.2. Impact of Solvent Selection on Metabolite Recovery

The choice of homogenization solvent significantly affects the efficiency of metabolite extraction. Different research facilities and tissue types utilize varying ratios of tissue weight to solvent volume [26, 27], and solvent composition plays a crucial role in determining which metabolites are extracted. When different homogenization solvents are used on the same homogenate slurry, the resulting metabolic profiles can differ substantially [30].

Temperature control is another critical factor in tissue homogenization. The lack of active cooling mechanisms influences metabolite integrity, as elevated temperatures can accelerate enzymatic and chemical degradation processes [31-34]. Without proper cooling, the metabolic profile of a sample can change due to heat-induced degradation, making temperature regulation an essential consideration in tissue homogenization workflows. Additionally, pipetting homogenate slurries poses challenges, as increased organic solvent content can lead to the accumulation of solid particles, increasing the likelihood of pipette tip blockage. These technical issues must be addressed to ensure consistency in tissue-based metabolomic studies.

2.1.3. Aim of the Study

This study aims to systematically evaluate the influence of tissue homogenization parameters on metabolite extraction efficiency. Specifically, the research focuses on optimizing tissue sample preparation by testing different solvent compositions and extraction procedures.

Pork tissue samples underwent extraction using six different solvent combinations with varying degrees of lipophilicity. A sequential two-step extraction approach was applied, first utilizing methanol (MeOH) to isolate polar metabolites, followed by a mixture of methyl-tert-butyl ether (MTBE) in MeOH to extract lipophilic ones. Metabolite recovery was compared between the supernatant and homogenate fractions. Sixty experimental conditions were tested with four replicates each, analyzing over 400 metabolites and lipids. Multidimensional analysis, including Upset plots, were performed to determine the optimal extracting condition of both polar and lipophilic metabolites.

Temperature control was also investigated to mitigate metabolite degradation during homogenization. Additionally, a prewetting correction (PWC) factor was introduced to improve pipetting accuracy and ensure reproducible metabolite quantification in high-organic solvent conditions.

For analytical validation, a targeted HPLC-ESI-QTRAP-MS/MS metabolomics platform was used to quantify a range of metabolite classes, including amino acids, organic acids, acylcarnitines, and phospholipids. Furthermore, the optimized homogenization and extraction protocol was applied to pancreas tissue samples from three mice to investigate intra-organ metabolic variations.

2.2. Material and Methods

2.2.1. Chemicals and Consumables

H ₂ O (LC-MS grade)	Merck, via Sigma-Aldrich, Schnelldorf, Germany
H ₂ O (HPLC grade)	Sigma-Aldrich, Schnelldorf, Germany
Methanol (MeOH)	Sigma-Aldrich, Schnelldorf, Germany
Acetonitrile (ACN)	Sigma-Aldrich, Schnelldorf, Germany
Isopropanol (IPA)	Sigma-Aldrich, Schnelldorf, Germany

Ethanol (EtOH, LC-MS grade)	Sigma-Aldrich, Schnelldorf, Germany
Methyl tert-butyl ether (MTBE)	Sigma-Aldrich, Schnelldorf, Germany
Phosphate buffer saline (PBS)	Gibco, via Sigma-Aldrich, Schnelldorf, Germany
PCR 96-well microplates (200 µL, conical, skirted)	Axygen, via Sigma-Aldrich, Schnelldorf, Germany
96 deep-well plates (1.2 mL, round bottom, low profile)	Brand, via Sigma-Aldrich, Schnelldorf, Germany
Human control plasma (Level I and II, used as individual control plasmas (CPI and CPII) and pooled quality controls (QCs))	ClinChek, Recipe, Munich, Germany
10 µL, 200 µL, and 1000 µL pipette tips	TipONE, StarLab, Hamburg, Germany
PCR microplate aluminum heat sealing foil	Eppendorf, Wesseling, Germany
Multipette M4	Eppendorf, Wesseling, Germany
HeatSealer S100	Eppendorf, Wesseling, Germany
ThermoMixer C (with well plate adapter)	Eppendorf, Wesseling, Germany
Polypropylene PCR microplate foil	RatioLab, Dreieichen, Germany
3 mm tungsten carbide beads	QIAGEN, Hilden, Germany
2 mL screw cap tubes	Sarstedt, Nümbrecht, Germany
2 mL reinforced screw caps	Omni-International, Biolabproducts GmbH, Bebensee, Germany

Tissue homogenizer Bead Ruptor-4 GmbH, Bebensee, Germany	Omni-International, Biolabproducts
Digital food thermometer HCP1	Habor, Taiping City, Taiwan
PRACTUM64-1S analytical balance KG, Goettingen, Germany	Sartorius Lab Instruments GmbH & Col.
Vortexer Germany	IKA®-Werke GmbH & Co. KG, Staufen,
ROTINA 380 R and MIKRO 22 R Hettich centrifuges KG, Tuttlingen, Germany	Andreas Hettich GmbH & Co.
NGM 22-LC/MS nitrogen generator Germany	CMC Instruments GmbH, Eschborn,
Nitrogen sample concentrator and related accessories (96-well block thermostat for Dri-block, Dri-Block DB100/3 heater, PTFE coated needles and sample concentrator) Germany	Techne, VWR, Darmstadt,

2.2.2. Sample Preparation

2.2.2.1. Processing of Pork Tissue

Pork chops were obtained from a local grocery store while still in the warranty period. The chops were rinsed using a sterile phosphate-buffered saline (PBS) solution and sectioned into pieces of approximately 100 mg \pm 10 mg using a disposable scalpel on a sanitized glass plate. Each tissue fragment was accurately weighed 4 times in a 2 mL screw-cap tube equipped with a reinforced lid. The prepared tissue fragments were subjected to rapid freezing in liquid nitrogen for 20 sec before being stored at -80 °C until performing homogenization.

2.2.2.2. Processing of Mouse Pancreas Tissue

Pancreatic tissues were sourced from Julia Alexandra Wolff (LMU Klinikum) and obtained from three female C57BL6/J mice housed under standard dietary and environmental conditions. The mice were sacrificed in compliance with §4 of Tierschutzgesetz (the German Animal Welfare Act) for research purposes. Tissue samples were collected from three individuals—one aged 17 weeks (M-1) and two aged 15 weeks (M-2 and M-3). Each pancreas was sectioned into three portions (A, B, and C), with each segment weighing approximately $50 \text{ mg} \pm 10 \text{ mg}$. To ensure accuracy, each sample was weighed three times in 2 mL screw-cap tubes with reinforced lids for subsequent homogenization, following in-house protocols. The samples were quickly flash-frozen in liquid nitrogen and stored at -80°C prior to processing homogenization.

2.2.3 Tissue Homogenization

2.2.3.1 Temperature Management During Homogenization

Tissue homogenization was carried out using the Bead Ruptor-4, a device that processes up to four tubes at a time but lacks a cooling feature. For each pork tissue sample, tubes were loaded with five 3 mm steel beads and 300 μL of PBS. A digital food thermometer was used to measure the temperature of both the homogenization solution and the resulting homogenate before (0 min) and post homogenization for varying durations (30 sec to 5 min) at intensity level 4 under different cooling conditions. Due to the rapid temperature increase, in-solution measurements were typically recorded once unless otherwise specified.

The following experiments were conducted to evaluate temperature control during homogenization:

Table 2.1. Experiment conditions for temperature management test.

Experiment	Cooling Method	Homogenization Duration	Additional Details
1 (Figure 2.1a)	One tube was flash-frozen in liquid nitrogen (-196°C) for 20 sec before each run	1, 2, 3, 4, 5 min	Same tube frozen at the start of each run; homogenate temperature measured four times for standard deviation
2 (Figure 2.1b)	One tube was cooled at - 20°C for 5 min before homogenization	0.5, 1.5, 3, 5 min	Zip-lock bag with crushed ice placed (ice bag) between sample tubes and homogenizer lid
3 (Figure 2.1c)	Tube cooled at -20°C for 5 min before homogenization	0.5, 1.0, 1.5 min	Ice bag was placed either under or on top of the homogenizer lid
4 (Figure 2.1d)	One tube was pre-cooled on crushed ice; two tubes cooled at -20°C for 5 min	30 sec	One of the two -20°C cooled samples was further cooled with a ice bag under the homogenizer lid

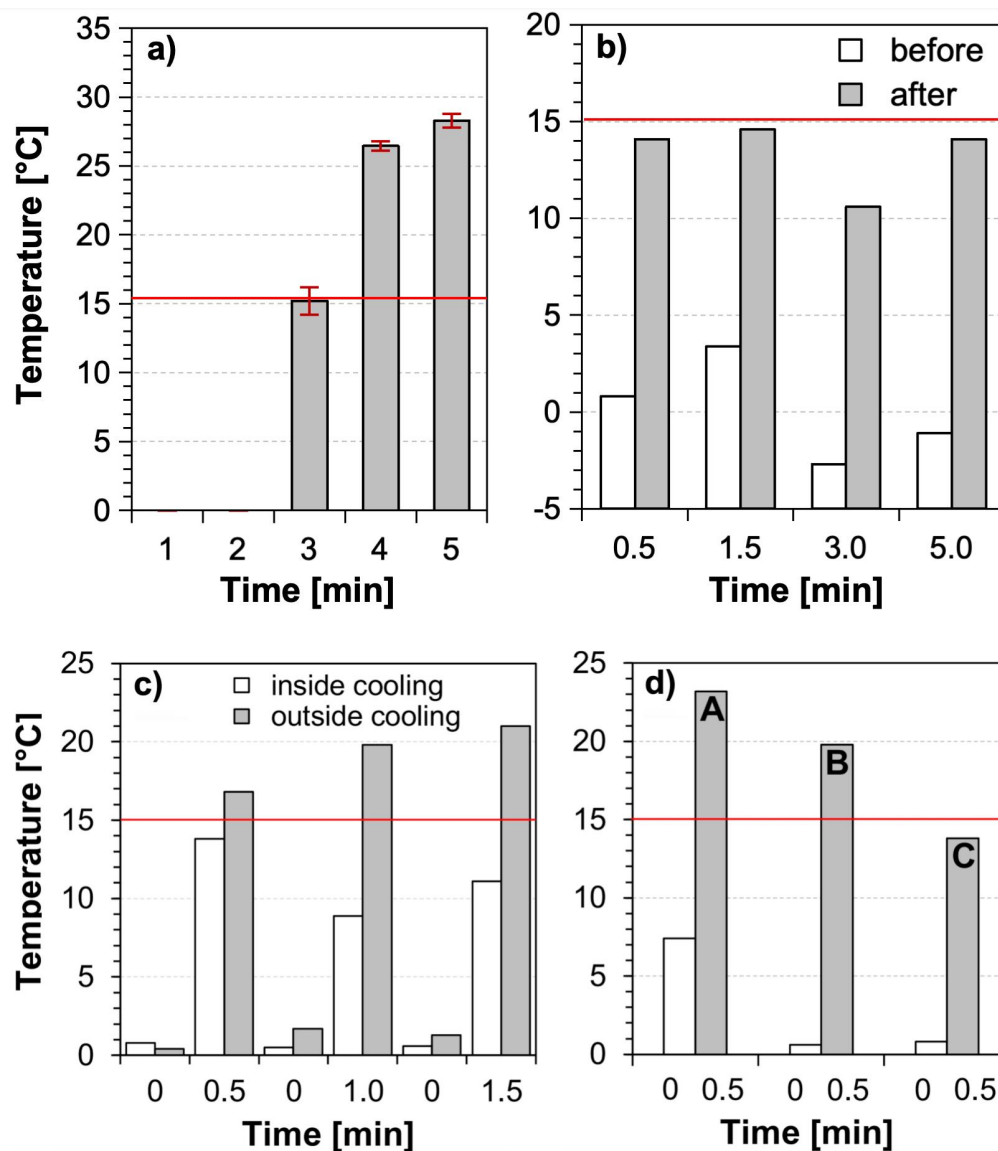


Figure 2.1. Temperature optimization test of tissue homogenization.

The test was performed at intensity level 4 with 5 * 3 mm steel beads in 300 μ L PBS. In part (a), the homogenization tubes ($n = 3$) were cooled in liquid nitrogen for 20 seconds before undergoing homogenization in 1-minute intervals at room temperature. In part (b), the homogenization tube ($n = 1$) was kept at -20°C for 5 minutes, followed by homogenization with an ice pack placed between the lid and the sample to ensure consistent cooling. Homogenate temperature was tested before and after homogenization. The red line shows the proposed upper limitation of homogenate temperature (15°C). In part (c), the homogenization tube ($n = 1$) was subsequently cooled for 5 minutes at -20°C prior to homogenizing for 0.5, 1.0, and 1.5 minutes with the ice bag putting between lid and sample (inside cooling) as well as on top of the lid (outside cooling). Homogenate temperature was tested before and after homogenization. In part (d), the homogenization tube ($n = 1$) was cooled for 5 minutes on crushed ice (A) or at -20°C (B and C) before homogenization for 30 sec. at room temperature (A and B) or with ice bag cooling (C), placing a ice bag between

sample tubes and homogenizer lid. Figure is cited from Y. Hao, et al [41] under the Creative Commons CC-BY license[42].

2.2.3.2. Effect of Solvent Polarity on Tissue Homogenization

Every pork tissue sample (100 mg; n = 4) was homogenized with 5 steel beads (3 mm) and 300 μ L of a designated homogenization solvent. The solvents included pure PBS, PBS/methanol (1:1; v/v), PBS/methanol (1:3; v/v), PBS/ethanol (15:85; v/v), methanol alone, and isopropanol (IPA). Homogenization was carried out at intensity level 4 for a duration of 5 minutes, with temperature control maintained by placing a zip-lock bag containing crushed ice (ice bag) beneath the lid of the Bead Ruptor 4. To minimize temperature fluctuations, all sample tubes were stored on ice both prior to and following homogenization, as well as throughout the metabolite extraction process. It is worth noting that none of the homogenized samples were subjected to re-freezing, and metabolite extraction was initiated immediately after homogenization.

Subsequent metabolite and lipid extractions were conducted for three different volumes of both homogenate and supernatant (10 μ L, 25 μ L, and 50 μ L), employing two separate two-step extraction procedures: (a) methanol followed by 25% MTBE in methanol, and (b) methanol followed by 75% MTBE in methanol. Notably, homogenate extraction was conducted prior to centrifugation, whereas supernatant extraction was carried out on the same homogenized samples post-centrifugation.

2.2.3.3. Background Contamination Check

Three distinct background contamination checks were conducted in quadruplicate to ensure analytical accuracy. The details of each blank experiment are summarized below:

Table 2.2. Blank types for background contamination investigation.

Blank Type	Description	Procedure
Blank 1	Empty tubes (n = 4) with 300 µL of homogenization solution and 5 * 3 mm steel beads	Homogenization was performed in parallel with pork tissue samples, followed by a two-step metabolite extraction process using 25% and 75% MTBE in MeOH in the second step
Blank 2	Same as above	The homogenization solution underwent the two-step metabolite extraction process directly, omitting the homogenization step
Blank 3	No tubes or beads were employed	Pipetting homogenization solution into the MeOH-ISTD solution and proceeded directly to the LC-MS related sample processings)

2.2.4. Extraction for Polar and Non-polar Metabolites

2.2.4.1. Extraction for Polar Metabolites

A methanolic ISTD mix solution (MeOH-ISTD, 450 µL) was added to pre-designed wells of a 96-deep-well plate (1.2 mL, well plate A) with the stepper pipette Multipette M4. Aliquots of 10 µL, 25 µL, and 50 µL from the vortexed homogenate slurry (n = 4 for each volume), along with 50 µL QC plasma (n = 6), 50 µL CPI (n = 2), 50 µL CPII (n = 2), and 50 µL H₂O (n = 1) for the ISTD blank, were pipetted directly into the MeOH-ISTD solution. The solutions were mixed by drawing and ejecting 20 times with a pipette tip, forming a fluffy protein precipitate for plasma and tissue samples.

The homogenate samples were then centrifuged at 10,000 rcf for 10 minutes at 4°C. Clear extracts (10 µL, 25 µL, and 50 µL) were carefully transferred from the supernatants (n = 4) to the MeOH-ISTD solution without disturbing the pellet. Notably, 10 µL extract volumes were excluded for experiments with 75% MTBE in MeOH. The

well plates were sealed with PCR foil, shaken at 25°C and 700 rpm for 20 minutes, and then refrigerated at 4°C for 20 minutes to finish the protein precipitation. After centrifugation for 5 minutes at 3,000 rpm and 22°C, the polar metabolite extract (extract A) was pipetted into a fresh 96-well plate (1.2 mL, well plate B; **Figure 2.2**).

2.2.4.2. Extraction of Lipids Using 25% and 75% MTBE in MeOH

Immediately, the protein precipitate in well plate A was resuspended in 50 µL H₂O by shaking at 800 rpm and 25°C for 20 minutes. Then 450 µL of 25% or 75% MTBE in MeOH was added, followed by mixing via pipette tip for 20 times to form a flocculent precipitate. The plate was then shaken, incubated at 4°C, and centrifuged using the same protocol as for polar analyte processing. The resulting supernatant extract was mixed together with the polar metabolite extract in well plate B (**Figure 2.2**).

The pooled extract was divided: 600 µL was then immediately transferred to a fresh 1.2 mL well plate (well plate C1), while the remaining 400 µL was retained in well plate B (well plate C2). Well plate C2, containing the MTBE-containing extract, was sealed with PCR foil and stored at -30°C for lipidomics analysis (acylcarnitines and phosphocholines) via UHPLC-ESI-QTRAP-MS/MS platform[35-37].

The extract in well plate C1 was dried at 25°C under a mild nitrogen stream and reconstituted in 300 µL of 10% H₂O in MeOH, representing a 1:1 concentration ratio. Well plate C1 was then sealed with PCR foil and stored at -30°C for subsequent analysis of polar metabolites, including organic acid, keto-acids and amino acids [38-40]. For long-term storage, extracts were kept at -80°C.

Tissue Homogenization

- 2 mL Screw cap tube with 3 mm steel beads (5x)
- 100 mg Pork tissue with 300 μ L homogenization solution
- Homogenize for 5 min at level 4
- Ice bag cooling between lid and tube



Homogenate or Supernatant

Addition of Internal Standard + Protein precipitation + Extraction of polar metabolites and lipids

- 1) Pipette 50 μ L (optionally 25 μ L or 10 μ L) of tissue homogenate (or supernatant after centrifugation) into 450 μ L of ISTD in MeOH in well plate A to extract polar metabolites.

Centrifuge protein pellet and transfer the polar extract to a new well plate B

- 2) Add 50 μ L water to resuspend the protein pellet in well plate A and add 450 μ L 75% (or 25%) MTBE in MeOH to extract lipids.

Centrifuge the protein pellet and transfer the lipophilic extract to well plate B.

- 3) Split the pooled extract to well plates C1 (600 μ L; concentrate to 300 μ L) and C2 (400 μ L; use as is) for polar metabolite and lipid analysis.

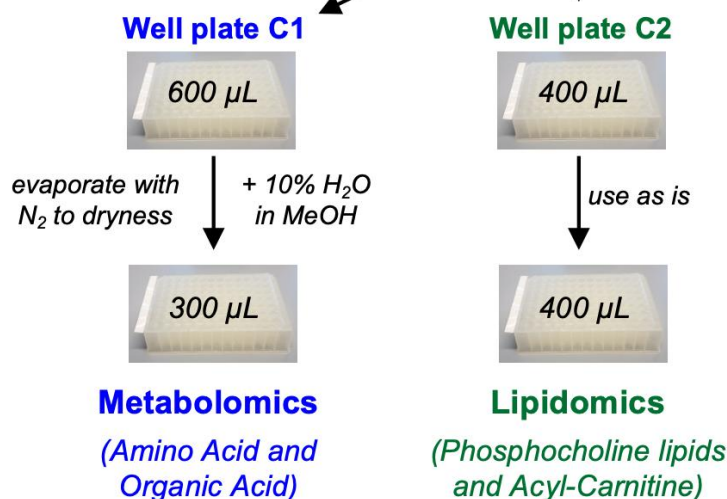


Figure 2.2. Workflow for tissue homogenization, followed by two-step extraction.

For polar metabolite extraction (well plate A), a methanol-ISTD solution was used, while lipid extraction for medium to non-polar compounds employed either 25% or 75% MTBE in MeOH. Post combining the extracts from well plate B, 400 μ L of the pooled extracts was directly utilized for lipidomics analysis (well plate C2). The remaining 600 μ L underwent evaporation, followed by reconstitution in 300 μ L of a 10% H_2O in MeOH solution for metabolomics

analysis (well plate C1). Figure is cited from Y. Hao, et al [41] under the Creative Commons CC-BY license[42].

2.2.5. Volume Adjustment for Homogenate Pipetting with Prewetting

To determine the volume correction factor when pipetting tissue homogenates with tip prewetting, four types of pipette tip conditions were weighed ($n = 5$): (A) empty tips, (B) tips retaining residual homogenate slurry (RHS) after prewetting and ejection, (C) tips containing homogenate without prewetting, and (D) tips filled with homogenate following prewetting. The prewetting process was conducted by performing multiple draw-and-eject cycles before pipetting the homogenate. This study utilized 10 μL and 200 μL TipONE pipette tips, testing pipetting volumes of 10 μL , 25 μL , and 50 μL . The pre-wetting correction factor (PWC-factor) was calculated only for homogenization solutions with a high organic solvent content, as fully aqueous PBS and 50% MeOH in PBS did not lead to tip blockage and could be pipetted directly (**Table 2.2a**, **Table 2.2b**).

The residual homogenate slurry (RHS) weight was calculated by Eq-I and Eq-III. Additionally, the weight of calculated pipetting volume (PV- I) with prewetting (Eq-II) was used to compared with the weight of right pipetting volume without prewetting (PV- II) by Eq-IV, and the weight of wrong pipetting volume after prewetting (Eq-V). The PWC-factor (%) was determined using Eq-VI and Eq-VII (**Table 2.2c**). PWC-factor-II was applied using Eq-VIII for the volume correction.

Equations:

$$\text{Eq-I} \quad \text{RHS-I} = B - A$$

$$\text{Eq-II} \quad \text{PV-I} = D - B$$

$$\text{Eq-III} \quad \text{RHS-II} = D - C$$

$$\text{Eq-IV} \quad \text{PV-II} = C - A$$

$$\text{Eq-V} \quad \text{PV} + \text{RHS} = D - A$$

$$\text{Eq-VI} \quad \text{PWC-factor-I} = (B-A) * 100 / (D-A)$$

$$\text{Eq-VII} \quad \text{PWC-factor-II} = (D-C) * 100 / (D-A)$$

$$\text{Eq-VIII} \quad \text{Concentration (corrected)} = (1 - \text{PWC-factor-II} / 100) * \text{Concentration (original)}$$

2.2.6. Extraction for Mouse Pancreas Tissue

Each mouse pancreas sample was put in a tube containing 300 μL of a 1:1 PBS/MeOH mixture (v/v) along with five 3 mm steel beads for homogenization. Homogenization was conducted for 5 minutes at intensity level 4, with cooling provided by a ice bag. For lipid and metabolite extraction, 50 μL of the homogenate ($n = 4$) was used without pre-wetting the pipette tips. The extraction process followed a two-step approach, first using MeOH with ISTD, followed by a 75% MTBE in MeOH solution. Metabolomics profiling was carried out using the same methodology for pork tissue samples.

2.2.7. Instruments and Analytical Methods

The targeted analysis was performed to quantify 20 proteinogenic amino acids, along with ornithine (Orn) and citrulline (Cit), using an Agilent 1100 HPLC system. This system included a degasser (G1379A), a binary pump (G1312A), a autosampler compatible with two plates (G1367A), a column oven (G1316A), and a 1290 thermostat (G1330B) from Agilent Technologies, Inc. (Waldbronn, Germany). The HPLC system was connected to an API 2000 triple quadrupole mass spectrometer equipped with an electrospray ionization (ESI) source, supplied by AB SCIEX Pte. Ltd. (Concord, Canada). Chromatographic separation was achieved using a Waters GmbH (Eschborn, Germany) XBridge C18 column (2.1 mm \times 150 mm, 3.5 μm) [38, 39].

For the targeted analysis of organic acids, keto-acids, and lipids, an Agilent 1260 HPLC system was employed, featuring a multi-sampler capable of handling eight plates (G7167A), a binary pump (G1312B) and a degasser (G1379B) from Agilent Technologies, Inc. (Waldbronn, Germany). This system was integrated with a MayLab

column oven (Vienna, Austria) and linked to a hybrid QTRAP 4000 mass spectrometer with an ESI source from AB SCIEX Pte. Ltd. (Concord, Canada). The separation of 15 organic and keto-acids was carried out using a Kinetex F5 column (2.1 mm × 150 mm, 2.6 µm) from Phenomenex (Aschaffenburg, Germany) [40]. Acylcarnitines, comprising 60 different analytes, were analyzed using a Kinetex EVO C18 column (2.1 mm × 150 mm, 2.6 µm) from the same manufacturer [35, 36]. Meanwhile, phosphocholine lipids—including LPCa, LPCe, PCaa, PCae, and SM, where "a" indicates acyl and "e" denotes ether—were examined using flow-injection analysis (FIA) mode without employing a chromatographic column [37].

2.2.8. Data Analysis

Data acquisition was carried out using Analyst 1.6.1, while quantitative data analysis was conducted with MultiQuant™ 3.0.3, both developed by SCIEX (Concord, Canada). Metabolite concentrations, initially measured in µmol/L, were converted to pmol/mg tissue by accounting for individual tissue weights, pipetting volumes, and, where applicable, the PWC-factor-II. Data visualization was carried out using R programming software (version 4.1.0) alongside R packages such as UpsetR [43], ComplexUpset [44], ggplot2, tidyr, scales, and dplyr, supplemented by MS Office Excel software. An in-house R script was used for automated peak integration, isotopic correction, as well as phosphatidylcholine lipid quantification.

For generating Upset plots, the complete dataset for 50 µL volumes of supernatant (S) and homogenate (H) was utilized, covering both metabolite extraction methods involving 25% and 75% MTBE in MeOH in the second extraction step. To compare extraction efficiencies, a 75% concentration threshold was applied to the highest concentration of each metabolite across the full dataset, which included results from all sample preparation conditions using 50 µL extract volumes (**Figure 2.4a**). To simplify the Upset plots visually, only intersection sizes ≥2 were displayed. A comparative Upset plot was created using a 75% concentration threshold for the most effective sample

processing condition (PBS:MeOH (1:1, v/v) for tissue homogenization coupled with 75% MTBE in MeOH in the second extraction step using homogenate). This condition was then compared to the extraction efficiencies of all other sample preparation conditions (**Figure 2.4b**).

2.3. Results and discussion

2.3.1. Temperature Managed Homogenization

The BeadRuptor 4 tissue homogenizer, despite its high efficiency and power, lacks an integrated cooling fitting, which poses a significant limitation. During homogenization with 5 * 3 mm steel beads per tube, the temperature rose unexpectedly fast, reaching nearly 30°C within 3 minutes post-thawing (**Figure 2.1a**). The primary objective was to identify an effective cooling method to maintain the homogenate temperature <15°C during homogenization period (5 min). This duration and intensity level 4 were selected to ensure robust processing of resilient biological samples, eliminating the need for subsequent re-optimization. The 15°C threshold was chosen for its practicality and ease of maintenance. Pre-freezing samples with homogenization solution and steel beads in liquid nitrogen resulted in a 2-minute delay as the samples remained frozen. Upon thawing, a rapid temperature increase of 15°C occurred within 1 minute (**Figure 2.1a**). The most effective cooling strategy maintained a consistent homogenate temperature of 12-15°C (**Figure 2.1b**), accomplished by adding a ice bag beneath the homogenizer lid (**Figure 2.1c**). Pre-cooling samples on crushed ice or at -20°C for 5 minutes before homogenization caused temperatures to rise to 28°C and 20°C, respectively, within 30 seconds (**Figure 2.1d**). Consequently, subsequent homogenization experiments utilized a 5-minute pre-cooling step at -20°C followed by icebag cooling during processing.

2.3.2. Prewetting Correction Factor for Volume Correction

The ability to pipette homogenate slurries accurately depends on the type of homogenization solvent, solvent mixtures, and pipette tip size (10 μL or 200 μL). In some cases, prewetting the pipette tip by drawing and ejecting the slurry was necessary to prevent tip blockage, while in others, prewetting was unnecessary for accurate volume measurement. It was noted that higher organic solvent content in the homogenate solution and smaller pipette tip sizes correlated with increased instances of tip blockage (**Table 2.3a**). For experiments requiring prewetting (**Table 2.3b**), a novel volume correction factor, termed the prewetting correction factor (PWC-factor), was introduced. This factor accounts for the additional volume retained in the pipette tip during prewetting, which can result in a 10% to 20% higher pipetted volume compared to non-prewetted tips. The PWC-factor-II, calculated using Eq-VII, was applied to all homogenate solutions pipetted with prewetting (**Table 2.3a**). Accurate pipetting is critical in the initial sample preparation step (**Figure 2.2**), which involves transferring biological samples into MeOH-ISTD solution. The PWC-factor-II was determined for four homogenization solutions, pipette tip size 10 μL and 200 μL , homogenate volume 10 μL , 25 μL , and 50 μL ($n = 5$ tips with each weighed 5 times).

For comparative purposes, **Table 2.3b** also includes results for PWC-factor-I (Eq-VI). Prolonged homogenization for 1 to 2 minutes did not reduce the particle size of solids in the homogenate. The size and volume of these solids increased with higher organic solvent content in the homogenization solution, likely due to protein precipitation in biological samples exposed to organic solvents. These solids are presumed to consist of a mixture of cell debris and protein precipitates. Once centrifuged and stored at low temperatures for extended periods, the resulting pellet cannot be re-dispersed into a homogeneous slurry. Consequently, metabolite and lipid extraction should be conducted immediately after tissue homogenization, ideally on the same day.

Table 2.3a. Frequency of pipette tip blockage caused by the homogenate precipitate (n out of 10) and PWC-factor-II.

	Tip Blockage Frequency			PWC-Factor-II \pm SD [%]		
	10	200	200	10	200	200
Pipette Tip Size [μ L]	10	25	50	10	25	50
PBS:MeOH (1:1)	2*	0	0	0*	0	0
PBS:MeOH (1:3)	6	0	1*	14.62 \pm 4.24	0	0*
MeOH	5	0	1*	15.62 \pm 6.26	0	0*
PBS:EtOH (15:85)	8	4	6	15.20 \pm 5.39	10.4 \pm 2.62	10.72 \pm 0.79
IPA	9	7	8	14.59 \pm 8.31	10.69 \pm 3.31	11.25 \pm 1.39

For frequencies ≤ 3 (*), experiments were repeated with new pipette tips without prewetting. Table is cited from Y. Hao, et al [41] under the Creative Commons CC-BY license[42].

Table 2.3b. Pipette tip prewetting for different homogenate solutions.

		Homogenate			Supernatant		
Pipette Tip Size [μ L]		10	200	200	10	200	200
Pipetted Volume [μ L]		10	25	50	10	25	50
25% MTBE	PBS	No	No	No	No	No	No
	PBS:MeOH 1:1	No	No	No	No	No	No
	PBS:MeOH 1:3	Yes	No	No	No	No	No
	MeOH	Yes	No	No	No	No	No
	PBS:EtOH 15:85	Yes	Yes	Yes	No	No	No
	IPA	Yes	Yes	Yes	No	No	No
75% MTBE	PBS	NA*	No	No	NA*	No	No
	PBS:MeOH 1:1	NA*	No	No	NA*	No	No
	PBS:MeOH 1:3	NA*	No	No	NA*	No	No
	MeOH	NA*	No	No	NA*	No	No
	PBS:EtOH 15:85	NA*	Yes	Yes	NA*	No	No
	IPA	NA*	Yes	Yes	NA*	No	No

NA: not applicable (experiment was not performed). Table is cited from Y. Hao, et al [41] under the Creative Commons CC-BY license[42].

Table 2.3c. Prewetting volume correction factor (PWC-factor) determination (n = 5 tips with each weighed 5 times) for different homogenization solvents

Homogenization Solvent		Homogenate [mg] (<i>n</i> = 5)			PWC Factor [%]		
	Pipette Tip [μL]	10	200	200	10	200	200
	Pipette Vol. [μL]	10	25	50	10	25	50
PBS	RHS-I	---	---	---			
	PV-I	---	---	---	---	---	---
	RHS-II	---	---	---			
	PV-II	---	---	---	---	---	---
	PV + RHS ⁵	---	---	---			
PBS:MeOH (1:1)	RHS-I	---	---	---			
	PV-I	---	---	---	---	---	---
	RHS-II	---	---	---			
	PV-II	---	---	---	---	---	---
	PV + RHS	---	---	---			
PBS:MeOH (1:3)	RHS-I	2.19 ± 0.36	---	---			
	PV-I	8.67 ± 0.46	---	---	20.18	---	---
	RHS-II	1.59 ± 0.46	---	---			
	PV-II	9.27 ± 0.56	---	---	14.62	---	---
	PV + RHS	10.86 ± 0.46	---	---			
MeOH	RHS-I	2.12 ± 0.63	---	---			
	PV-I	8.10 ± 0.64	---	---	20.70	---	---
	RHS-II	1.60 ± 0.64	---	---			
	PV-II	8.62 ± 0.43	---	---	15.62	---	---
	PV + RHS	10.22 ± 0.64	---	---			
PBS:EtOH (15:85)	RHS-I	1.92 ± 0.25	3.88 ± 0.76	6.99 ± 0.40			
	PV-I	7.92 ± 0.53	21.96 ± 0.68	45.34 ± 0.41	19.55	15.02	13.36
	RHS-II	1.50 ± 0.53	2.69 ± 0.68	5.61 ± 0.41			
	PV-II	8.34 ± 0.64	23.15 ± 0.80	46.73 ± 1.03	15.20	10.40	10.72
	PV + RHS	9.84 ± 0.53	25.84 ± 0.68	52.34 ± 0.41			
IPA	RHS-I	2.07 ± 0.74	3.61 ± 0.88	6.72 ± 0.65			
	PV-I	7.20 ± 0.77	21.80 ± 0.83	45.08 ± 0.72	22.32	14.34	12.98
	RHS-II	1.35 ± 0.77	2.69 ± 0.83	5.83 ± 0.72			
	PV-II	7.91 ± 0.72	22.46 ± 0.39	45.98 ± 0.51	14.59	10.69	11.25
	PV + RHS	9.26 ± 0.77	25.15 ± 0.83	51.81 ± 0.72			

---: no pipette tip blockage was observed. Table is cited from Y. Hao, et al [41] under the Creative Commons CC-BY license[42].

2.3.3. Volume Choice of Homogenate and Extract

The analysed metabolites were categorized into substance classes based on their polarity and lipophilicity, ranging from organic acids and amino acids to acylcarnitines, lyso-phosphatidylcholines (Lyso-PCs), phosphatidylcholines (PCs), and

sphingomyelins (SMs). Within each class, lipophilicity increases with longer alkyl-chain lengths, as demonstrated in **Figure 2.3a** for acylcarnitines (Carn 4:0 < Carn 9:0 < Carn 16:0) and phospholipids (LPC < LPC 24:0; PC 18:2 < PC 38:0; SM 26:4 < SM 42:1). Additionally, the presence of polar functional groups, such as hydroxyl (OH) and carboxylic acid (DC), further influences polarity, as seen in acylcarnitines (Carn 4:0 DC > Carn 4:0 OH > Carn 4:0). Unless specified, PC and LPC compounds are of the di-acyl and mono- types (PCaa and LPCa), while their acyl-alkyl and mono-alkyl variants (PCae and LPCe) were analyzed but not discussed in detail. Given the extensive dataset of 401 metabolites, changes in metabolite profiles were evaluated based on extract type (supernatant vs. homogenate), homogenate solution polarity, extract volume (10 μ L vs. 25 μ L vs. 50 μ L), and lipid extraction solution (75% MTBE vs. 25% MTBE), with results presented for selected metabolites. Concentrations were calculated to pmol/mg tissue from μ mol/L, accounting for extract volume, tissue weight and pipette tip prewetting.

To facilitate comparison of extraction efficiencies, results were normalized to a 50 μ L extraction volume in **Figure 2.3b**, while **Figure 2.3a** focuses on 50 μ L of supernatant and homogenate data. A consistent tissue-to-solution ratio of 1:3 (100 mg tissue to 300 μ L homogenization solution) was maintained. The homogenization solutions spanned a wide polarity range, including PBS, PBS:MeOH (1:1), PBS:MeOH (1:3), PBS:EtOH (15:85), MeOH, and IPA. Notably, PBS:EtOH (15:85) and IPA are recommended in literature for use with Biocrates metabolomics and lipidomics kits [45] and are thus compared directly in **Figure 2.3a** and **Figure 2.3b**. Pipetting homogenate slurries proved challenging for small volumes with high organic solvent content, particularly for highly lipophilic ones. However, homogenate slurries provided more consistent results for 25 μ L and 50 μ L volumes compared to supernatants and were less dependent on homogenization solution type. For long-chain lipids like SM 42:1 (**Figure 2.3a**), solutions with low organic content significantly reduced extraction efficiency from supernatants, whereas homogenates yielded reproducible results

independent of solution or volume (**Figure 2.3b**). While lipophilic solvents like IPA generally enhanced lipid extraction, this trend was not always evident in supernatants (**Figure 2.3a**). Surprisingly, PBS:MeOH (1:1) or PBS:MeOH (1:3) combined with 75% MTBE in MeOH outperformed IPA for both lipid and polar metabolite extraction.

For polar metabolites, adding organic solvents like MeOH (50% and 75%) or EtOH (85%) to PBS improved recoveries compared to pure PBS. Quantitative results for polar compounds were comparable between homogenates and supernatants, with higher recoveries using 75% MTBE in MeOH versus 25% MTBE in MeOH. Smaller homogenate volumes were preferable for lipids, while polar metabolites showed this trend only with polar homogenization solutions (**Figure 2.3b**). Overall, PBS:MeOH (1:1) or PBS:MeOH (1:3) combined with 75% MTBE in MeOH provided higher recoveries, particularly for long-chain lipids like Carn 16:0, LPCa 24:0, PCaa 38:0, and SM 42:1. The choice of homogenization and extraction solutions was critical for achieving adequate recovery rates, especially for LPC 24:0. Within acylcarnitines, Carn 4:0 DC and Carn 4:0 showed a preference for PBS with 25% MTBE in MeOH, while long-chain acylcarnitines required homogenates with 75% MTBE in MeOH. Polar metabolites like Asp, which contains a carboxylic acid group, mirrored Carn 4:0 DC in favoring 25% MTBE, whereas amino acids like Ser and Ile showed comparable results for both 25% and 75% MTBE in MeOH (**Figure 2.3a**).

In parallel, blank samples (three types) were prepared to assess potential contamination [46, 47]: Blank 1 (tissue homogenization consumables), Blank 2 (metabolite and lipid extraction process), and Blank 3 (solvents and LC-MS/MS system). Blank 3 exhibited the highest contamination levels, suggesting that background contaminants primarily originated from the LC-MS/MS system and solvents (**Table 2.4**).

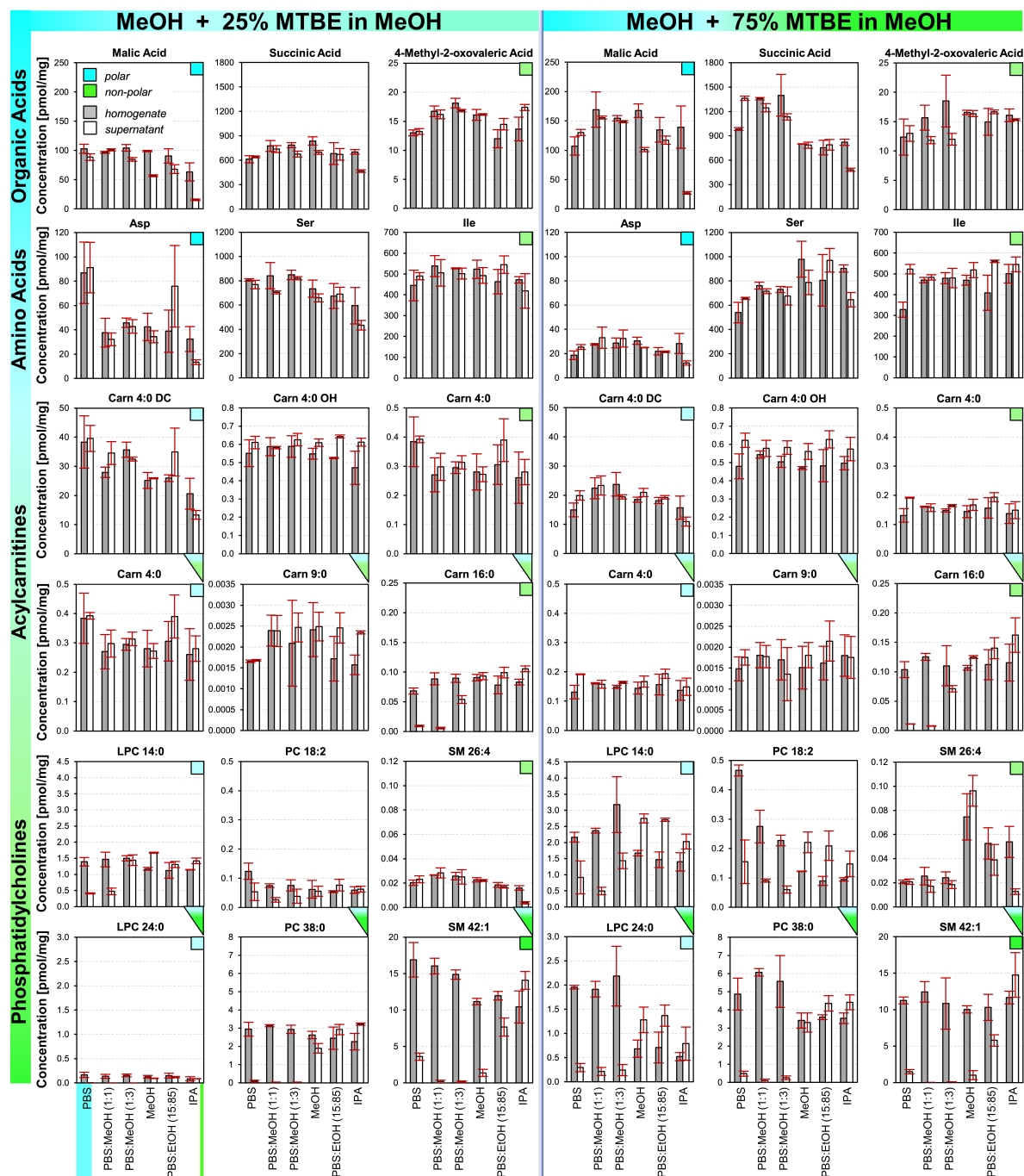
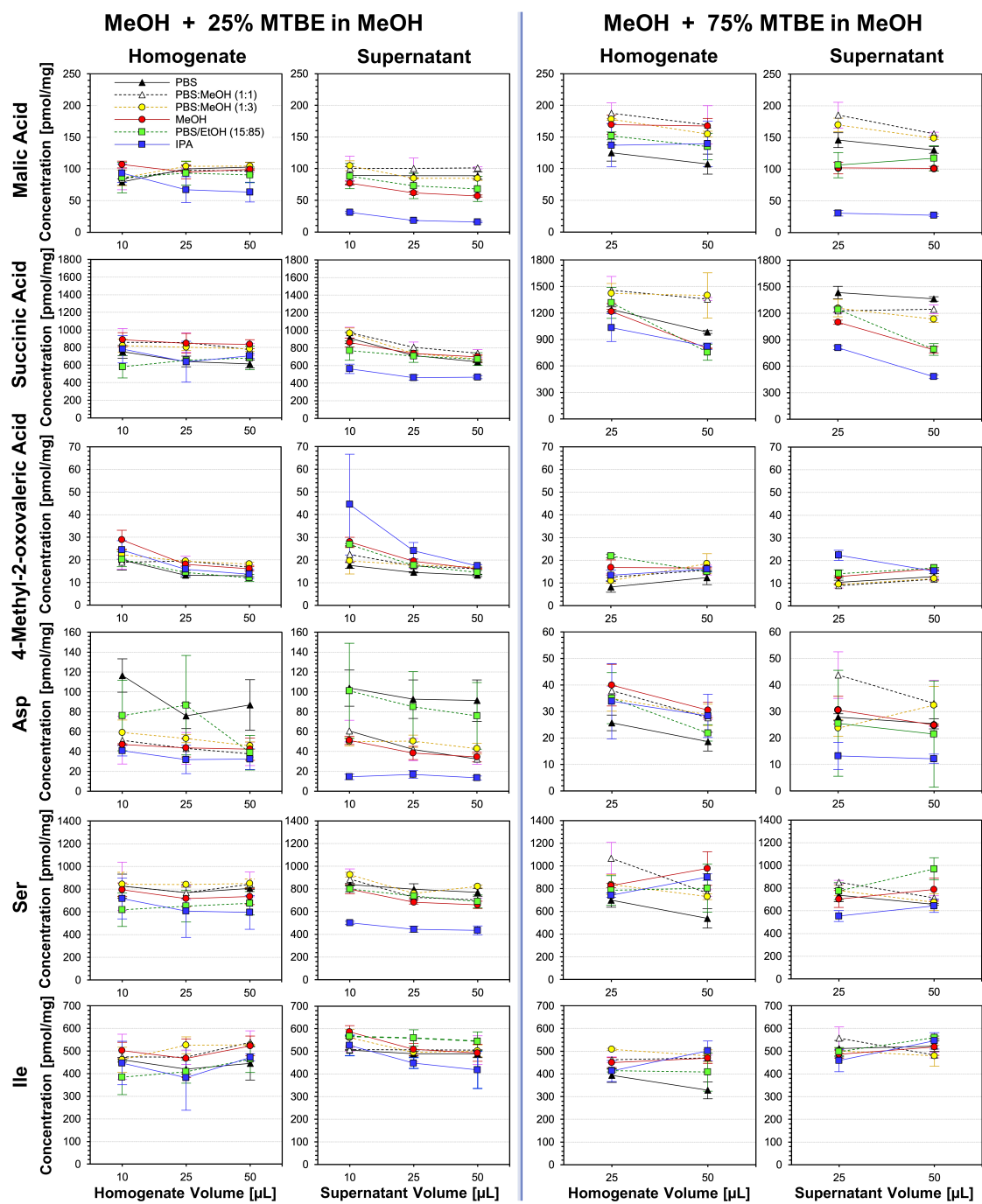
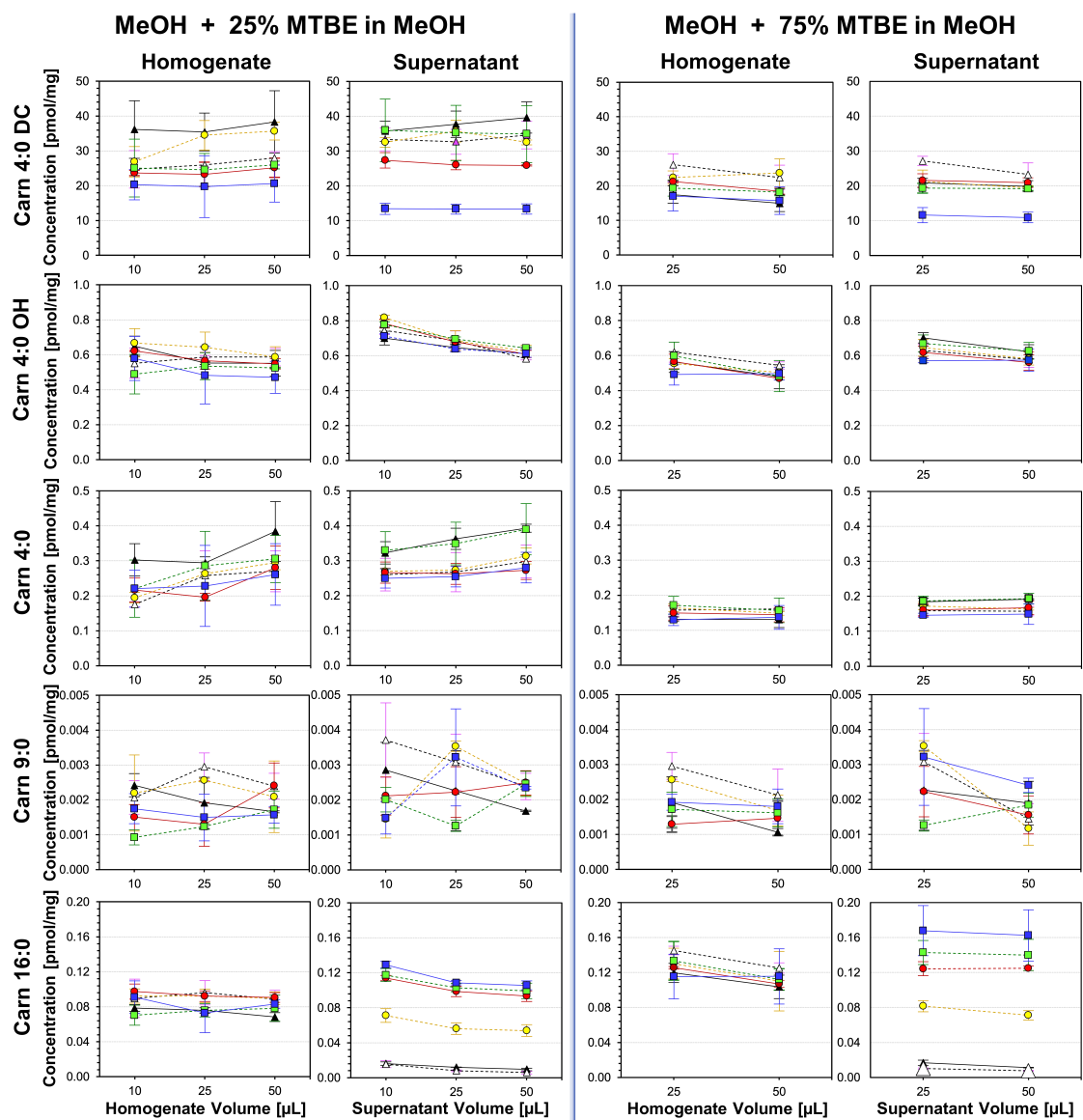


Figure 2.3a. Recoveries of selected lipid and polar metabolite for pork tissue samples (Bar charts).

Tissue samples were homogenized with six different solutions. Subsequently, 50 μL of supernatant and homogenate were processed with the in-house two-step extraction method. Figure is cited from Y. Hao, et al [41] under the Creative Commons CC-BY license[42].



(Figure 2.3b continued in next two pages.)



(Figure 2.3b continued in next two pages.)

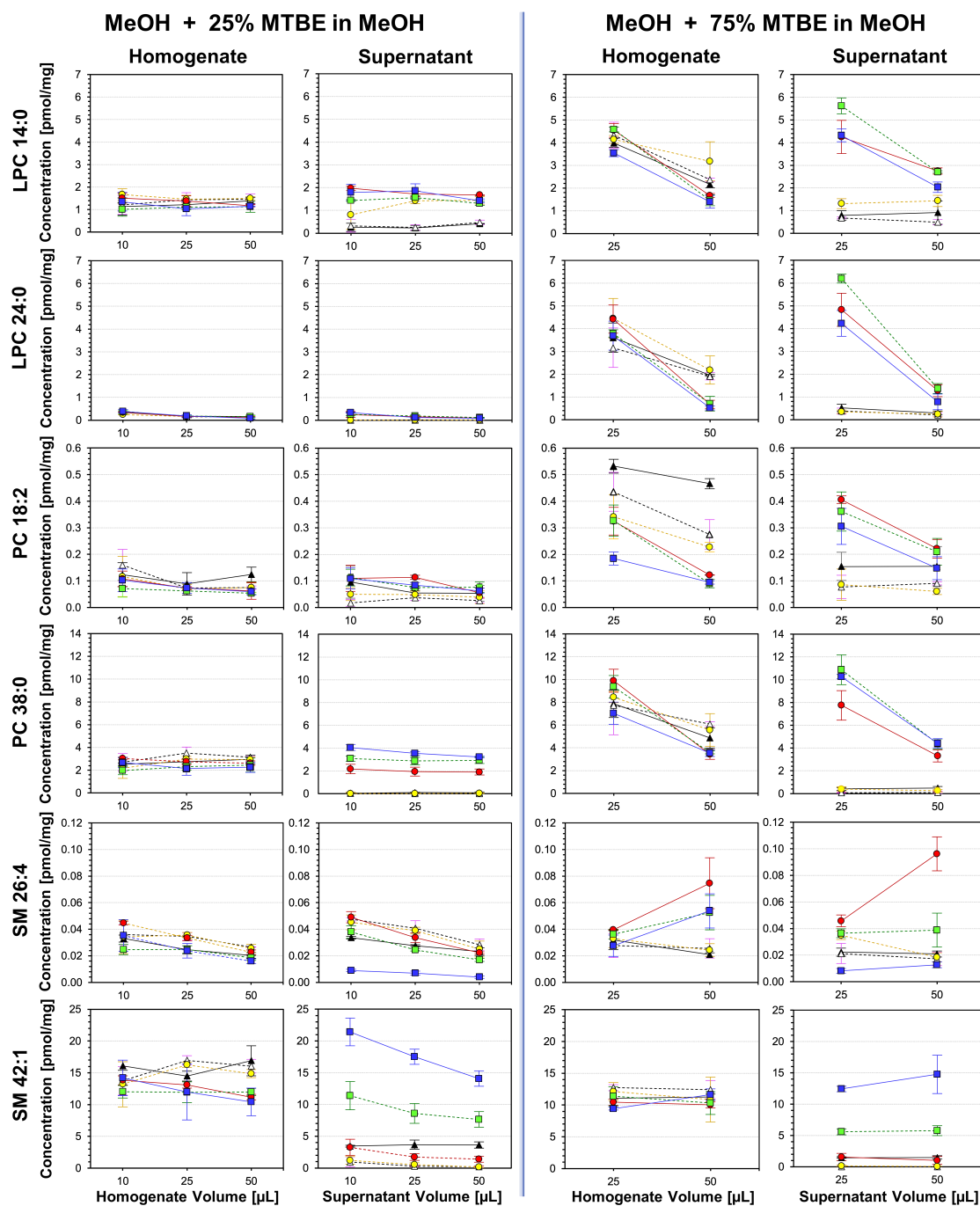


Figure 2.3b. Recoveries of selected lipid and polar metabolite for pork tissue samples (Line charts).

Tissue samples were homogenized with six different solutions. Subsequently, 50 μL of supernatant and homogenate were processed with the in-house two-step extraction method. Figure is cited from Y. Hao, et al [41] under the Creative Commons CC-BY license[42].

Table 2.4. Background contamination shown for a selection of metabolites.

	Metabolite	Blank-1 [pmol/mg (%)]	Blank-2 [pmol/mg (%)]	Blank-3 [pmol/mg (%)]
Organic Acids	Malic Acid	0.57 ± 0.18 (0.34)	0.31 ± 0.25 (0.18)	0.61 ± 0.34 (0.36)
	Succinic Acid	NA	NA	NA
	4-Methyl-2-oxo-valeric Acid	NA	NA	NA
Amino Acids	Asp	0.46 ± 0.66 (1.68)	1.48 ± 0.10 (5.37)	NA
	Ser	NA	NA	NA
	Ile	3.01 ± 0.48 (0.64)	2.43 ± 0.07 (0.52)	3.22 ± 0.55 (0.68)
Acylcarnitines	Carn 4:0 DC	0.00054 ± 0.00016 (0.0024)	0.00070 ± 0.000069 (0.0031)	0.00043 ± 0.00012 (0.0019)
	Carn 4:0 OH	0.00021 ± 0.000064 (0.038)	0.00026 ± 0.00011 (0.048)	0.00015 ± 0.000035 (0.028)
	Carn 4:0	0.000038 ± 0.000016 (0.024)	0.000039 ± 0.000024 (0.025)	0.0011 ± 0.00011 (0.66)
	Carn 9:0	0.00017 ± 0.000073 (8.23)	0.00020 ± 0.000076 (9.26)	0.00027 ± 0.00010 (12.74)
	Carn 16:0	0.00059 ± 0.00011 (0.47)	0.00069 ± 0.0001433 (0.55)	0.00062 ± 0.00016 (0.50)
Phosphatidylcholines	LPC 14:0	0.12 ± 0.081 (5.25)	0.30 ± 0.17 (12.73)	0.64 ± 0.30 (26.97)
	LPC 24:0	0.035 ± 0.018 (1.85)	0.069 ± 0.23 (3.62)	NA
	PC 18:2	0.032 ± 0.022 (11.76)	0.017 ± 0.021 (6.03)	0.072 ± 0.055 (26.33)
	PC 38:0	0.0090 ± 0.013 (0.15)	0.0054 ± 0.0076 (0.088)	0.027 ± 0.11 (0.45)
	SM 26:4	0.016 ± 0.0030 (63.48)	0.015 ± 0.0028 (57.03)	0.018 ± 0.0046 (69.66)
	SM 42:1	NA	NA	NA

The specific experimental condition was using PBS:MeOH (1:1) as the homogenization solution combined with lipid extraction using 75% MTBE in MeOH using 50 µL “extract” volume (Mean ± SD (%-contribution)). NA: not applicable, since no signal was detected. Table is cited from Y. Hao, et al [41] under the Creative Commons CC-BY license[42].

2.3.4. Comparison of Metabolite Extraction Efficiencies

Upset plots proved effective for visualizing extraction efficiencies in complex datasets [7], outperforming Venn diagrams [17] for comparisons involving more than four datasets. To assess and compare the extraction efficiencies of all metabolites, a threshold (Threshold A)—set at 75% of the largest metabolite concentration—was applied to each metabolite across all homogenization test solutions. This analysis focused exclusively on 50 µL supernatant and homogenate samples extracted with

either 25% MTBE or 75% MTBE. **Figure 2.4a** shows the Upset plot which reveals that PBS:MeOH (1:1) achieved the highest extraction recoveries and the greatest number of extracted metabolites, followed by PBS:MeOH (1:3) and PBS, particularly when combined with homogenate extraction using 75% MTBE. PBS:EtOH (15:85) ranked fourth, especially in the case of supernatant extraction with 75% MTBE. In contrast, IPA used for tissue homogenization paired with 25% MTBE for homogenate extraction performed the worst, likely due to the high solid content generated during IPA homogenization, resulting in thick, clumpy slurries that are challenging to pipette, even with 200 μ L pipette tips and pre-wetting.

Figure 2.4b shows the Upset plot generated by applying a second threshold (Threshold B)—75% of the metabolite concentrations from the top-performing condition, PBS:MeOH (1:1)—and all sample preparation conditions were compared with PBS:MeOH (1:1), the same top four conditions were identified. However, PBS:MeOH (1:1) combined with 25% MTBE for supernatant lipid extraction emerged as the least effective option.

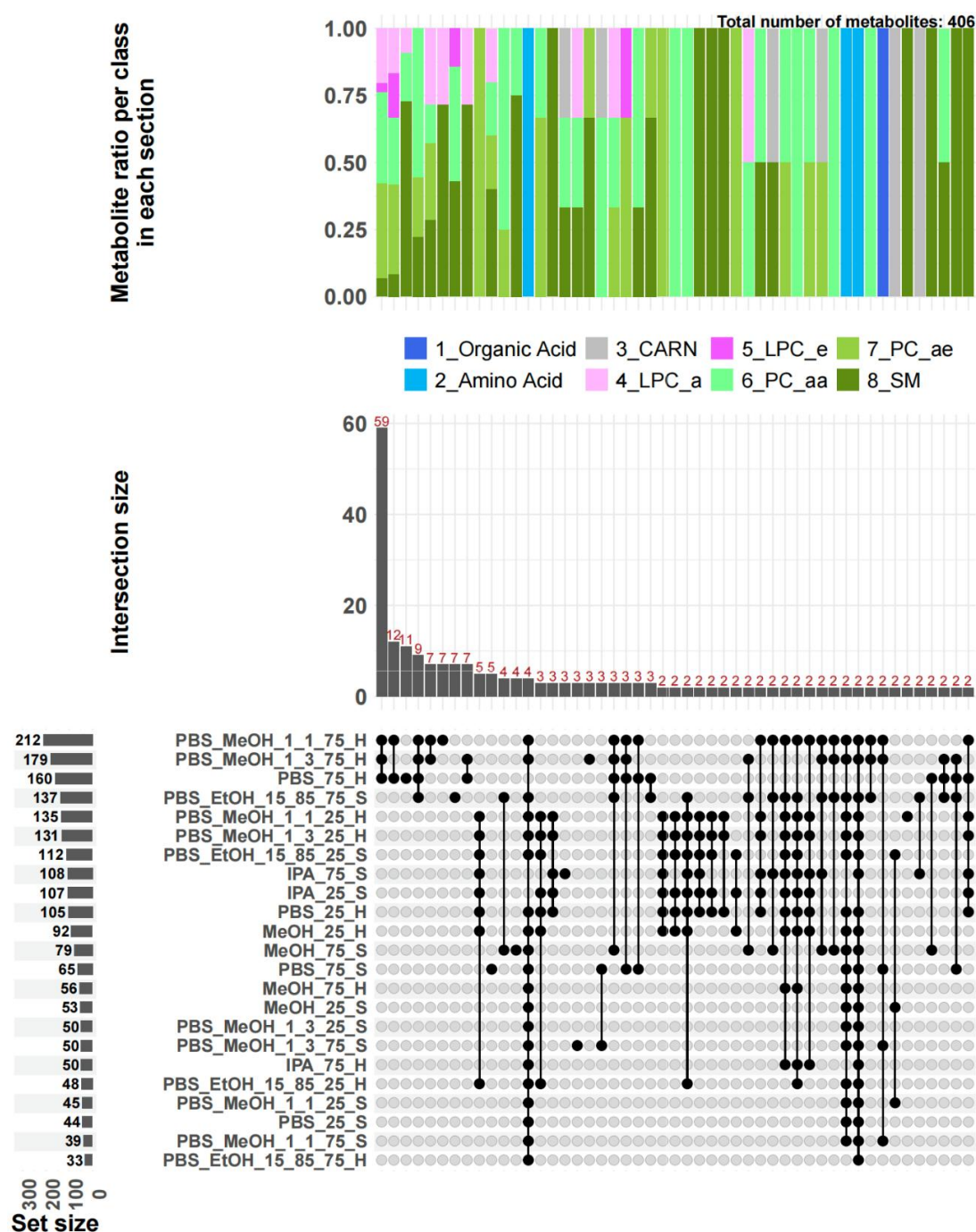
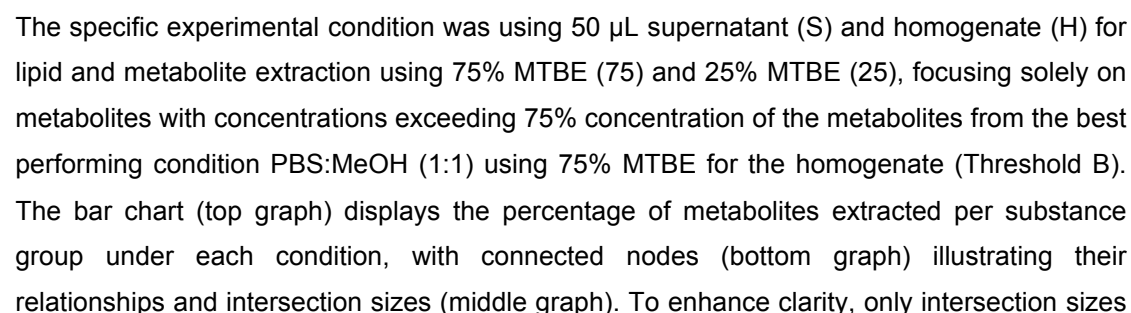


Figure 2.4a. Upset Plot Analysis of Metabolite Extraction Recoveries Across Homogenization Solutions (Threshold A).

The specific experimental condition was using 50 μ L supernatant (S) and homogenate (H) for lipid and metabolite extraction using 75% MTBE (75) and 25% MTBE (25), focusing solely on metabolites with concentrations exceeding 75% of the highest concentration observed across all sample preparations (Threshold A). The bar chart (top graph) displays the percentage of metabolites extracted per substance group under each condition, with connected nodes (bottom graph) illustrating their relationships and intersection sizes (middle graph). To enhance clarity, only intersection sizes ≥ 2 were displayed. Figure is cited from Y. Hao, et al [41] under the Creative Commons CC-BY license[42].



≥2 were displayed. Figure is cited from Y. Hao, et al [41] under the Creative Commons CC-BY license[42].

2.3.5 Mouse Pancreas Tissue

Figure 5 illustrates the outcomes of metabolite extraction from three pancreas tissue samples (A, B, and C; 50 mg ± 10 mg) obtained from three distinct mice (M-1, M-2, and M-3). Homogenization was conducted using a PBS:MeOH mixture (1:1), followed by lipid extraction of 50 µL homogenate using a 75% MTBE protocol. Given the small tissue weight, metabolite extractions were processed in quadruplicates for each homogenization experiment. Generally, error bars were smaller for higher-concentration metabolites and increased as metabolite concentrations decreased.

The three pancreas tissue pieces from each mouse were analysed in randomly, without regard to their anatomical location. The final quantitative results were normalized to tissue weight, with intermediate µmol/L values switched to pmol/mg tissue. Mouse M-1 was sacrificed at 17 weeks, M-2 and M-3 were sacrificed 2 weeks early. Despite their minimal age difference and shared genetic background, biological heterogeneity among mice likely contributed to variations in metabolite profiles. Additionally, anatomical differences, such as variations in blood supply and pancreas islet distribution [48], may account for the differing metabolite profiles observed in the samples from the same mouse.

Metabolites such as PC 18:2, Carn 16:0 and malic acid exhibited different concentrations between the two age groups, whereas Carn 4:0 DC showed no significant variations across tissue sections or different mice. Concentration spikes in specific tissue pieces could reflect varying metabolic activities in different anatomical regions of the pancreas. However, limited research has explored this phenomenon, highlighting a promising area for future studies.

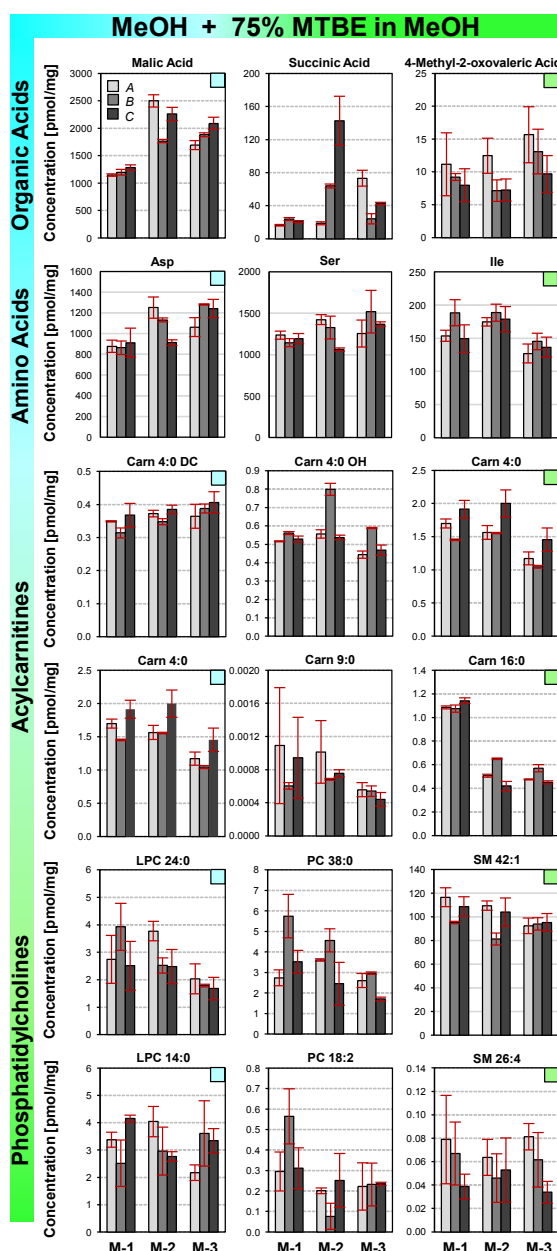


Figure 2.5. Recoveries of selected lipid and polar metabolite for 9 mouse pancreas tissue pieces from three mice (Bar charts).

9 pancreas tissue pieces (A, B, and C of each mouse among three mice M-1, M-2 and M3) were homogenized with 300 μ L of PBS:MeOH (1:1) with 5 * 3 mm steel beads for 5 min at level 4 with ice bag under the homogenizer lid. Subsequently, 50 μ L of supernatant and homogenate were processed with the optimized extraction method using MeOH and 75% MTBE in MeOH in turn. Figure is cited from Y. Hao, et al [41] under the Creative Commons CC-BY license[42].

2.4. Conclusions

This study outlines the optimization of tissue homogenization and metabolite extraction protocols, focusing on the comprehensive recovery of polar and very lipophilic metabolites. By evaluating six homogenization solutions, two lipid extraction methods, and three extract volumes, a total of 60 conditions were analysed using technical replicates $n = 4$ for approximately 400 metabolites and lipids. In alignment with green analytical chemistry (GAC) principles [49], only non-halogenated solvents were utilized, and waste was minimized through the use of 96-well plate formats and reduced solvent volumes. The study also introduced a novel prewetting correction factor (PWC-factor) for accurate homogenate pipetting and explored cooling strategies during homogenization. Quantification of lipid and metabolite was performed using a targeted HPLC-ESI-QTRAP-MS/MS platform, encompassing four analytical modules for amino acids, organic acids, acylcarnitines, and phosphocholine lipids.

PBS:MeOH (1:1), PBS:MeOH (1:3), and PBS demonstrated superior extraction efficiencies for polar metabolites, with homogenates outperforming supernatants. Recoveries of metabolites with high lipophilicity were also significantly higher in homogenates. While MeOH and IPA improved lipid extraction from supernatants, combining MeOH with PBS and employing a two-step extraction procedure (MeOH for polar metabolites and 75% MTBE in MeOH for lipids) yielded higher reproducibility and recovery rates. Increased organic solvent content led to higher solid content in homogenates, causing pipette tip blockages, particularly with 10 μL tips. In such cases, the PWC-factor can be applied, though its use is not recommended by the authors. The solids in homogenates, likely composed of cell debris and protein precipitates, acted as adsorbents, reducing lipid extraction efficiency from supernatants. While higher organic solvent content improved lipid recovery from supernatants, it also increased polar metabolite loss.

The study deliberately separated homogenization (300 μL) from metabolite extraction (25 μL or 50 μL homogenate), further dividing the extraction into polar metabolites (450

μL MeOH) and lipids (450 μL 75% MTBE in MeOH). This approach, inspired by liquid-liquid extraction principles, enhanced overall extraction efficiency, metabolite coverage, and reproducibility.

The optimal condition identified was PBS:MeOH (1:1) coupled with the homogenate extraction approach using a two-step procedure, MeOH and 75% MTBE in MeOH. However, alternative combinations of homogenization solutions, extract types (supernatant or homogenate), and extraction conditions hold the potential to yield tissue compartment-specific insights. For example, low-organic homogenization solutions combined with supernatant extraction may primarily recover polar metabolites, whereas the presented method aims for comprehensive polar and lipid profiling. While this study addressed numerous experimental factors influencing metabolic profiles, extra parameters such as tissue-to-homogenate volume ratios, tissue type, tissue weight, and organ-specific sections remain to be fully explored. These will be detailed in future research. A preliminary investigation of 9 pancreas tissue sections from three mice revealed significant metabolic profile variations based on anatomical location, highlighting the need for further exploration in this area.

2.5. References

- [1] A. Matsika, R. Gallagher, M. Williams, C. Joy, E. Lowe, G. Price, L. Webb, L. Marquart, A. Pelecanos, J. Harraway, D.J. Venter, J.E. Armes, DNA extraction from placental, fetal and neonatal tissue at autopsy: what organ to sample for DNA in the genomic era?, *Pathology* 51(7) (2019) 705-710. <https://doi.org/10.1016/j.pathol.2019.09.001>.
- [2] Y. Gao, X. Zhao, sncRiboTag-Seq: cell-type-specific RiboTag-Seq for cells in low abundance in mouse brain tissue, *STAR protocols* 2(1) (2021) 100231. <https://doi.org/10.1016/j.xpro.2020.100231>.
- [3] A.A. Karpiński, J.C. Torres Elguera, A. Sanner, W. Konopka, L. Kaczmarek, D. Winter, A. Konopka, E. Bulska, Study on Tissue Homogenization Buffer Composition

for Brain Mass Spectrometry-Based Proteomics, *Biomedicines* 10(10) (2022) 2466. <https://doi.org/10.3390/biomedicines10102466>.

[4] P.B. Naidu, P. Ponmurugan, M.S. Begum, K. Mohan, B. Meriga, R. RavindarNaik, G. Saravanan, Diosgenin reorganises hyperglycaemia and distorted tissue lipid profile in high-fat diet-streptozotocin-induced diabetic rats, *J Sci Food Agric* 95(15) (2015) 3177-82. <https://doi.org/10.1002/jsfa.7057>.

[5] J. Berg, J. Tymoczko, L. Stryer, Each Organ Has a Unique Metabolic Profile, *Biochemistry*, W.H.Freeman Co Ltd., New York, 2006, pp. 851-854.

[6] K. Kishida, N. Furusawa, Simultaneous determination of sulfamonomethoxine, sulfadimethoxine, and their hydroxy/N(4)-acetyl metabolites with gradient liquid chromatography in chicken plasma, tissues, and eggs, *Talanta* 67(1) (2005) 54-8. <https://doi.org/10.1016/j.talanta.2005.02.005>.

[7] B. Wancewicz, M.R. Pergande, Y. Zhu, Z. Gao, Z. Shi, K. Plouff, Y. Ge, Comprehensive Metabolomic Analysis of Human Heart Tissue Enabled by Parallel Metabolite Extraction and High-Resolution Mass Spectrometry, *Anal Chem* 96(15) (2024) 5781-5789. <https://doi.org/10.1021/acs.analchem.3c04353>.

[8] S.W. Gooding, M.A. Chrenek, S. Ferdous, J.M. Nickerson, J.H. Boatright, Set screw homogenization of murine ocular tissue, including the whole eye, *Mol Vis* 24 (2018) 690-699.

[9] S.C. Yan, Z.F. Chen, H. Zhang, Y. Chen, Z. Qi, G. Liu, Z. Cai, Evaluation and optimization of sample pretreatment for GC/MS-based metabolomics in embryonic zebrafish, *Talanta* 207 (2020) 120260. <https://doi.org/10.1016/j.talanta.2019.120260>.

[10] M. Horing, S. Krautbauer, L. Hiltl, V. Babl, A. Sigrüener, R. Burkhardt, G. Liebisch, Accurate Lipid Quantification of Tissue Homogenates Requires Suitable Sample Concentration, Solvent Composition, and Homogenization Procedure-A Case Study in Murine Liver, *Metabolites* 11(6) (2021) 365. <https://doi.org/10.3390/metabo11060365>.

[11] T. Zuellig, M. Troetzmueller, H.C. Koefeler, Lipidomics from sample preparation to data analysis: a primer, *Anal Bioanal Chem* 412(10) (2020) 2191-2209. <https://doi.org/10.1007/s00216-019-02241-y>.

[12] M. Horing, C.S. Ejlsing, S. Krautbauer, V.M. Ertl, R. Burkhardt, G. Liebisch, Accurate quantification of lipid species affected by isobaric overlap in Fourier-transform

mass spectrometry, J Lipid Res 62 (2021) 100050.
<https://doi.org/10.1016/j.jlr.2021.100050>.

[13] C. Andresen, T. Boch, H.M. Gegner, N. Mechtel, A. Narr, E. Birgin, E. Rasbach, N. Rahbari, A. Trumpp, G. Poschet, D. Hübschmann, Comparison of extraction methods for intracellular metabolomics of human tissues, *Front Mol Biosci* 9 (2022) 932261.
<https://doi.org/10.3389/fmolb.2022.932261>.

[14] S. Redanz, A. Podbielski, P. Warnke, Improved microbiological diagnostic due to utilization of a high-throughput homogenizer for routine tissue processing, *Diagn Microbiol Infect Dis* 82(3) (2015) 189-93.
<https://doi.org/10.1016/j.diagmicrobio.2015.03.018>.

[15] D. Hicks, M.J. Ryan, A. Allahham, L.W. Barrett, S. Lee, B. Bartlett, H. Ludewick, N.C. Ward, R.L. Loo, G. Dwivedi, J.K. Nicholson, J. Wist, E. Holmes, N. Gray, Evaluation of Tissue-Specific Extraction Protocols for Comprehensive Lipid Profiling, *Analytica Chimica Acta* (2025) 343791.
<https://doi.org/https://doi.org/10.1016/j.aca.2025.343791>.

[16] A.M. Jones, M.T. Van de Wyngaerde, E.T. Machtinger, E.G. Rajotte, T.C. Baker, Choice of Laboratory Tissue Homogenizers Matters When Recovering Nucleic Acid From Medically Important Ticks, *J Med Entomol* 57(4) (2020) 1221-1227.
<https://doi.org/10.1093/jme/tjaa006>.

[17] P. Cuevas-Delgado, N. Warmuzińska, K. Łuczykowski, B. Bojko, C. Barbas, Exploring sample treatment strategies for untargeted metabolomics: A comparative study of solid phase microextraction (SPME) and homogenization with solid-liquid extraction (SLE) in renal tissue, *Anal Chim Acta* 1312 (2024) 342758.
<https://doi.org/10.1016/j.aca.2024.342758>.

[18] D.B. Dias, R. Fritsche-Guenther, F. Gutmann, G.N. Duda, J. Kirwan, P.S.P. Poh, A Comparison of Solvent-Based Extraction Methods to Assess the Central Carbon Metabolites in Mouse Bone and Muscle, *Metabolites* 12(5) (2022).
<https://doi.org/10.3390/metabo12050453>.

[19] J. Balog, L. Sasi-Szabó, J. Kinross, M.R. Lewis, L.J. Muirhead, K. Veselkov, R. Mirnezami, B. Dezső, L. Damjanovich, A. Darzi, J.K. Nicholson, Z. Takáts, Intraoperative tissue identification using rapid evaporative ionization mass

spectrometry, *Science translational medicine* 5(194) (2013) 194ra93.
<https://doi.org/10.1126/scitranslmed.3005623>.

[20] E. Manoli, S. Mason, L. Ford, A. Adebesein, Z. Bodai, A. Darzi, J. Kinross, Z. Takats, Validation of Ultrasonic Harmonic Scalpel for Real-Time Tissue Identification Using Rapid Evaporative Ionization Mass Spectrometry, *Anal Chem* 93(14) (2021) 5906-5916.
<https://doi.org/10.1021/acs.analchem.1c00270>.

[21] M. Stoeckli, P. Chaurand, D.E. Hallahan, R.M. Caprioli, Imaging mass spectrometry: a new technology for the analysis of protein expression in mammalian tissues, *Nat Med* 7(4) (2001) 493-6. <https://doi.org/10.1038/86573>.

[22] C. Sun, A. Wang, Y. Zhou, P. Chen, X. Wang, J. Huang, J. Gao, X. Wang, L. Shu, J. Lu, W. Dai, Z. Bu, J. Ji, J. He, Spatially resolved multi-omics highlights cell-specific metabolic remodeling and interactions in gastric cancer, *Nat Commun* 14(1) (2023) 2692. <https://doi.org/10.1038/s41467-023-38360-5>.

[23] F. Li, R. Karongo, D. Mavridou, J. Horak, A. Sievers-Engler, M. Lämmerhofer, Automated sample preparation with 6-Aminoquinolyl-N-hydroxysuccinimidyl carbamate and iodoacetamide derivatization reagents for enantioselective liquid chromatography tandem mass spectrometry amino acid analysis, *J Chromatogr A* 1708 (2023) 464349.
<https://doi.org/10.1016/j.chroma.2023.464349>.

[24] E.G. Bligh, W.J. Dyer, A rapid method of total lipid extraction and purification, *Canadian journal of biochemistry and physiology* 37(8) (1959) 911-7.
<https://doi.org/10.1139/o59-099>.

[25] C. Calderón, C. Sanwald, J. Schlotterbeck, B. Drotleff, M. Lämmerhofer, Comparison of simple monophasic versus classical biphasic extraction protocols for comprehensive UHPLC-MS/MS lipidomic analysis of HeLa cells, *Anal Chim Acta* 1048 (2019) 66-74. <https://doi.org/10.1016/j.aca.2018.10.035>.

[26] H.M. Gegner, N. Mechtel, E. Heidenreich, A. Wirth, F.G. Cortizo, K. Bennewitz, T. Fleming, C. Andresen, M. Freichel, A.A. Teleanu, J. Kroll, R. Hell, G. Poschet, Deep Metabolic Profiling Assessment of Tissue Extraction Protocols for Three Model Organisms, *Front Chem* 10 (2022) 869732. <https://doi.org/10.3389/fchem.2022.869732>.

[27] S. Zukunft, C. Prehn, C. Rohring, G. Moller, M. Hrabe de Angelis, J. Adamski, J. Tokarz, High-throughput extraction and quantification method for targeted

metabolomics in murine tissues, *Metabolomics* 14(1) (2018) 18. <https://doi.org/10.1007/s11306-017-1312-x>.

[28] T. Bogl, F. Mlynek, M. Himmelsbach, W. Buchberger, Comparison of one-phase and two-phase extraction methods for porcine tissue lipidomics applying a fast and reliable tentative annotation workflow, *Talanta* 236 (2022) 122849. <https://doi.org/10.1016/j.talanta.2021.122849>.

[29] E. Dorochow, R. Gurke, S. Rischke, G. Geisslinger, L. Hahnefeld, Effects of Different Storage Conditions on Lipid Stability in Mice Tissue Homogenates, *Metabolites* 13(4) (2023). <https://doi.org/10.3390/metabo13040504>.

[30] R.W. Jiang, K. Jaroch, J. Pawliszyn, Solid-phase microextraction of endogenous metabolites from intact tissue validated using a Biocrates standard reference method kit, *J Pharm Anal* 13(1) (2023) 55-62. <https://doi.org/10.1016/j.jpha.2022.09.002>.

[31] S. Ayache, M. Panelli, F.M. Marincola, D.F. Stroncek, Effects of Storage Time and Exogenous Protease Inhibitors on Plasma Protein Levels, *Am J Clin Pathol* 126(2) (2006) 174-184. <https://doi.org/10.1309/3wm7xj7rd8bclnkx>.

[32] M. Schwaiger-Haber, E. Stancliffe, V. Arends, B. Thyagarajan, M. Sindelar, G.J. Patti, A Workflow to Perform Targeted Metabolomics at the Untargeted Scale on a Triple Quadrupole Mass Spectrometer, *ACS Meas Sci Au* 1(1) (2021) 35-45. <https://doi.org/10.1021/acsmeasuresciau.1c00007>.

[33] A. Sens, S. Rischke, L. Hahnefeld, E. Dorochow, S.M.G. Schafer, D. Thomas, M. Kohm, G. Geisslinger, F. Behrens, R. Gurke, Pre-analytical sample handling standardization for reliable measurement of metabolites and lipids in LC-MS-based clinical research, *Journal of mass spectrometry and advances in the clinical lab* 28 (2023) 35-46. <https://doi.org/10.1016/j.jmsacl.2023.02.002>.

[34] C.E. Ramsden, Z.X. Yuan, M.S. Horowitz, D. Zamora, S.F. Majchrzak-Hong, B.S. Muhlhausler, A.Y. Taha, M. Makrides, R.A. Gibson, Temperature and time-dependent effects of delayed blood processing on oxylipin concentrations in human plasma, *Prostag Leukotr Ess* 150 (2019) 31-37. <https://doi.org/10.1016/j.plefa.2019.09.001>.

[35] P. Giesbertz, J. Ecker, A. Haag, B. Spanier, H. Daniel, An LC-MS/MS method to quantify acylcarnitine species including isomeric and odd-numbered forms in plasma and tissues, *J Lipid Res* 56(10) (2015) 2029-39. <https://doi.org/10.1194/jlr.D061721>.

- [36] J. Marques, E. Shokry, O. Uhl, L. Baber, F. Hofmeister, S. Jarmusch, M. Bidlingmaier, U. Ferrari, B. Koletzko, M. Drey, Sarcopenia: investigation of metabolic changes and its associated mechanisms, *Skelet Muscle* 13(1) (2023) 2. <https://doi.org/10.1186/s13395-022-00312-w>.
- [37] S. Rauschert, O. Uhl, B. Koletzko, F. Kirchberg, T.A. Mori, R.-C. Huang, L.J. Beilin, C. Hellmuth, W.H. Oddy, Lipidomics reveals associations of phospholipids with obesity and insulin resistance in young adults, *Journal of Clinical Endocrinology & Metabolism* 101(3) (2016) 871-879. <https://doi.org/10.1210/jc.2015-3525>.
- [38] U. Harder, B. Koletzko, W. Peissner, Quantification of 22 plasma amino acids combining derivatization and ion-pair LC-MS/MS, *Journal of chromatography. B, Analytical technologies in the biomedical and life sciences* 879(7-8) (2011) 495-504. <https://doi.org/10.1016/j.jchromb.2011.01.010>.
- [39] E. Newton-Tanzer, H. Demmelmair, J. Horak, L. Holdt, B. Koletzko, V. Grote, Acute Metabolic Response in Adults to Toddler Milk Formulas with Alternating Higher and Lower Protein and Fat Contents, a Randomized Cross-Over Trial, *Nutrients* 13(9) (2021) 3022. <https://doi.org/10.3390/nu13093022>.
- [40] K.L. Lindsay, C. Hellmuth, O. Uhl, C. Buss, P.D. Wadhwa, B. Koletzko, S. Entringer, Longitudinal Metabolomic Profiling of Amino Acids and Lipids across Healthy Pregnancy, *PLoS One* 10(12) (2015) e0145794. <https://doi.org/10.1371/journal.pone.0145794>.
- [41] Y. Hao, J. Horak, Z. Stijepic, S.N. Can, L. Tu, J.A. Wolff, B. Koletzko, Comprehensive tissue homogenization and metabolite extraction for application in clinical metabolomics, *Analytica Chimica Acta* 1344 (2025) 343728. <https://doi.org/https://doi.org/10.1016/j.aca.2025.343728>.
- [42] I. Copyright Clearance Center, Copyright Link-Comprehensive tissue homogenization and metabolite extraction for application in clinical metabolomics, 2025. <https://s100.copyright.com/AppDispatchServlet?publisherName=ELS&contentID=S0003267025001229&orderBeanReset=true>. (Accessed 16th February 2025).
- [43] J.R. Conway, A. Lex, N. Gehlenborg, UpSetR: an R package for the visualization of intersecting sets and their properties, *Bioinformatics* 33(18) (2017) 2938-2940. <https://doi.org/10.1093/bioinformatics/btx364>.

- [44] M. Krassowski, ComplexUpset, 2020. https://krassowski.github.io/complex-upset/articles/Examples_R.html. (Accessed 23rd October 2024).
- [45] A. Marton, Z. Mohácsi, B. Decsi, B. Csillag, J. Balog, R. Schäffer, T. Karancsi, G.T. Balogh, High-Throughput Drug Stability Assessment via Biomimetic Metalloporphyrin-Catalyzed Reactions Using Laser-Assisted Rapid Evaporative Ionization Mass Spectrometry (LA-REIMS), *Pharmaceutics* 16(10) (2024) 1266.
- [46] S. Sofalvi, E.S. Lavins, C.K. Kaspar, H.M. Michel, C.L. Mitchell-Mata, M.A. Huestis, L.G. Apollonio, Development and Validation of an LC-MS-MS Method for the Detection of 40 Benzodiazepines and Three Z-Drugs in Blood and Urine by Solid-Phase Extraction, *Journal of analytical toxicology* 44(7) (2020) 708-717. <https://doi.org/10.1093/jat/bkaa072>.
- [47] S.P. Maputla, W. Van Dalen, A. Joubert, J. Norman, S. Castel, M. van der Merwe, L. Wiesner, A validated liquid chromatography-tandem mass spectrometry assay for the analysis of isoniazid and its metabolite acetyl-isoniazid in urine, *Journal of mass spectrometry and advances in the clinical lab* 32 (2024) 11-17. <https://doi.org/10.1016/j.jmsacl.2024.02.001>.
- [48] J. Dolenšek, M.S. Rupnik, A. Stožer, Structural similarities and differences between the human and the mouse pancreas, *Islets* 7(1) (2015) e1024405. <https://doi.org/10.1080/19382014.2015.1024405>.
- [49] A. Gałuszka, Z. Migaszewski, J. Namieśnik, The 12 principles of green analytical chemistry and the SIGNIFICANCE mnemonic of green analytical practices, *TrAC Trends in Analytical Chemistry* 50 (2013) 78-84. <https://doi.org/https://doi.org/10.1016/j.trac.2013.04.010>.

Acknowledgements

First and foremost, I would like to express my deepest appreciation to my supervisor, Prof. Dr. med. Dr. hc. Berthold Koletzko, chair of the Division of Metabolic and Nutritional Medicine, Department of Paediatrics, Dr. von Hauner Childrens Hospital, LMU-Klinikum. His enthusiasm, meticulousness, and patience were instrumental in navigating challenges and completing my projects. His exemplary guidance have shaped my future career in medical research and clinical practice. I am incredibly grateful for the opportunity to be one of his PhD candidates and for his invaluable mentorship, which extended beyond the academic realm, providing both spiritual and financial support throughout my PhD training.

I am equally thankful to my other two supervisors, Dr. rer. nat. Jeannie Horak, Laboratory Head of the MS-Core Facility and Dr. rer. nat. Sultan Nilay Can, Biostatistician and Bioinformatician of the MS-Core Facility. Their expertise, encouragement, and professional guidance have been fundamental to the success of my research.

Special thanks go to my research team for their dedication and hard work. In particular, I am grateful to Luke Tu, my work and running partner, as well as my "German translator," for her continuous companionship and support. I also want to extend my thanks to Zorica Stijepic and Stephanie-Katrin Magdalena Winterstetter for their essential contributions to my experimental work. I am deeply appreciative of Dr. Hans Demmelmair and Dr. Thu Giang Le Thi for generously sharing their scientific expertise. Additionally, I would like to thank Sonja Kunz, Shobhit Madan, Christiane Haesner-Stricker, Andrea Vielhauer, Vanessa Jäger, and Karin Kantke for their optimism, friendliness, and enthusiasm, which have been a source of motivation throughout my PhD journey.

I extend my gratitude to Prof. Dr. Klaus Parhofer, Prof. Dr. Sebastian Theurich, Prof. Dr. Kristina Adorjan, Prof. Dr. Sibylle Koletzko, Prof. Dr. Alexander Choukér, Prof. Dr.





Oliver T. Keppler, PD Dr. Helga P. Török, Prof. Dr. Veit Hornung, Dr. Paul R. Wratil, and Dr. Ana Zhelyazkova for their insightful advice, invaluable feedback, and ongoing support during my research.

I am deeply indebted to the China Scholarship Council (CSC) for their financial support during my time studying abroad.

To my parents, wife, and sister—words cannot express my gratitude for your unconditional love and support throughout my educational journey.

Finally, to all those who have contributed to my PhD work, in one way or another, thank you!

Affidavit

			
Affidavit			

Hao, Yuntao

Surname, first name

Lindwurmstr. 4

Street

80337, Munich, Germany

Zip code, town, country

I hereby declare, that the submitted thesis entitled:

Plasma Metabolite Correlates of Immune Response in Health Care Workers Post Two Doses of mRNA COVID-19 Vaccines and Methodological Advances in Tissue Metabolomics for Clinical Applications

.....

is my own work. I have only used the sources indicated and have not made unauthorised use of services of a third party. Where the work of others has been quoted or reproduced, the source is always given.

I further declare that the dissertation presented here has not been submitted in the same or similar form to any other institution for the purpose of obtaining an academic degree.

Munich, 05.08.2025

place, date

Yuntao Hao

Signature doctoral candidate

Confirmation of congruency



Confirmation of congruency between printed and electronic version of the doctoral thesis

Hao, Yuntao

Surname, first name

Lindwurmstr. 4

Street

80337, Munich, Germany

Zip code, town, country

I hereby declare, that the submitted thesis entitled:

Plasma Metabolite Correlates of Immune Response in Health Care Workers Post Two Doses of mRNA COVID-19 Vaccines and Methodological Advances in Tissue Metabolomics for Clinical Applications

.....

is congruent with the printed version both in content and format.

Munich, 05.08.2025

place, date

Yuntao Hao

Signature doctoral candidate